The 8th International Conference on Micro-Pattern Gaseous Detectors
Oct.14th - Oct.18th 2024 USTC·Hefei, China

Technical challenges for the new T2K High Angle TPCs

17 October 2024

Stefano Levorato

on behalf of the T2K ND280 upgrade group

Outlook

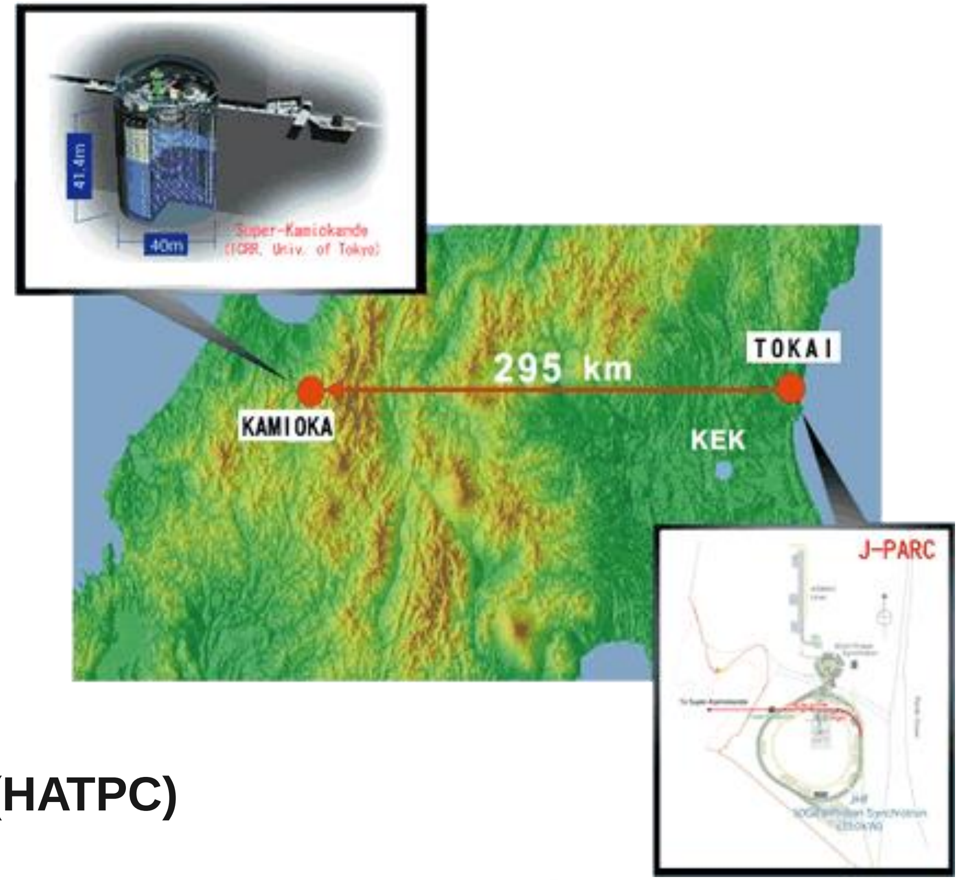

- **The T2K ND280 experiment**
- **The ND280 upgrade project**
  - The motivations
  - The upgrade
- **The High Angle Time Projection Chambers (HATPC)**
  - A short detector description
- **The Encapsulated Resistive Anode Micromegas (ERAM)**
  - Construction
  - Quality assessment
  - Performance
- **Conclusions**

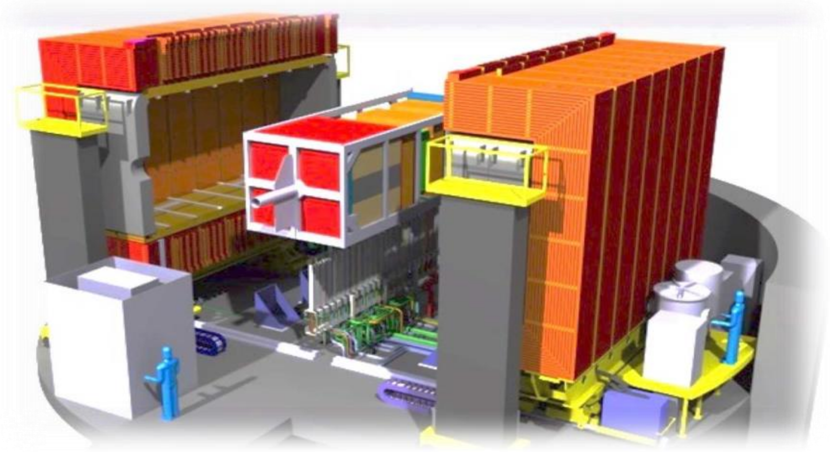

The T2K experiment and the role of ND280

High intensity, 0.6 – 2.2 GeV ν_μ beam produced at J-PARC (Tokai) → ν or $\bar{\nu}$ mode by changing the horn polarity

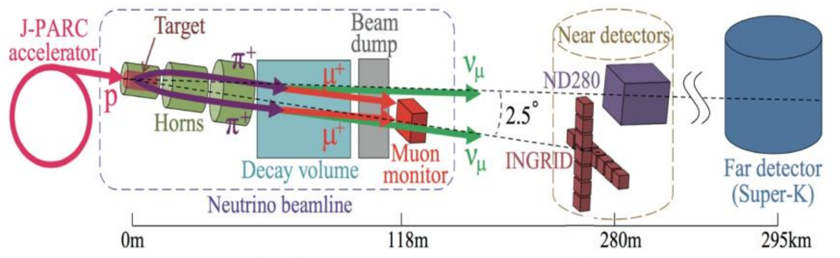

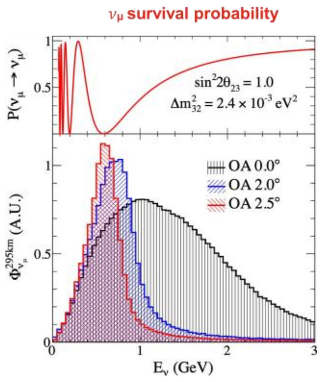

Near Detector complex at 280 meters from the target

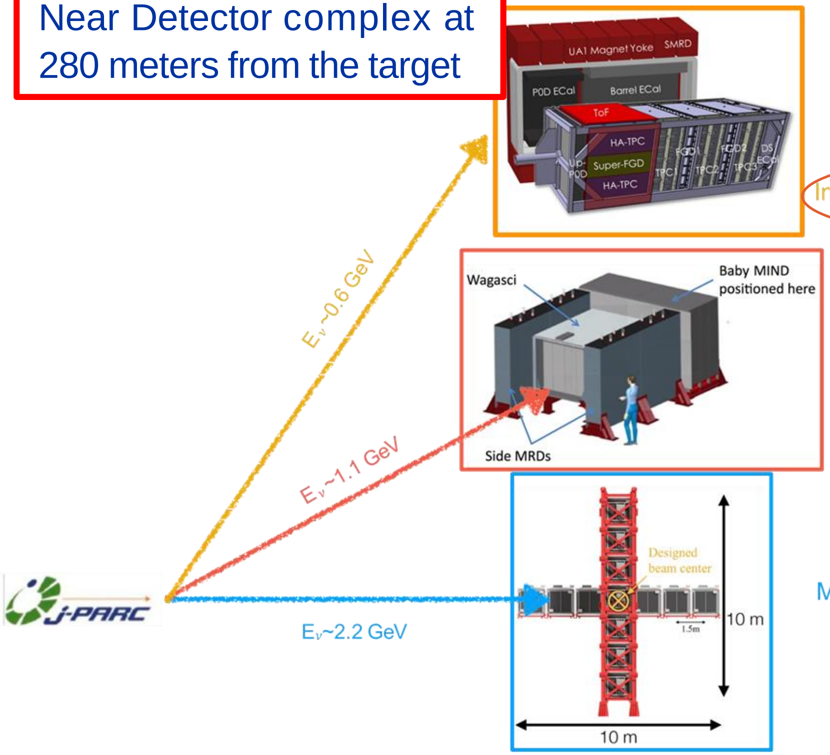

Off-Axis ND280
Constraint systematics in T2K oscillation analyses
Measure neutrino cross-sections
In operation since 2010 and upgraded in 2023

WAGASCI/BabyMIND
Installed in 2019
Cross-sections on water

INGRID: on-axis detector
Monitoring ν beam profile day-by-day
Cross-section measurements
In operation since 2009

8

Neutrinos detected at the Near Detector (ND280) and at the Far Detector (Super-Kamiokande)

- ν_e and $\bar{\nu}_e$ appearance → determine θ_{13} and δ_{CP}
- Precise measurement of ν_μ disappearance → θ_{23} and $|\Delta m^2_{32}|$

Several detectors installed to monitor the beam reduce systematic uncertainties in oscillation analyses, and measure ν and $\bar{\nu}$ cross-sections

ND to measure un-oscillated beam flux and ν cross sections

The ND280 experiment: the upgrade

- Reduced angular acceptance ν events, mostly reconstruct forward going tracks entering the TPCs
- Low efficiency to reconstruct low momenta protons

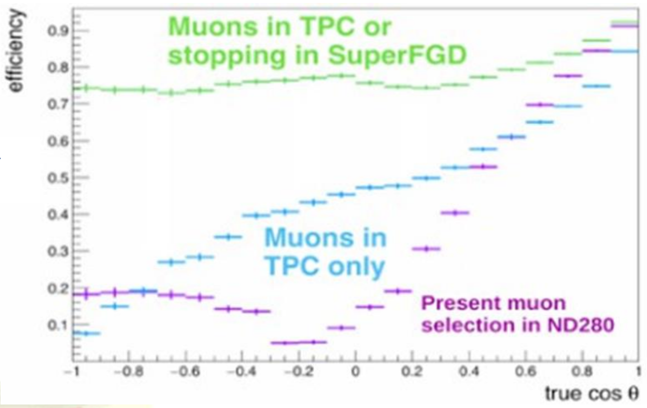

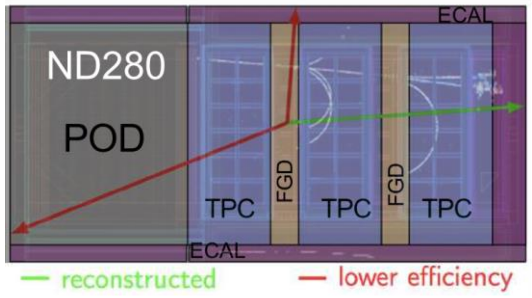

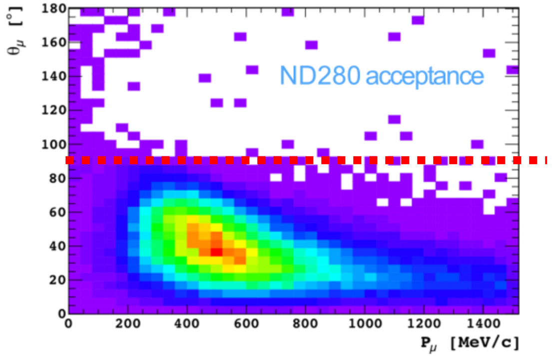

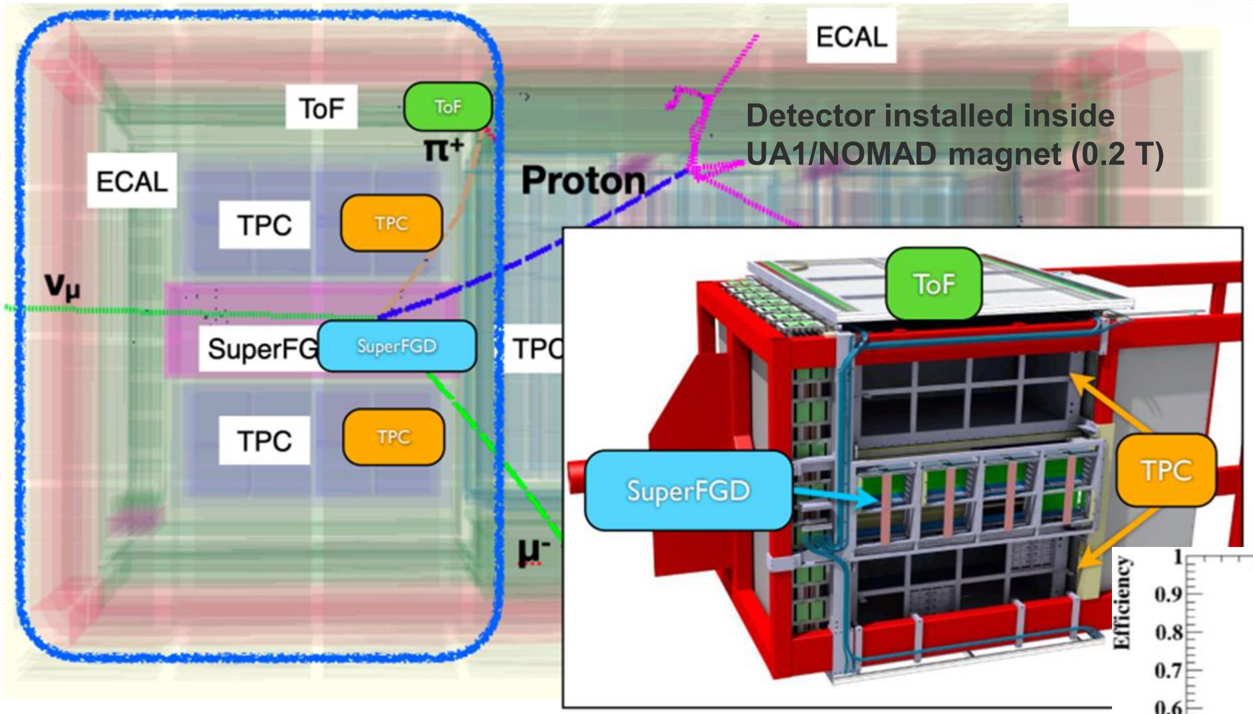

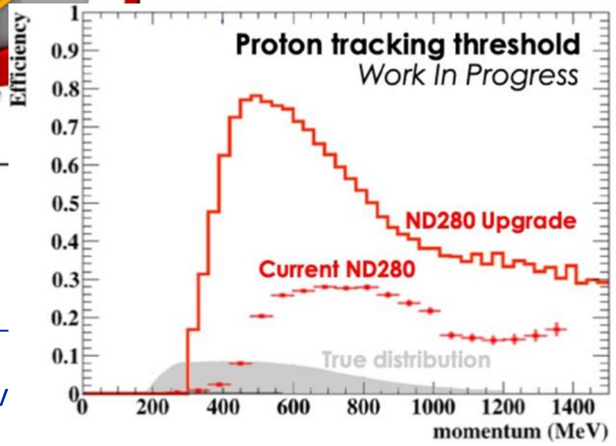

New detectors to extend acceptance for tracks at high angles

ND280: the upgrade detectors

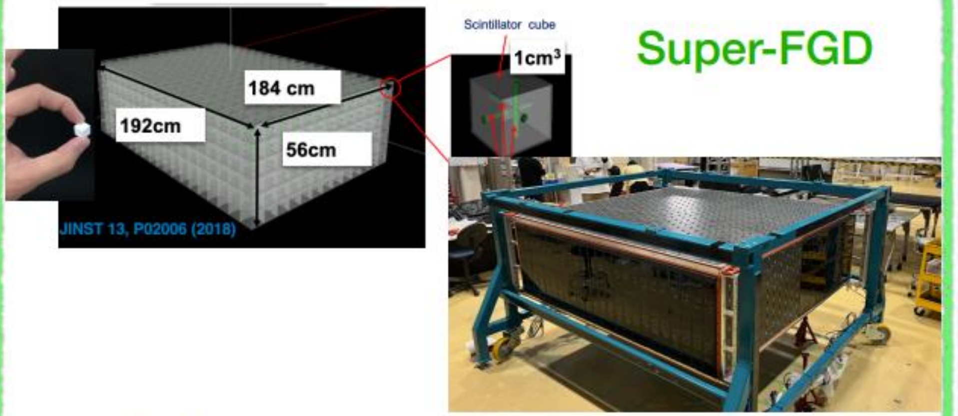

Super-FGD

- New concept of detectors, $2x10^6$ $1cm^3$ cubes
- Each cube is read by 3 WLS → 3D view

High-Angle TPCs

- New TPCs instrumented with Encapsulated Resistive Anode MicroMegas (ERAM)

TOF

6 TOF planes to reconstruct track direction
Time resolution ~150 ps

6

ND280: upgrade completed! Top-HATPC installed in the end of April 2024

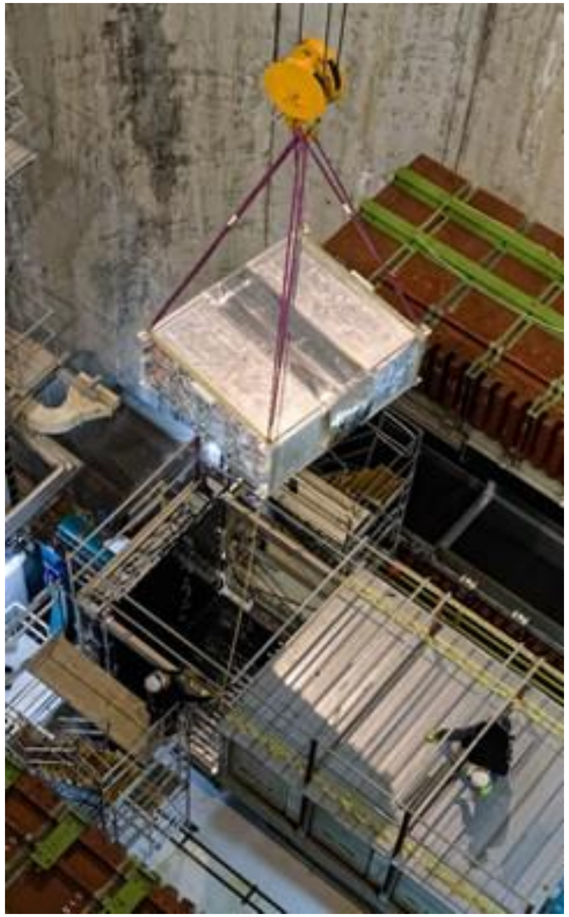

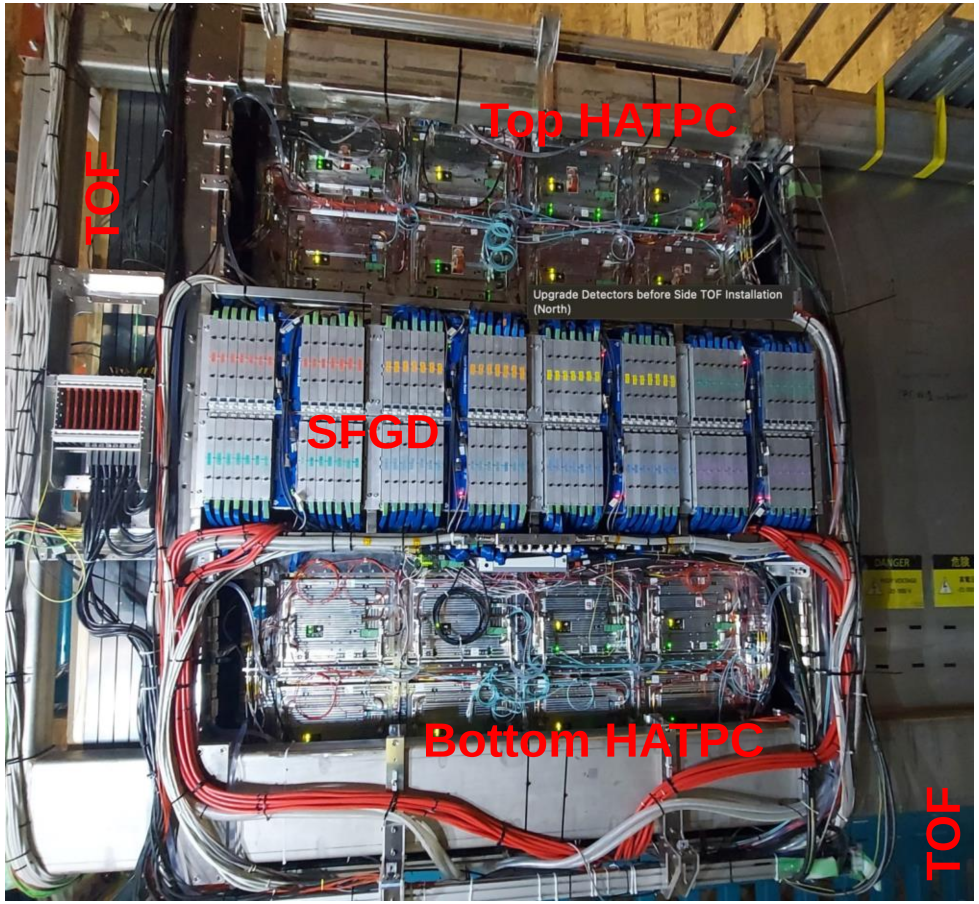

ND280: upgrade completed! Top-HATPC installed in the end of April 2024

Installation of the Detectors of the ND280 upgrade successfully completed in May 2024!

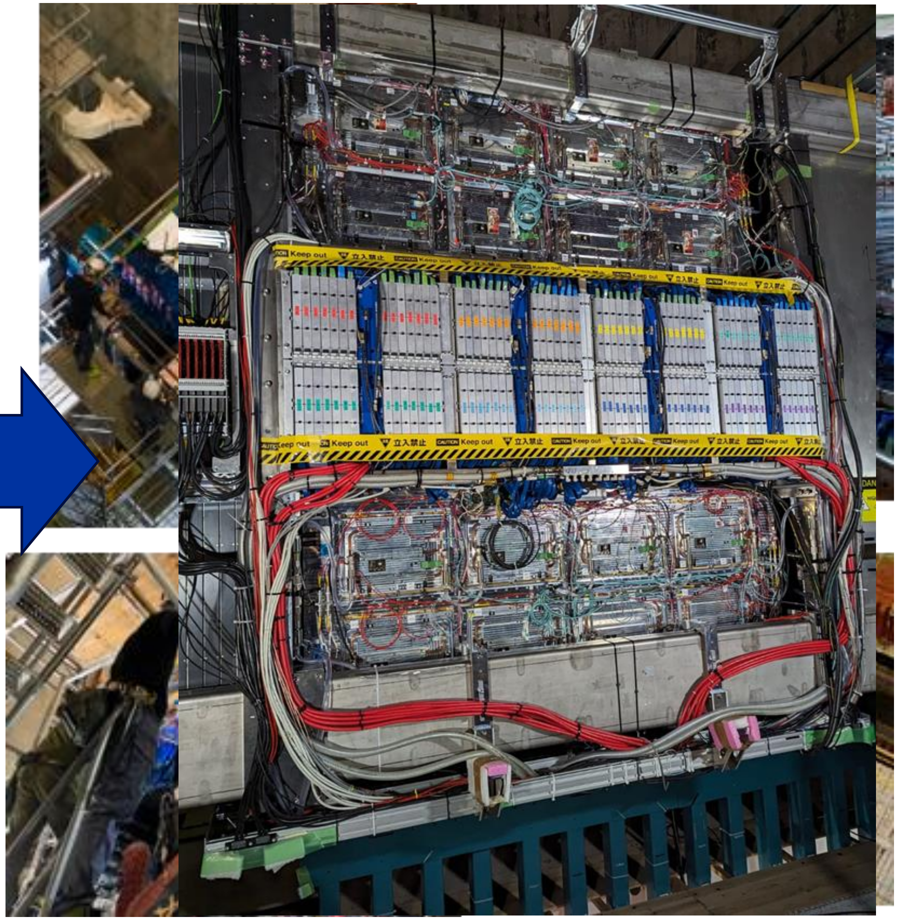

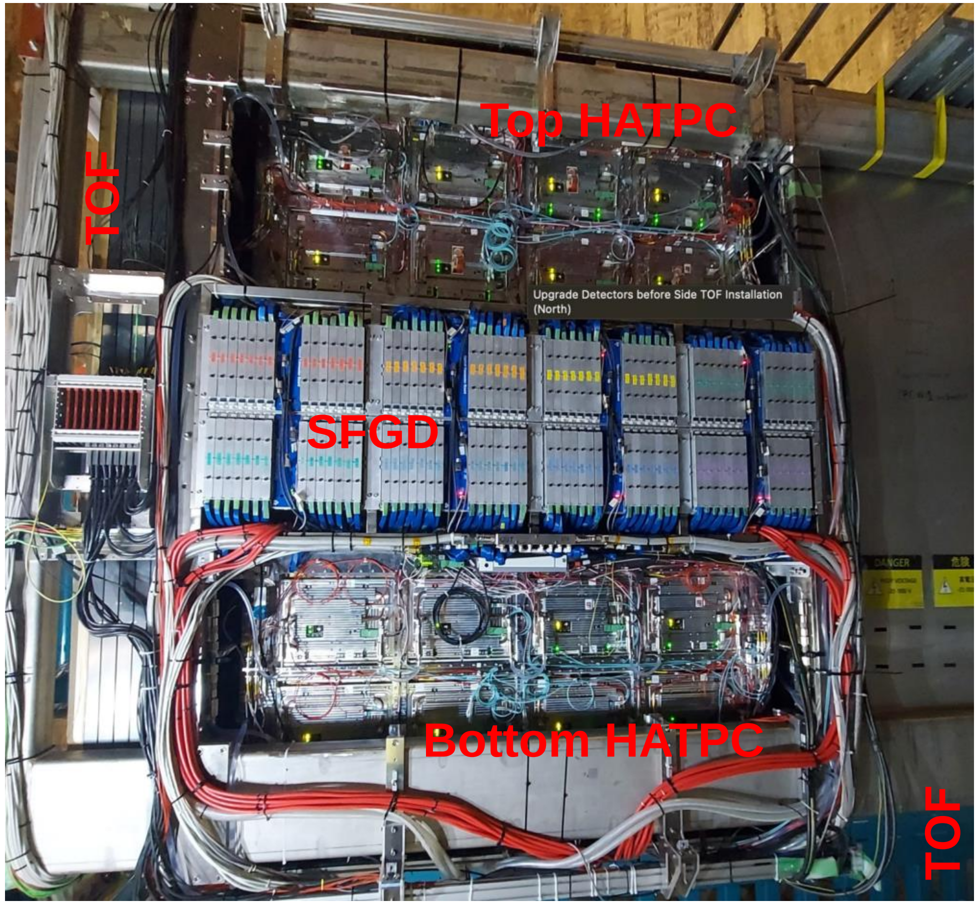

The ND280 experiment: High Angle TPC highlights

- The HATPC detector
  - A short introduction
- Encapsulated Resistive Anode Micromegas (ERAMs)
  - The realization of the 50 ERAM sensors
  - The ERAM characterization
  - Detector response, signal
- HATPC performance

The ND280 experiment: HATPC requirements

Momentum resolution σ_p/p < 9% at 1GeV/c
(neutrino energy)

Energy resolution $\sigma_{dE/dx}$< 10%
(PID muons and electrons)

Space resolution O(500 μm)
(3D tracking & pattern recognition)

Low material budget walls ~ 3% X_0
(matching tracks from neutrino active target)

High Angle TPC

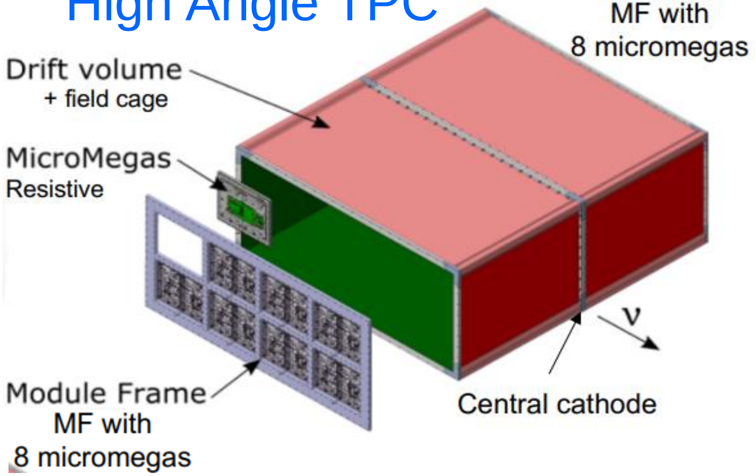

Atmospheric pressure TPC

- Gas: T2K mixture (Ar-CF4-isoC4H10 = 95-3-2)
- Gas contaminants better than O(10 ppm) level
- Drift length 1m
- Central Cathode @ -27kV
- E field unif. < 10^{-3} @1cm from walls
- Low material budget, thin walls
- Active volume ~ O(3m^3)

Resistive MicroMegas sensors (ERAMs)

- Overall anode active surface ~ O(3m^2)
- Sampling length ~ 80-160 cm
- pads ~ 1x1cm^2
- 10k+10k channels / TPC @ End Plates (Anodes)

HATPC, an overview on the main elements

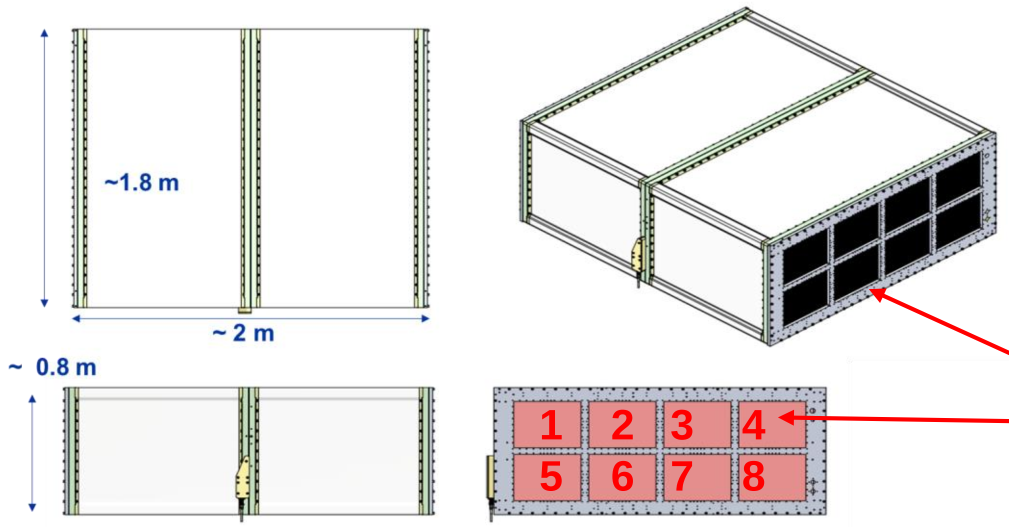

- HATPC in two half FCs
- Central cathode
- Special cathode flanges w/ HV ft
- Two End Plates (Al)
- 8 Readout Modules each

Looking for defects on strips and strip-strip short-circuits and repairing them

Soldering voltage divider resistors

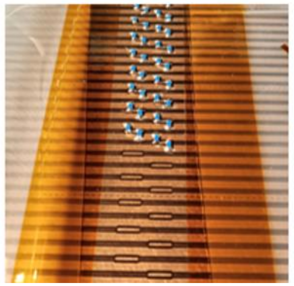

Produced at CERN EP-DT LAB

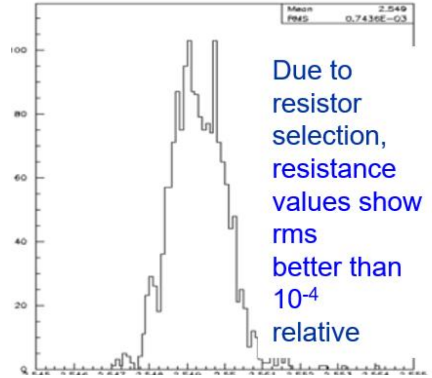

Measuring single resistors

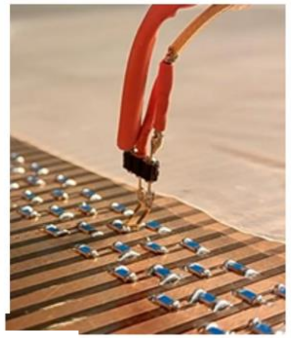

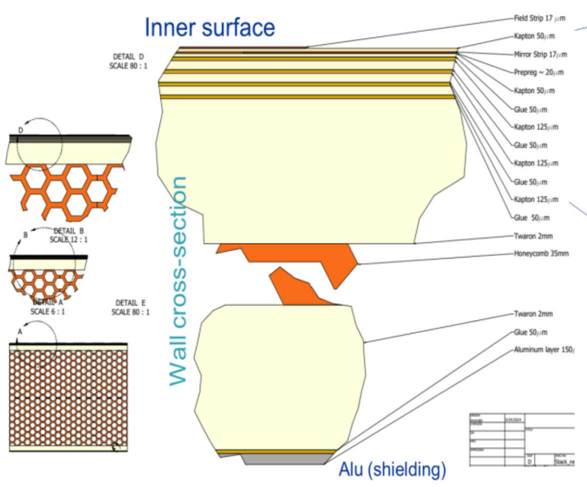

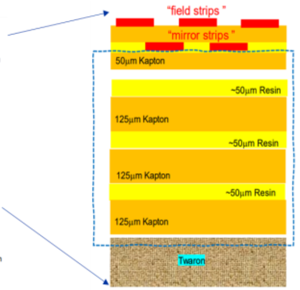

Wall thickness
~ 40 mm
~ 2% radiation length

Electric field shaping by two Cu strips layers ('Field' and 'Mirror' strips)

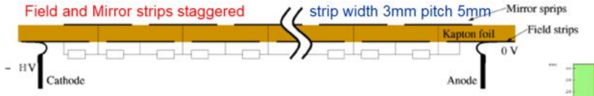

Double layer of strips on Kapton foil
Dimensions = 5m (inner surface cage perimeter) x 1m (drift distance)
Resistors soldered on the inners surface (contact Mirror strips by vias

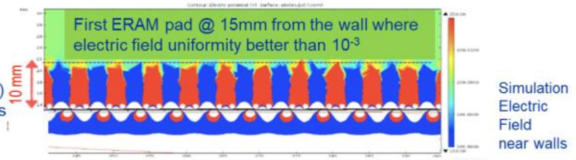

Two voltage dividers In parallel ~400 5.1MΩ resistors each: Overall R ~ 1GΩ

The ND280 experiment: High Angle TPC highlights

- The HATPC detector
  - A short introduction
- Encapsulated Resistive Anode Micromegas (ERAMs)
  - The realization of the 50 ERAM sensors
  - The ERAM characterization
  - Detector response, signal
- HATPC performance

ERAM: MicroMegas with DLC resistive foil

Resistive layer enables charge spreading
→ space resolution below 500μm with larger pads
→ less FEE channels (lower cost)
→ improved resolution at small drift distance
(where transverse diffusion cannot help)

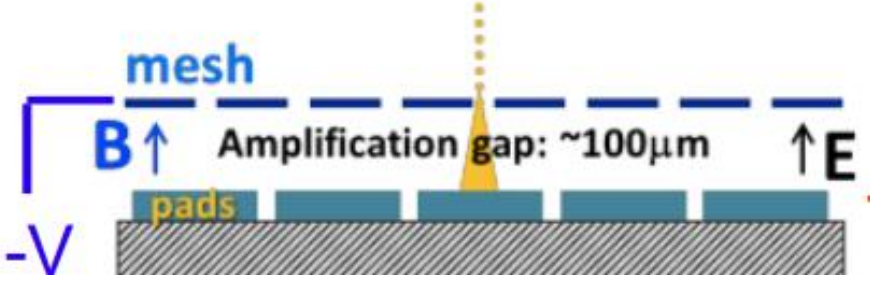

Resistive layer prevents charge build-up and quench sparks
→ enables operation at higher gain
→ no need for spark protection circuits for ASICs
→ compact FEE → max active volume

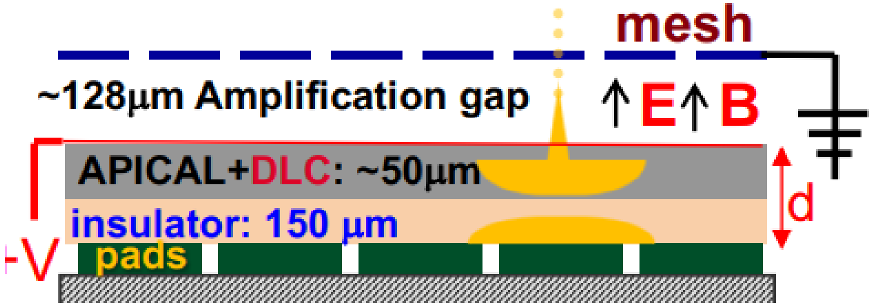

Resistive layer encapsulated and properly insulated from GND
→ Mesh at ground and Resistive layer at +HV
→ improved field homogeneity → reduced track distortions
→ better shielding from mesh and DLC → potentially better S/N

ERAM Module breakout

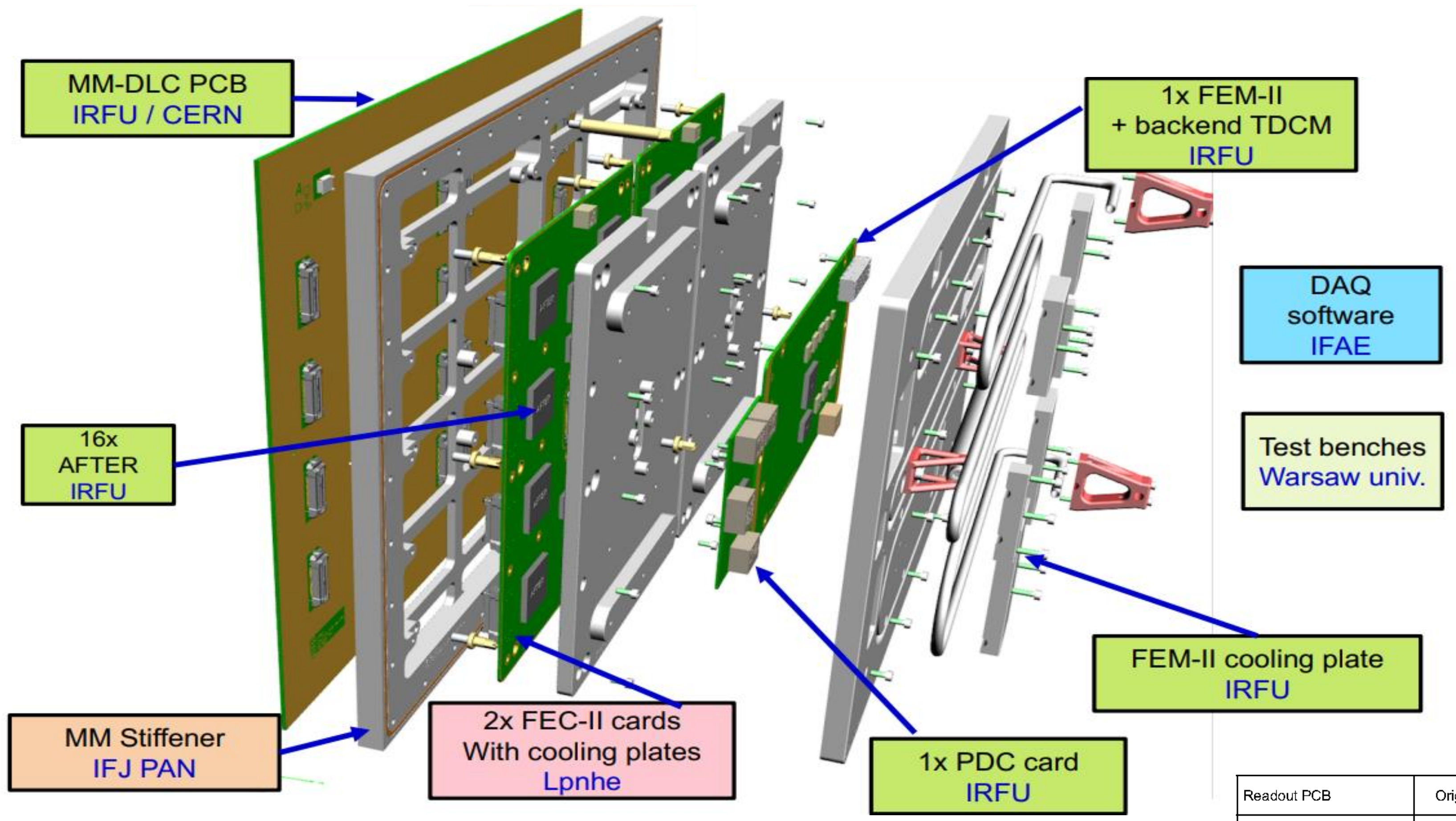

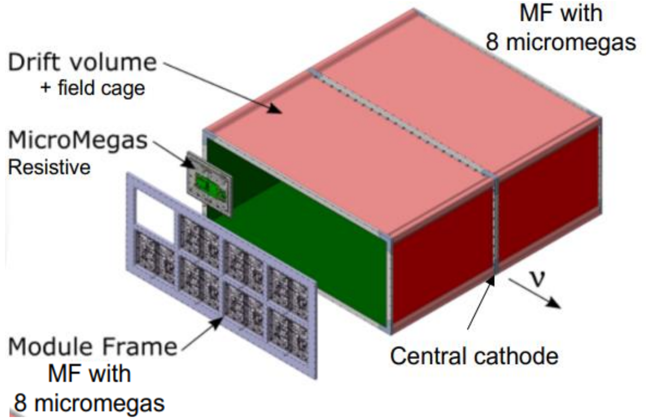

8 + 8 ERAMs per HATPC

← **Very compact Electronics parallel to the detector**

36x32=1152 pads : 2 x 576 ch. FEC + 1 FEM2 + 1 PDC

Readout PCB	Original T2K-TPC	HA-TPC V1 + ARC FEE	HA-TPC V2 + final FEE V1	HA-TPC V2 + final FEE V2
Size	34 × 36 cm²	34 × 42 cm²	34 × 42 cm²	34 × 42 cm²
Pads	48 × 36 cm²	32 × 36 cm²	32 × 36 cm²	32 × 36 cm²
Pad size	6,85 × 9,65 mm²	10,09 × 11,18 mm²	10,09 × 11,18 mm²	10,09 × 11,18 mm²
Number of pads	1728	1152	1152	1152

Charge spread on *low* resistivity foil

Charge Spreading 2D telegraph eqn. solution
time scale is driven by RC

R- surface resistivity
C- capacitance/unit area

Gaussian spread

$$\frac{\partial \rho}{\partial t} = h\left[\frac{\partial^2 \rho}{\partial r^2} + \frac{1}{r}\frac{\partial \rho}{\partial r}\right] \rightarrow \rho(r,t) = \frac{RC}{2t} e^{-r^2 RC/(4t)}$$

$$\sigma_r = \sqrt{\frac{2t}{RC}} \quad \begin{cases} t \approx \text{shaping time (few 100 ns)} \\ RC_{[ns/mm^2]} = \dfrac{180\, R_{[M\Omega/\blacksquare]}}{d_{[\mu m]}/175} \end{cases}$$

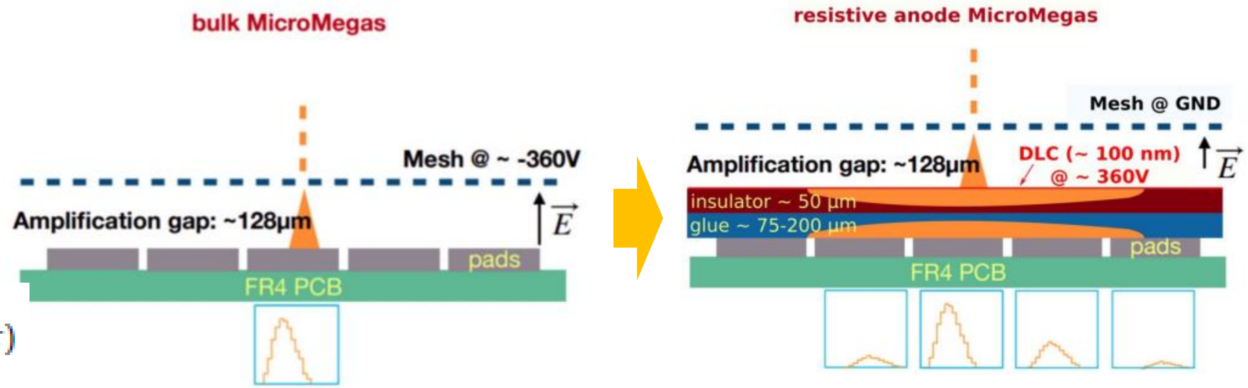

Final ERAM layout choice for series production:

Considering pads of 11x10 mm^2 parameters
- 400 kΩ/□ DLC resistivity – low resistivity
- 150 µm thickness glue – $C_{dlc\text{-}pad/gnd}$ ~ O(20pF)

→ RC ~ O(100ns/mm^2)

Trade-off optimal charge spread VS spark protection

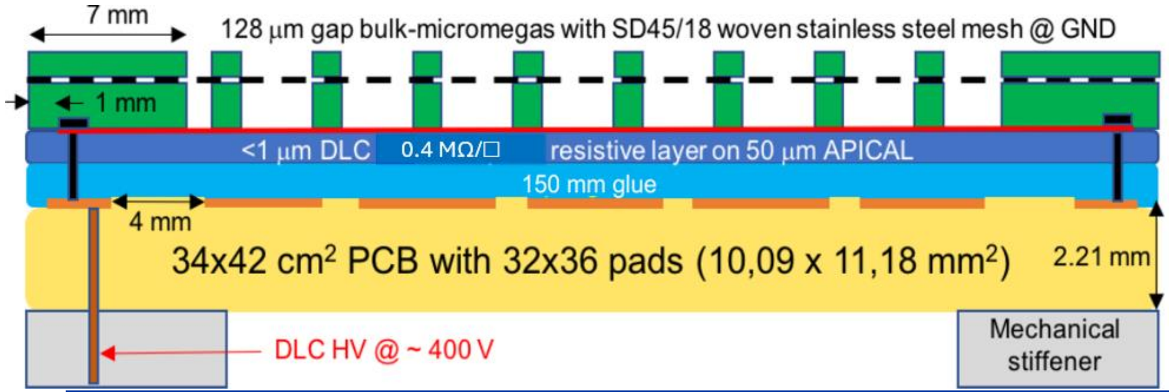

Gain not affected by resistivity
(transparency to induced signals is guaranteed)

ERAM production ~ 50 detectors

Crucial steps in production
(CERN EP-DT MPGD workshop)

1) Selecting DLC foil resistivity
- Large variations from DLC provider
- Value stable after annealing

2) Gluing steps by Pressing
- DLC to PCB
- Stiffener to DLC-PCB

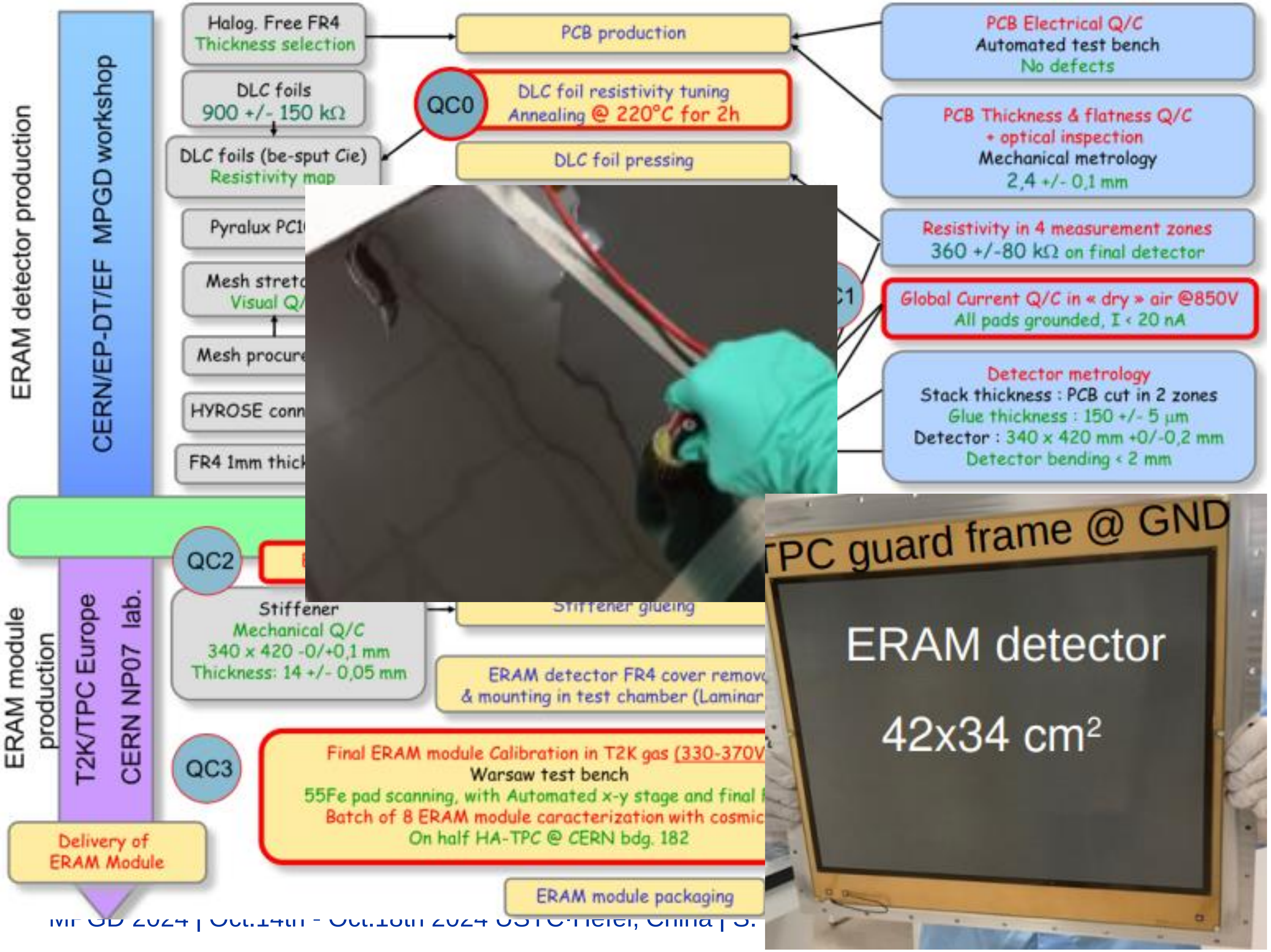

DLC layer: foil selection, QC

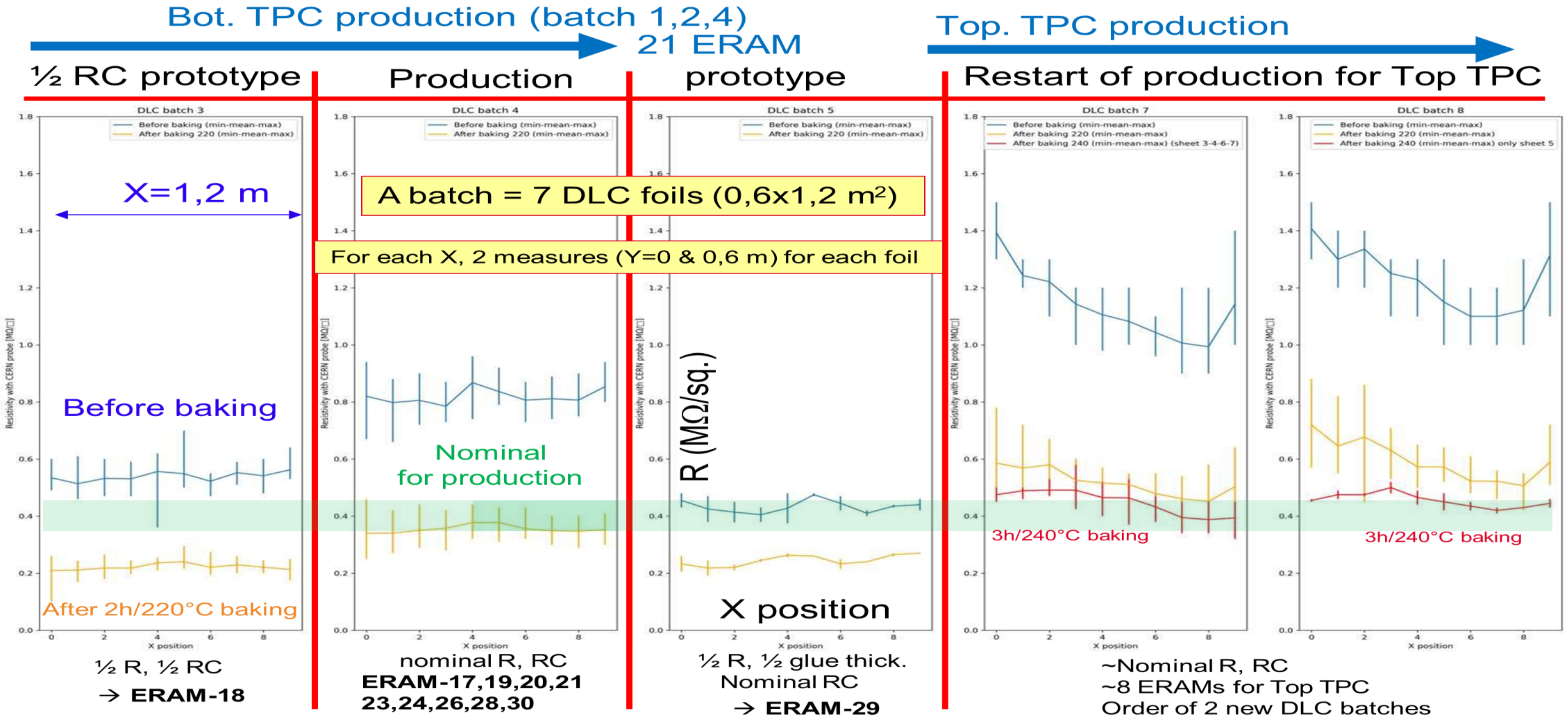

ERAM Series production experience: X-ray scan

X-rays Test Bench at CERN fundamental to

1) Qualify, characterize and calibrate all prototypes and series ERAMs

2) Support the development of detailed ERAM response model

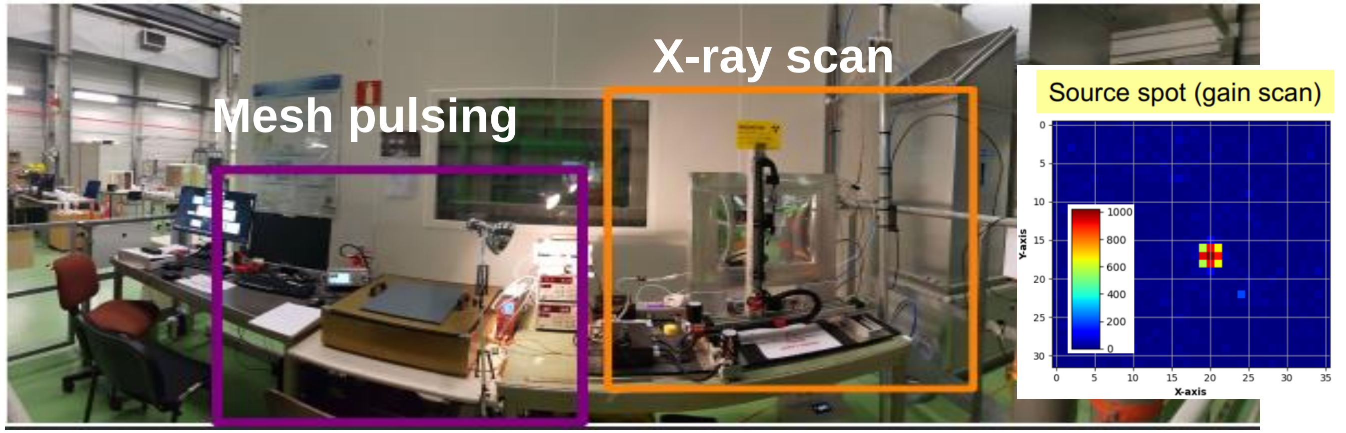

A) Mesh Pulsing: before and after stiffener gluing
Aim: detector geom defects (i.e. pillar detach), stiffener gluing issues, electronic noise

B) X-ray scan of finalized detectors with final electronic modules. Remote controlled station for scanning with mm step fine steps
Aim: QC and fine calibration in terms of gain, resolution and RC

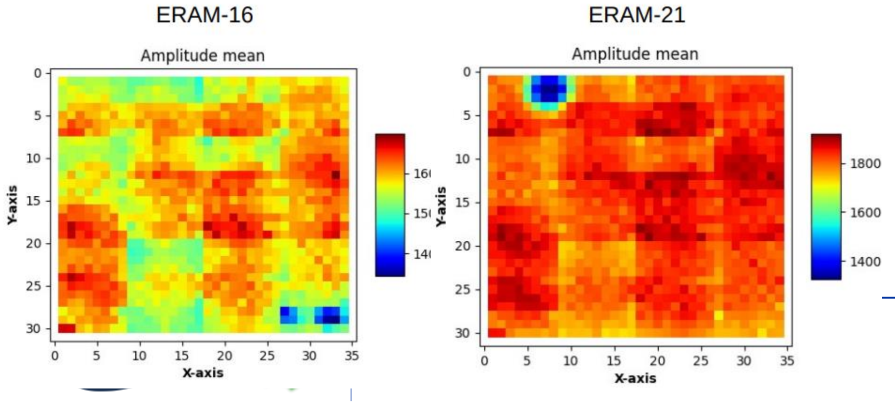

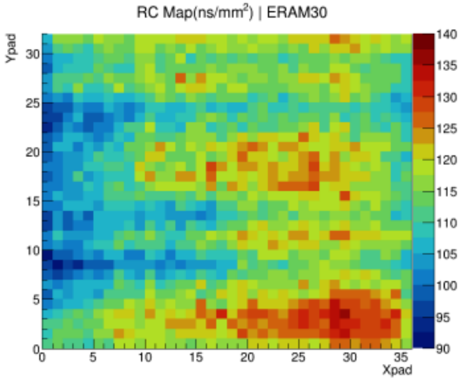

RC map of ERAM30

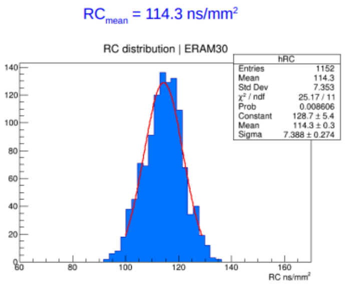

RC distribution of ERAM30

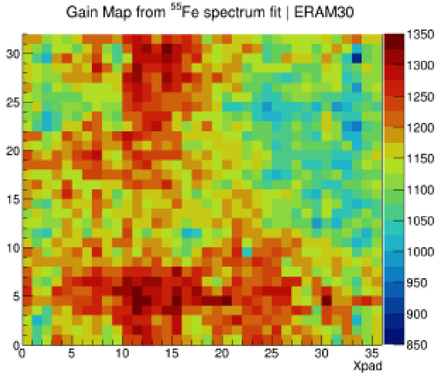

Gain map of ERAM30

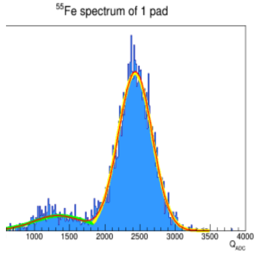

ERAM Series production experience: X-ray scan

Production steps: tough!
(needed long tuning)

1) Selecting DLC foil resistivity
- Large variations from DLC provider
- Stable values only after annealing

2) Gluing steps by Pressing
- DLC to PCB
- Stiffener to DLC-PCB

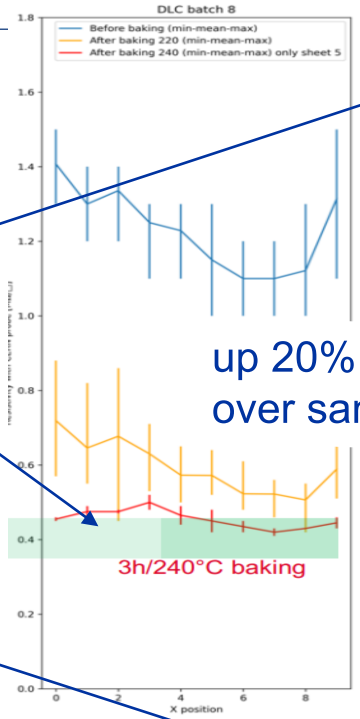

up 20% RC variation
over same ERAM

RC map of ERAMS on bottom HATPC EP1

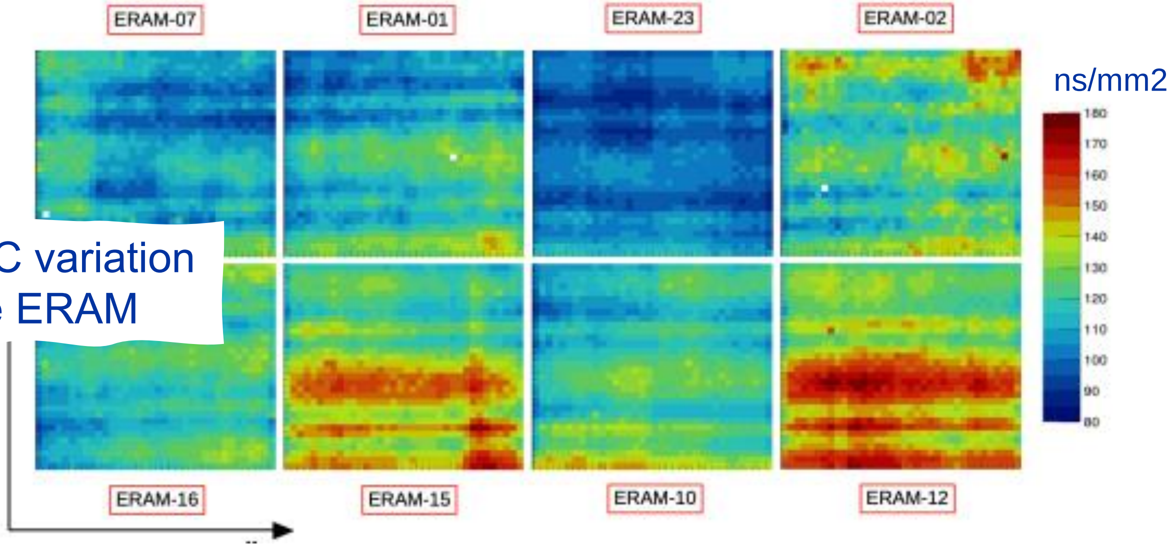

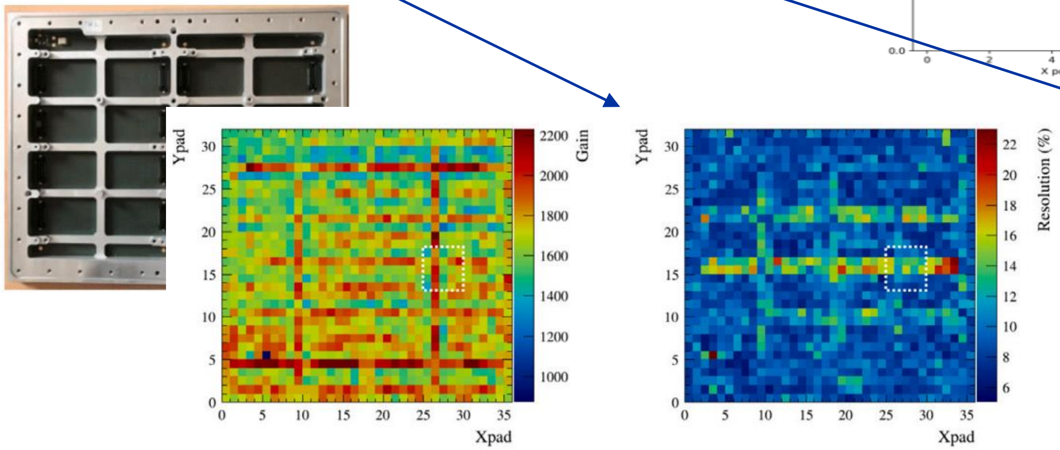

ERAM with DLC-PCB gluing issue

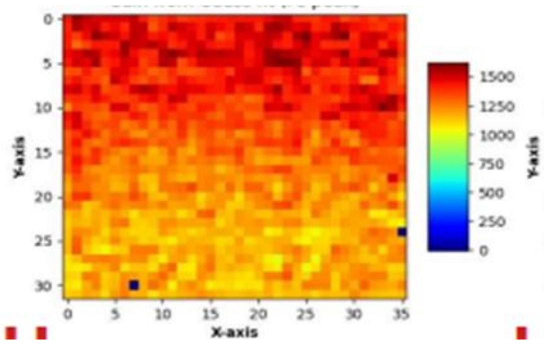

Gain map of ERAM OK

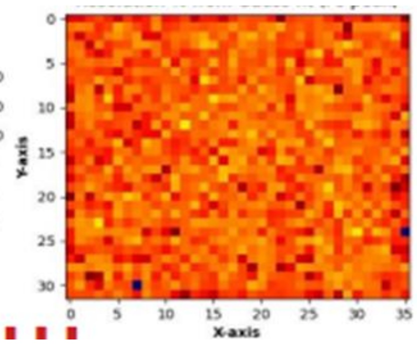

1μm mesh-DLC gap variation => 10% variation in gain

ERAM Series production experience: X-ray scan the importance of the (fast) QA

Gain maps of eight ERAMs tested together in a field cage prototype

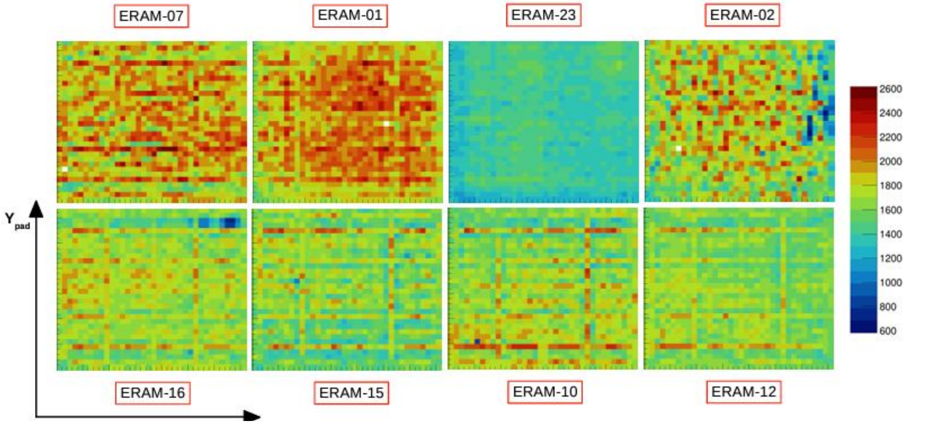

A map of gain non-uniformity within a pad.
relative shift of the mean amplitude reconstructed in the top, bottom, left or right region of each pad under study w.r.t mean amplitude of the pad

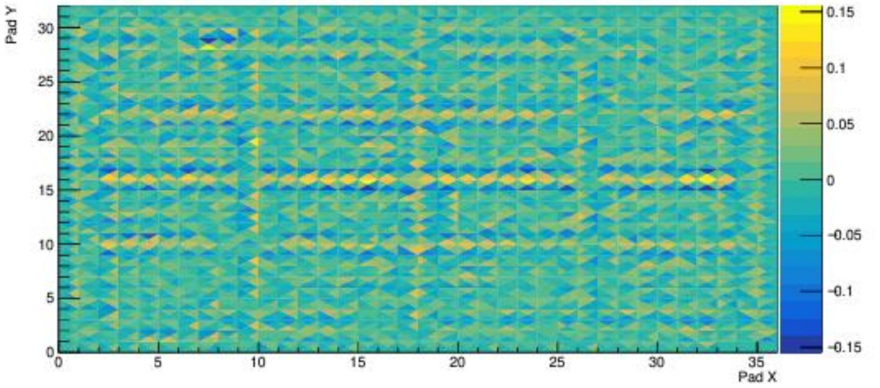

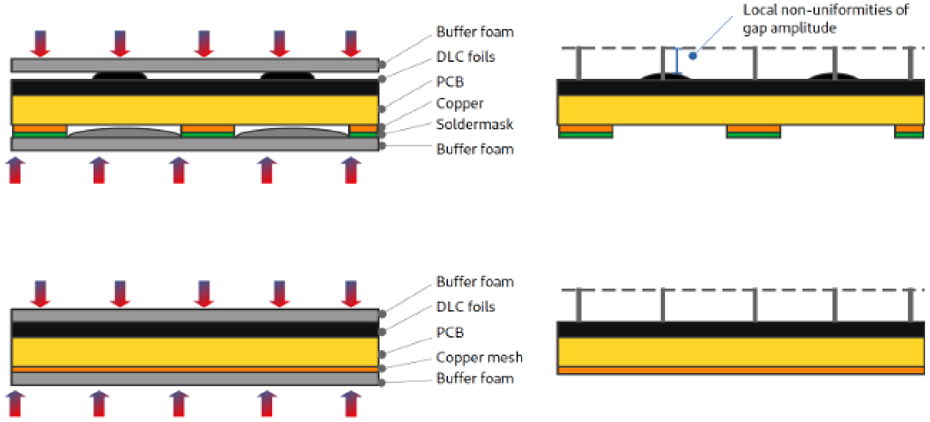

DLC pressing on the PCB during detector assembly resulting in the non-uniformities observed on the 2D gain and energy resolution maps
→ The solder mask is removed and replaced by the copper mesh.

ERAM Series production: a summary table

Gain distribution @350V

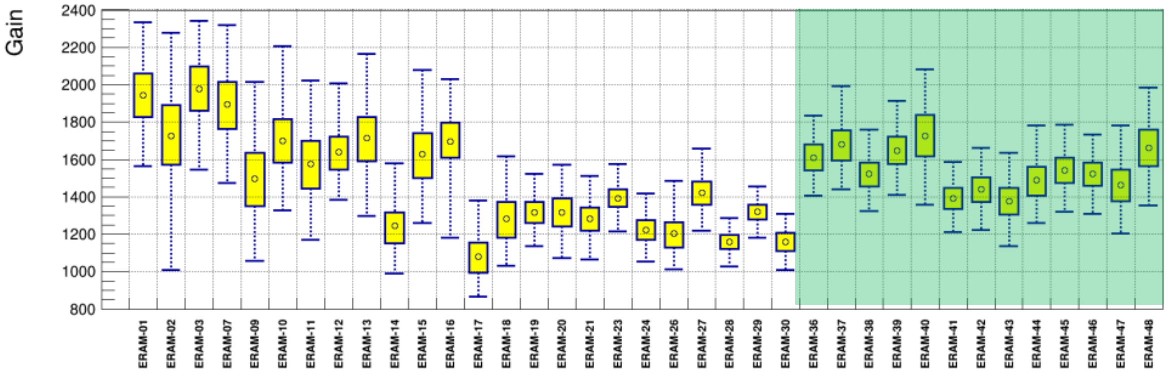

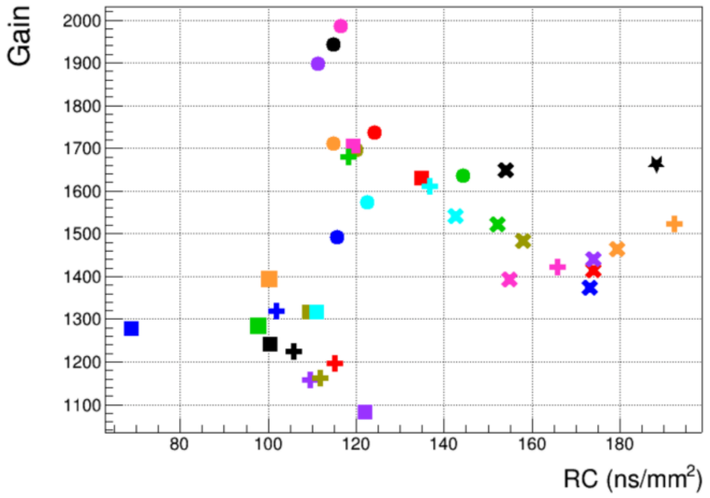

Energy resolution

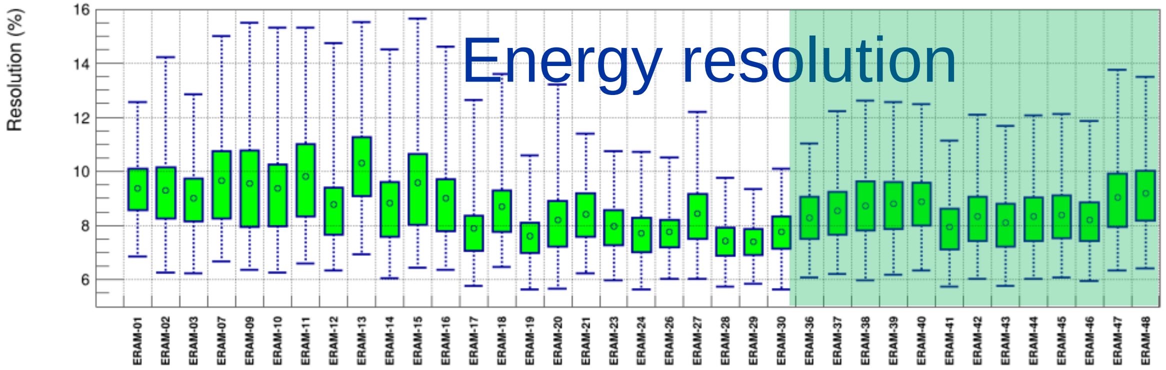

RC distribution

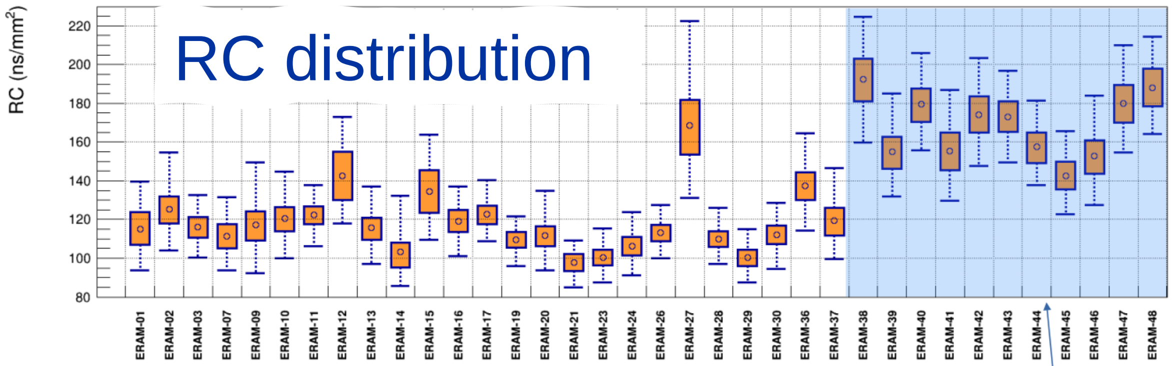

DLC resistivity ≈ 500kΩ/□
Glue thickness: 150 μm

- Lower and upper bounds of box: [Mean – 25%, Mean + 25%] of distribution (50% of values within box).
- Lower and upper bounds of bars: [Mean – 49%, Mean + 49%] of distribution (98% of values within bars).

ERAM Assembly and Operation experience

Low resistivity DLC O(~500kΩ/□) [after annealing] features

- Optimal charge spread → uniform response across pad (combined with C ~ O(20pF/cm^2))
- Fast Q removal and Effective Protection against sparks included at moderate rates ~ O(1kHz) tracks crossing pads
- Leakage currents at level of few nA in normal conditions (no beam)

ERAM @ test beam 2022

ERAM stability

- We have operated 8 ERAM modules during ~ 7.7 days @ CERN 2022
  - Intense beam activity
  - One ERAM module was not working during cosmic test (solved by hammering on it)

- **We have observed no major issue**
- The spark rate is between 0.8 and 1.7 per day (higher than 2uA)

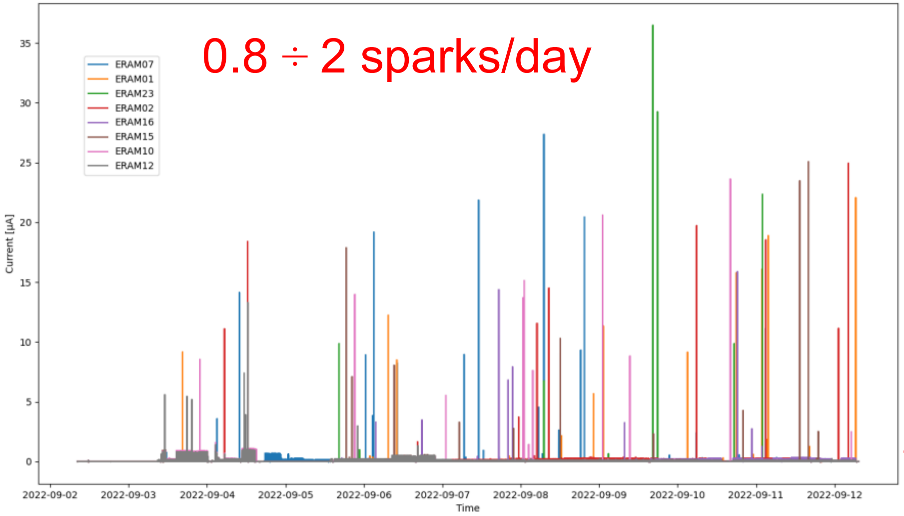

Challenging installation conditions

→ high sensitivity to dust
→ low H2O level (100ppm) before HV on

→ **Confirmed by the detector operation at T2K**

Noise: stability of the installed detector

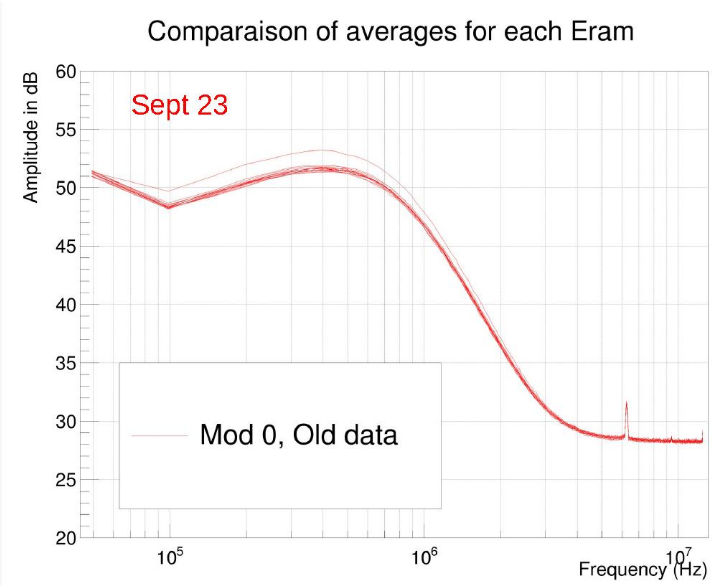

•15 Erams are quasi-identical

•One Eram singles out:
Eram 27
double layer of glue
⇒ Higher capacitance
⇒ Higher noise

RMS of the ADC distributions in Eram 27 is 7.0 against 6.0 for the others Erams

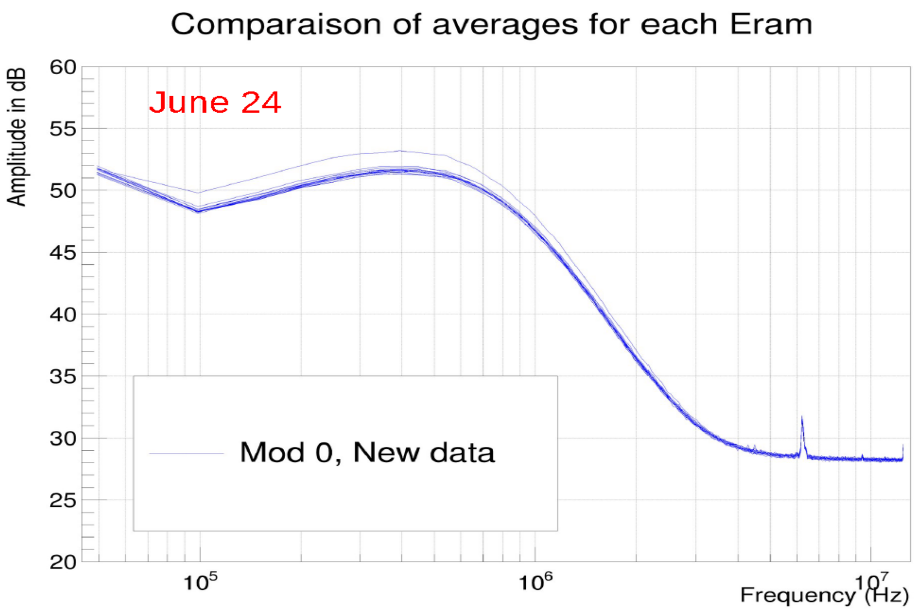

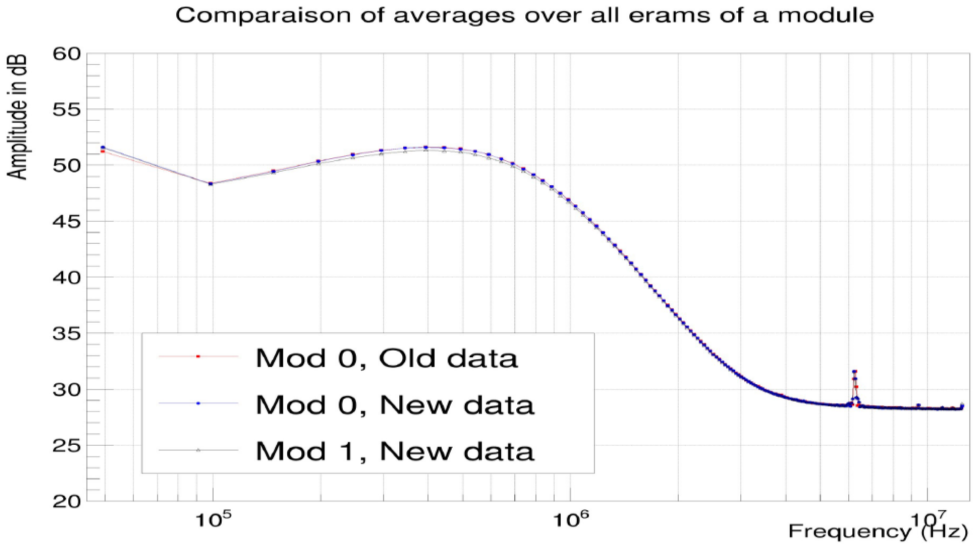

Noise in module 0 has been stable between September 23 and June 24
All the Erams are quasi-identical but one, Eram 27, due its higher capacitance

→ the excellent uniformity of the electronics and of the mechanical definition of the glue layer driving the detector capacitance

ERAM detector response – Noise model

Previous conclusions supported by the noise detailed model included in the MC for Simulation of charge deposition in events

Record of the baseline (no trigger) by D. Calvet

One record
T_p= 412 ns
F_s = 25 MHz

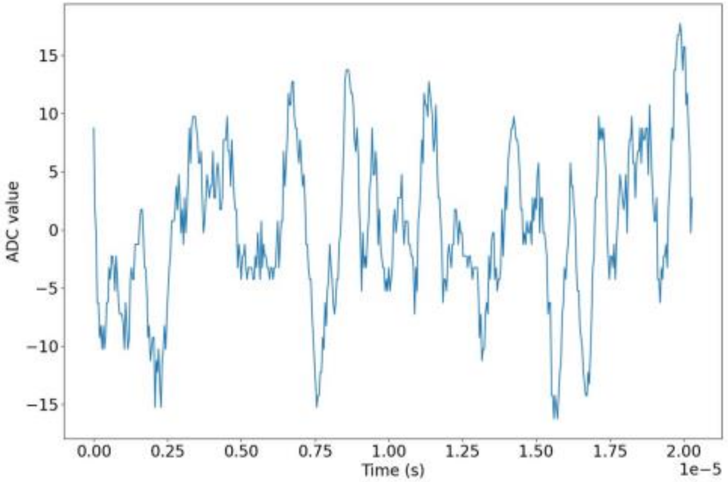

T_p= 412 ns
F_s = 25 MHz

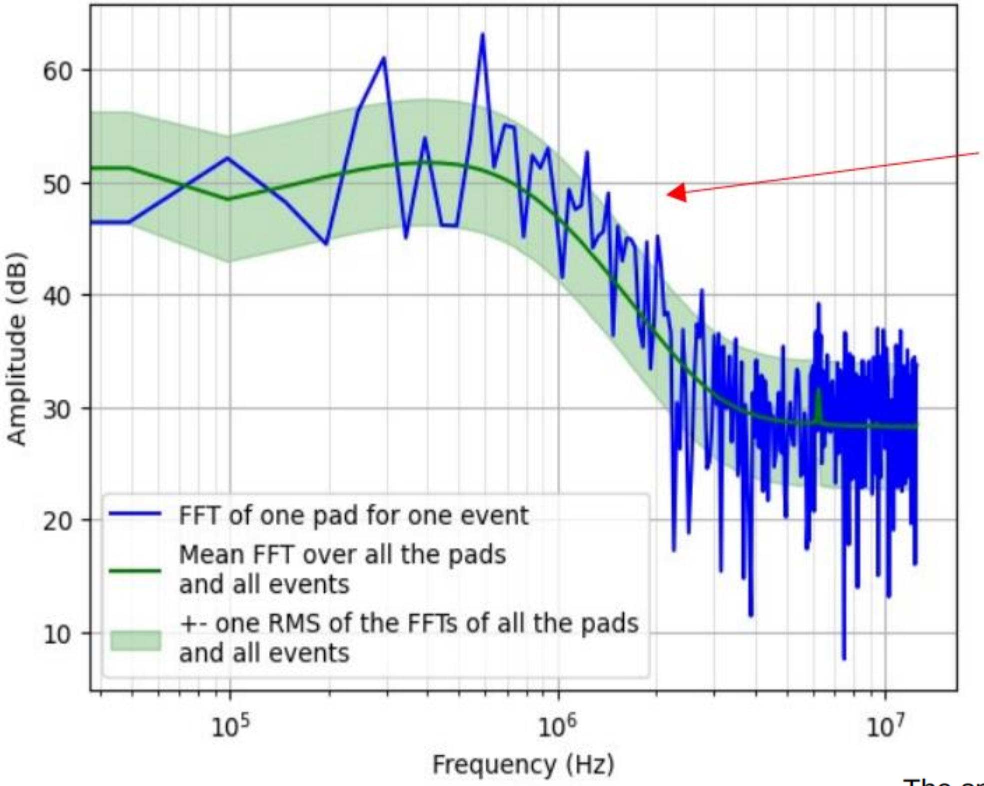

Dominated by frequencies lower than 1 MHz

$$
\begin{aligned}
S(t_b) = & A_{\max}\left(1-\frac{\pi}{2}\left|\sin\left(\frac{\pi(t_b-t_{\max})}{t_w}\right)\right|\right) \\
& + A\cos\left(2\pi\frac{f_s}{4}t_b+\pi\right) \\
& + \sum_f I(f)\,|H(i2\pi f)|\cos\left(\omega t_b+\phi_H+\phi_{\boldsymbol{R}}\right) \\
& + \mathcal{N}(0,\sigma)
\end{aligned}
$$

The spectrum can be fitted quite decently with a “simple” analytical function

$$\sqrt{\left[\frac{A_0}{f^2}\right]^2+\left[A_1\sqrt{f}\,H_{after}(f)\right]^2+A_2^2}$$

The ND280 experiment: High Angle TPC highlights

- The HATPC detector
  - A short introduction
- Encapsulated Resistive Anode Micromegas (ERAMs)
  - The realization of the 50 ERAM sensors
  - The ERAM characterization
  - Detector response, signal
- HATPC performance

The ND280 experiment: High Angle TPC highlights

How does the signal look ? Point deposition for example

Charge deposited punctually
on a pad (X ray)

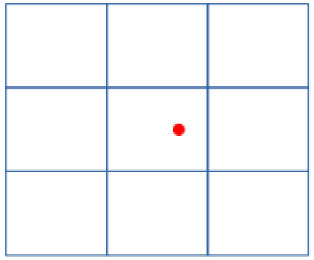

ADC signal : max 4096 counts
Time window of 511 time bins
Time bin (typ.): 40 ns (25 MHz sampling)
Peaking time (typ.) : 412 ns

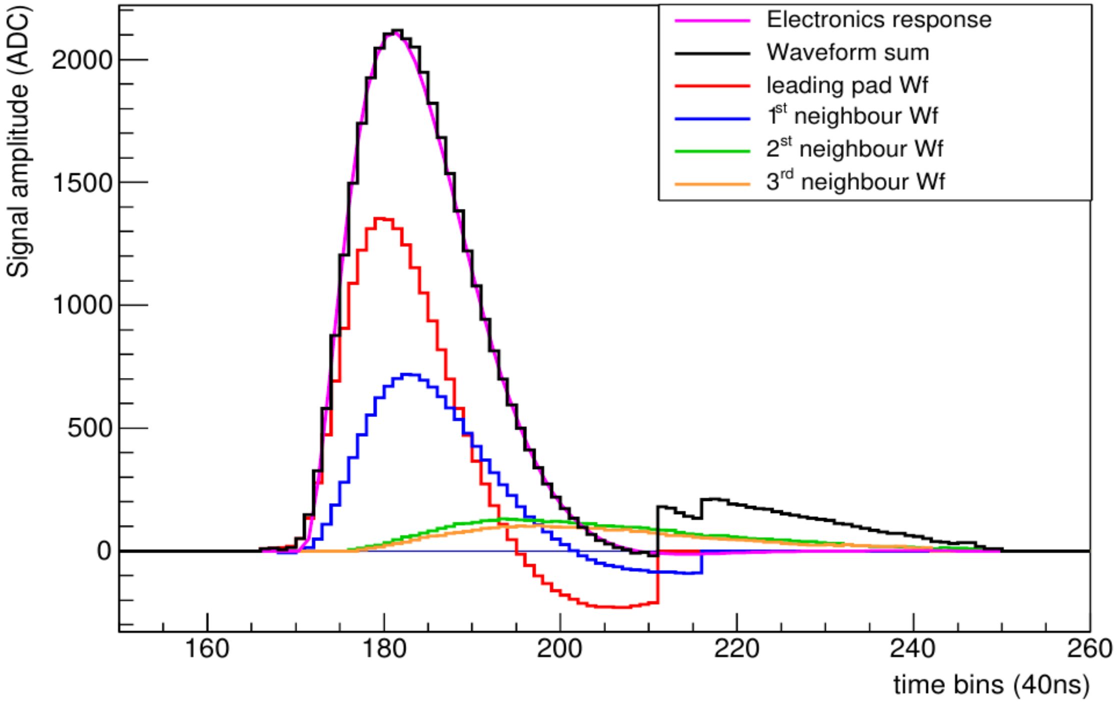

Leading pad: highest and earliest signal
⇒ current induced on pads from by avalanche, ie **ions** signal (as electrons' signal is too fast)
Adjacent pads: lower and later signals
⇒ current induced by potential field adjustments after **electrons** are collected by on DLC
(current induction by "charge spread on resistive layer")

Reconstruction of charge deposition 1/2

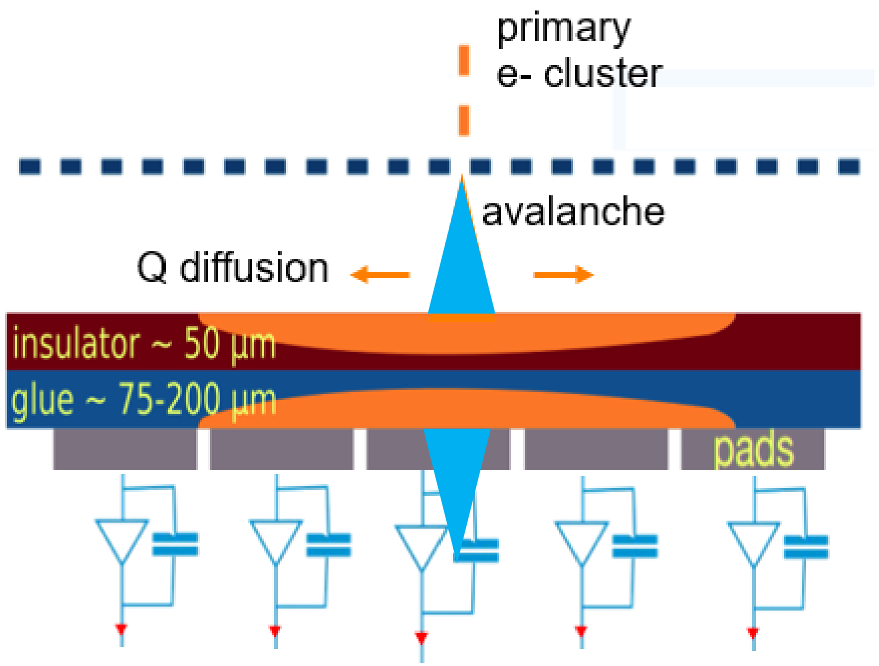

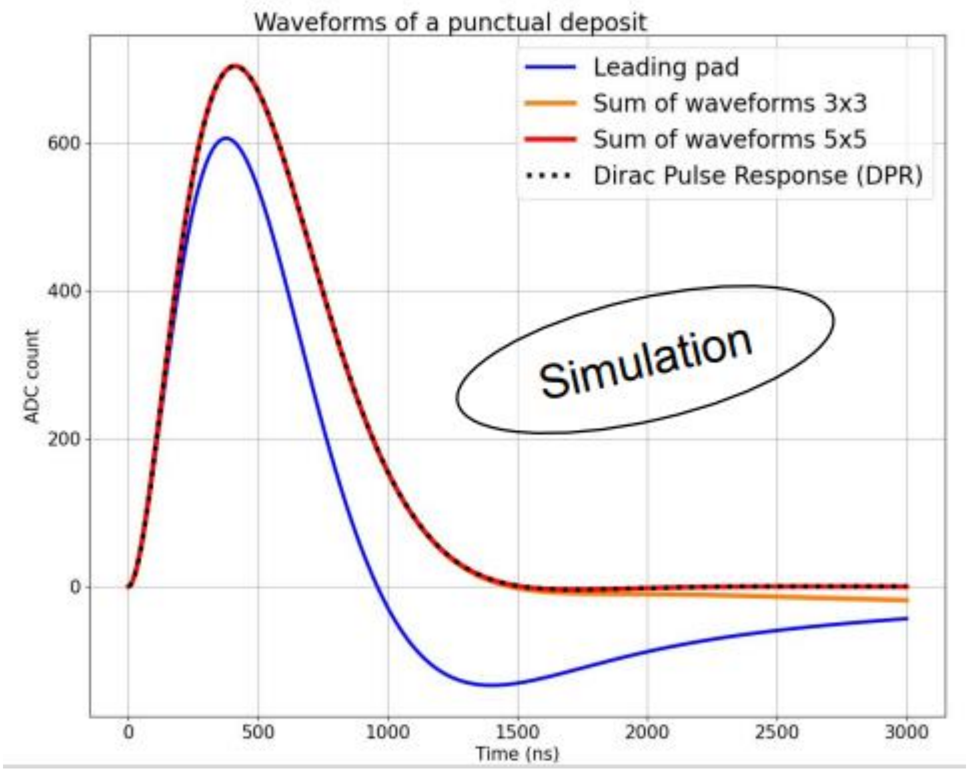

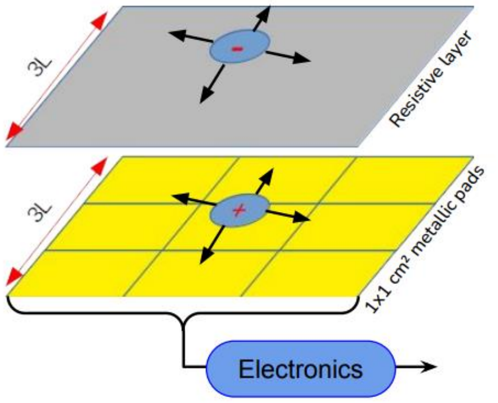

Recovering information about deposited Q is not trivial

Within our electronics shaping time scale
in primary pads, the signal of ions is *diluted* by the signal of charge spreading
=> Need to combine information of all pads (primary and secondary)

Reconstruction of charge deposition 2/2

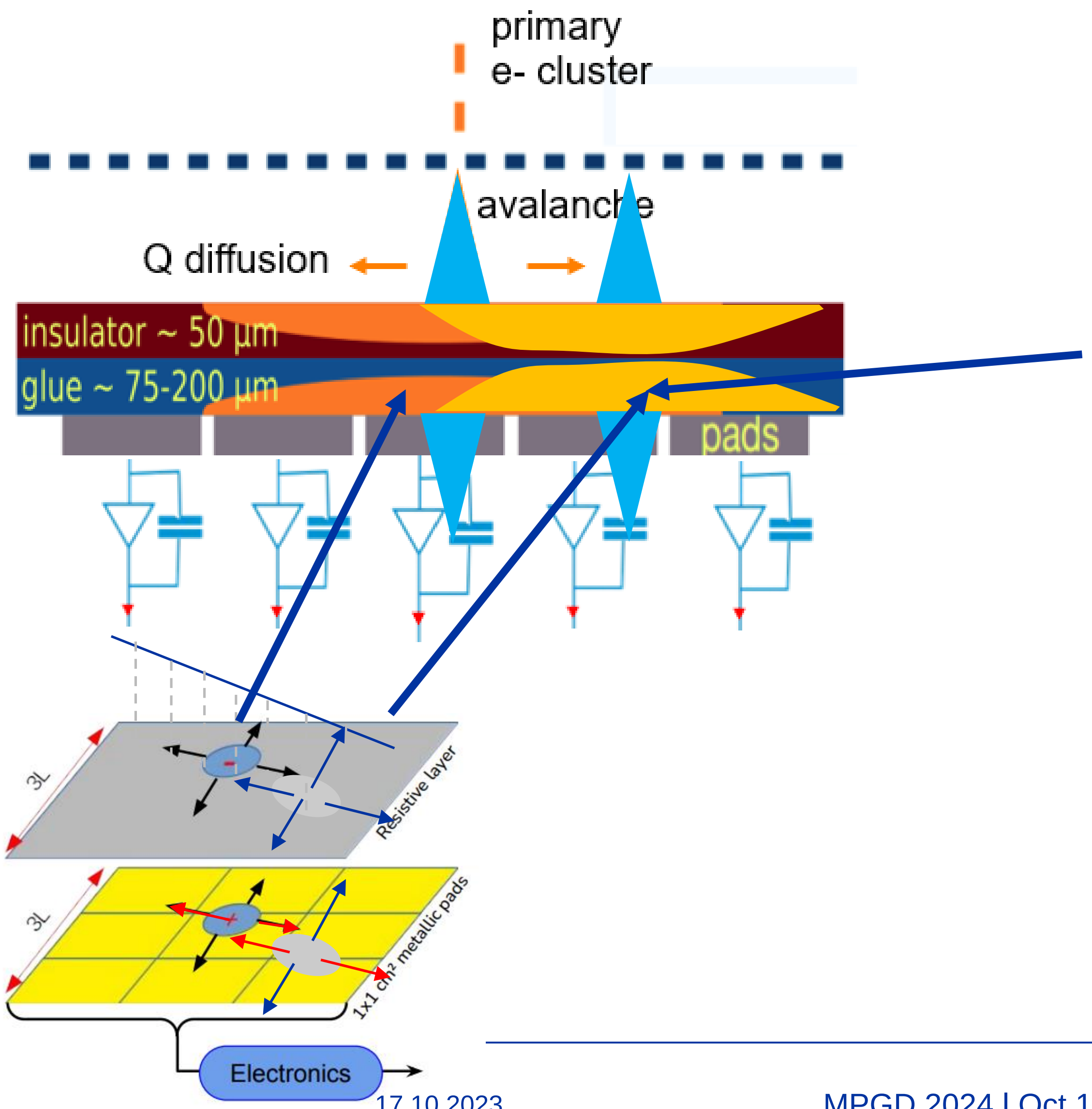

Charge on DLC spreads along any direction including track direction «**longitudinal correlation**» across primary pads within our electronics shaping time scale

requires a dedicated signal formation model

ERAM response – Signal formation model

Main ingredients

In the time scale of our shaping time O(100ns)
Charge spread is properly described by

Solutions of 2D diffusion eqn.

$$\Rightarrow \frac{\partial^2 \rho}{\partial^2 t} = \frac{1}{RC}\left(\frac{\partial^2 \rho}{\partial^2 x} + \frac{\partial^2 \rho}{\partial^2 y}\right) \quad \text{with } RC = \frac{C_S}{\sigma} \text{ in } s/m^2$$

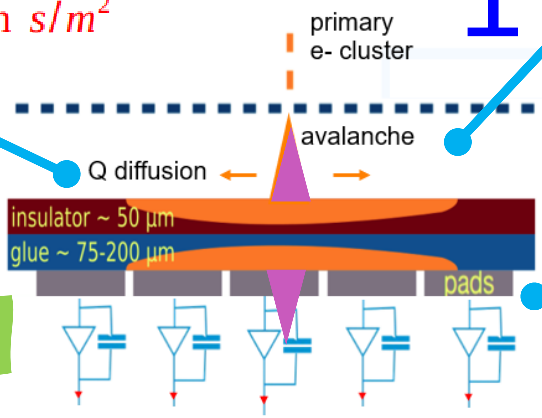

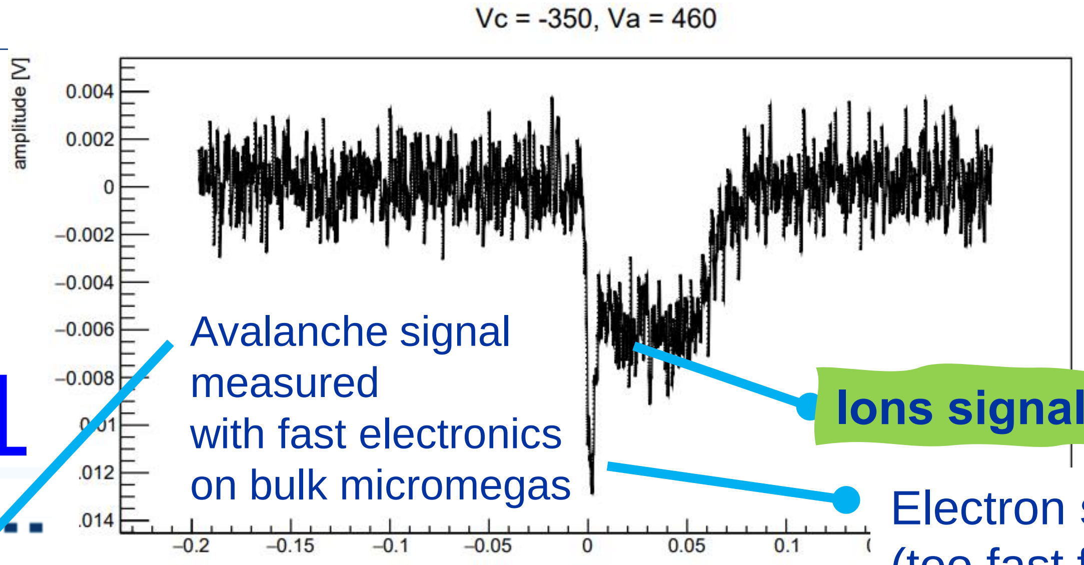

Avalanche signal measured with fast electronics on bulk micromegas

Ions signal (slow)

Electron signal (too fast for our shaping times)

Electrical model of the sensor

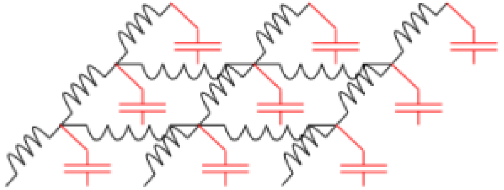

FEE Response Function

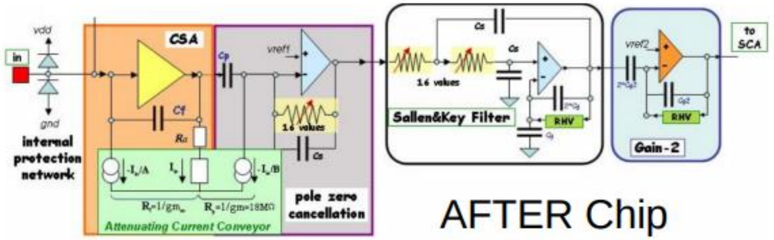

AFTER Chip

$$f(t; w_S, Q) = e^{-w_s t} + e^{\frac{-w_s t}{2Q}}\left[\sqrt{\frac{2Q-1}{2Q+1}}\sin\left(\frac{w_s t}{2}\sqrt{4-\frac{1}{Q^2}}\right) - \cos\left(\frac{w_s t}{2}\sqrt{4-\frac{1}{Q^2}}\right)\right]$$

w_s~1/Peaking time and Q quality factor

Note: Of course, **gas transport properties** (L, T diffusion) have to be accounted for

ERAM response – Signal formation model

Main ingredients

In the time scale of our shaping time O(100ns)
Charge spread is properly described by

Solutions of 2D diffusion eqn.

$$\Rightarrow \frac{\partial^2 \rho}{\partial^2 t} = \frac{1}{RC}\left(\frac{\partial^2 \rho}{\partial^2 x} + \frac{\partial^2 \rho}{\partial^2 y}\right) \text{ with } RC = \frac{C_S}{\sigma} \text{ in } s/m^2$$

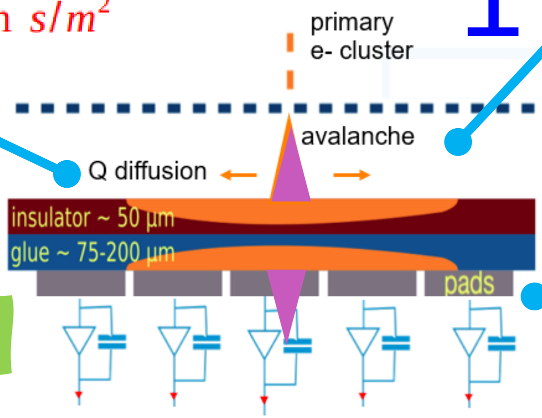

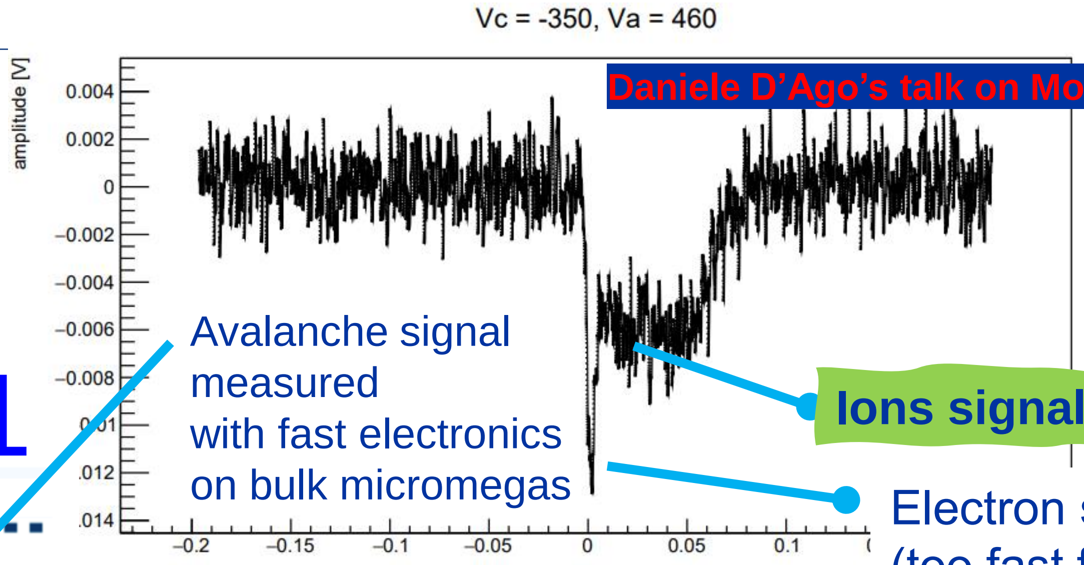

Avalanche signal measured with fast electronics on bulk micromegas

Ions signal (slow)

Electron signal (too fast for our shaping times)

Electrical model of the sensor

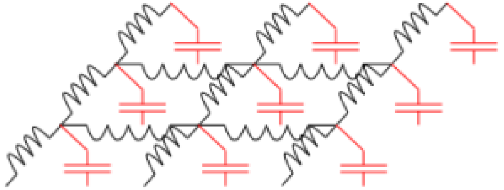

FEE Response Function

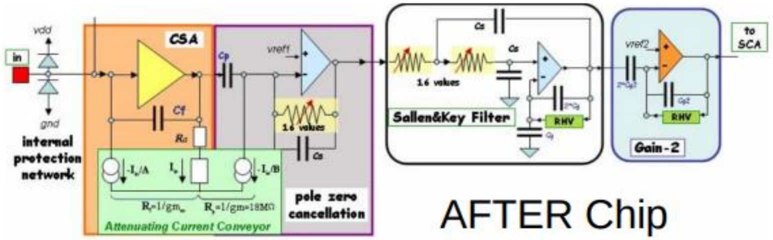

AFTER Chip

$$f(t; w_S, Q) = e^{-w_s t} + e^{\frac{-w_s t}{2Q}}\left[\sqrt{\frac{2Q-1}{2Q+1}}\sin\left(\frac{w_s t}{2}\sqrt{4-\frac{1}{Q^2}}\right) - \cos\left(\frac{w_s t}{2}\sqrt{4-\frac{1}{Q^2}}\right)\right]$$

w_s~1/Peaking time and Q quality factor

Note: Of course, **gas transport properties** (L, T diffusion) have to be accounted for

The ND280 experiment: High Angle TPC highlights

- The HATPC detector
  - A short introduction

- Encapsulated Resistive Anode Micromegas (ERAMs)
  - The realization of the 50 ERAM sensors
  - The ERAM characterization
  - Detector response, signal

- HATPC performance

ERAM detector response: impact on reconstruction

Use of the model for Reconstructing the charge deposition

Due to square shape of ERAM pads, the classical method (PRF+clustering) works OK only for tracks with horizontal or vertical direction (wrt pads coordinates)

Better methods use solutions of telegraph equation in order to
1) compute the pattern templates for charge diffusion on DLC
2) calculate the overall expected signal waveform per each pad
3) find the best matching with the recorded waveforms

Its computationally heavy → different approximations are used for different analysis
1) X-rays analysis – ERAM characterization
2) Measurement of dE/dx – Particle Identification
3) Track reconstruction – momentum measurement

Reconstructing X-rays charge deposition

$Q_{pad}(t)$ = Solution of 2D Teq. for diffusion of initial Q deposited charge (point-like, delta-pulse initial conditions)

$$Q_{pad}(t) = \frac{Q_e}{4} \times \left[erf\left(\frac{x_{high} - x_0}{\sqrt{2}\sigma(t)}\right) - erf\left(\frac{x_{low} - x_0}{\sqrt{2}\sigma(t)}\right) \right] \times \left[erf\left(\frac{y_{high} - y_0}{\sqrt{2}\sigma(t)}\right) - erf\left(\frac{y_{low} - y_0}{\sqrt{2}\sigma(t)}\right) \right]$$

$$\sigma(t) = \sqrt{\frac{2t}{RC}}$$

- Obtained from Telegrapher's equation for charge diffusion.
- Integrating charge density function over area of 1 readout pad.
- Parameterized by 5 variables:
  - x_0 } Initial charge position
  - y_0
  - t_0: Time of charge deposition in leading pad
  - RC : Describes charge spreading
  - Q_e : Total charge deposited in an event

x_H, x_L: Upper and lower bound of a pad in x-direction
y_H, y_L: Upper and lower bound of a pad in y-direction

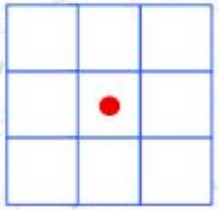

RC = 60 ns/mm²
Q_e = 4 e⁻

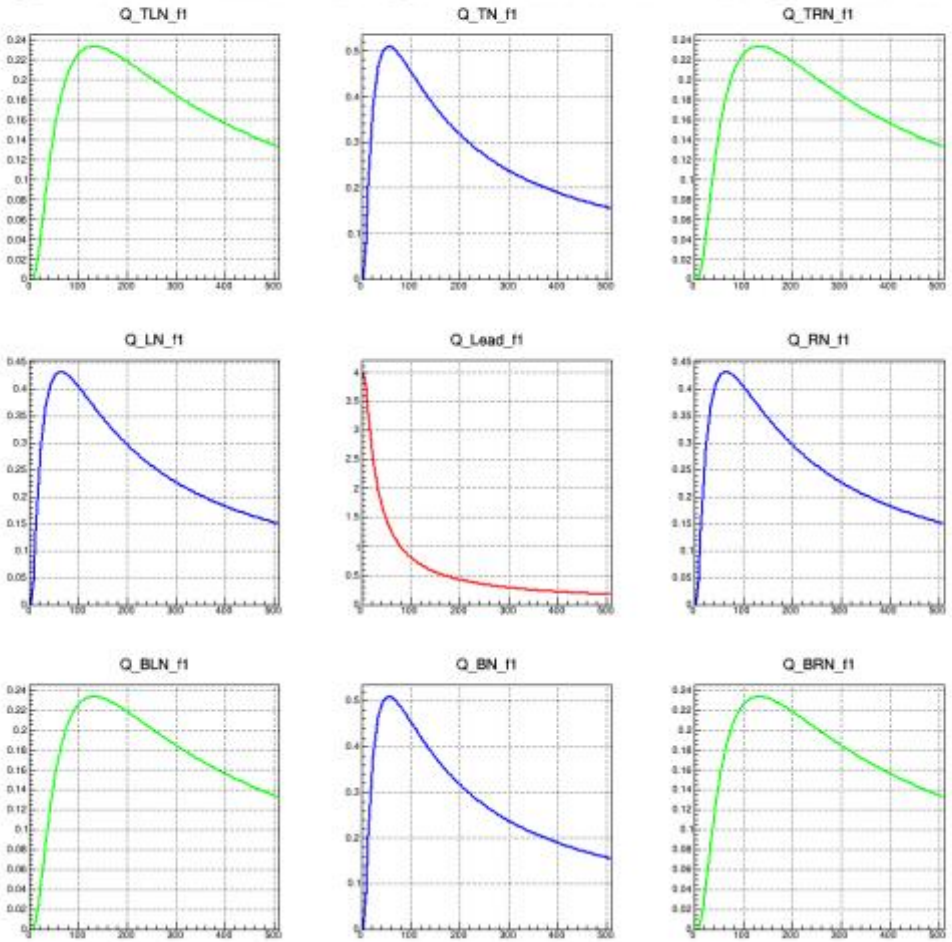

Reconstructing X-rays charge deposition

WF templates

Current induced on a pad dQpad(t) / dt
to be convoluted with
electronics transfer function R(t)
$dQ/dt \otimes R(t) = Q(t) \otimes dR(t)/dt$
$Q(t) \otimes dR(t)/dt$ is more practical

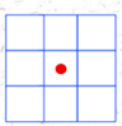

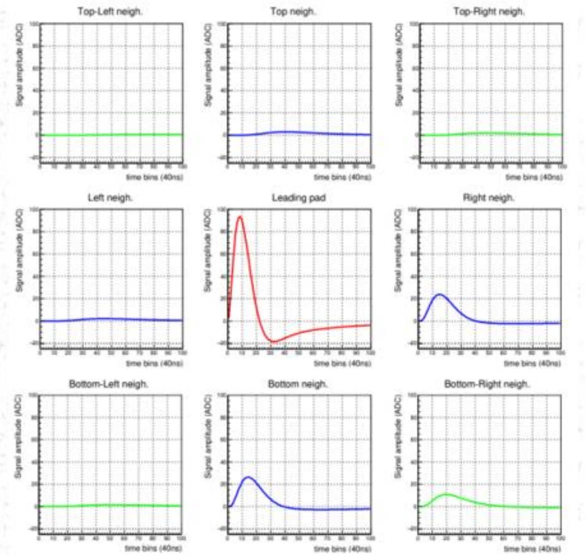

WF fit against templates

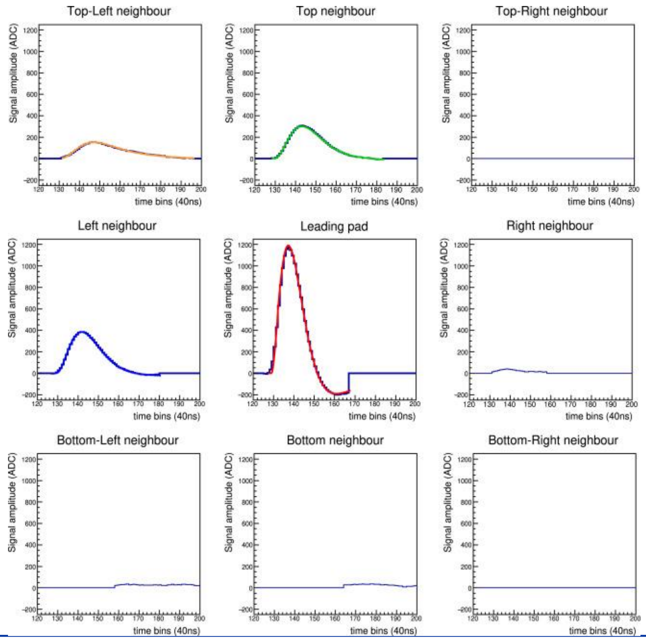

Simultaneous fit of waveforms of Leading pad + Neighboring pads to get the best 5 parameters

- x_0 } Initial charge position
- y_0
- t_0: Time of charge deposition in leading pad
- RC : Describes charge spreading
- Q_e : Total charge deposited in an event

x_H, x_L: Upper and lower bound of a pad in x-direction
y_H, y_L: Upper and lower bound of a pad in y-direction

Results about Gain and RC

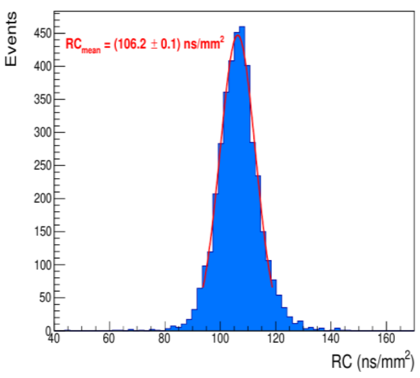

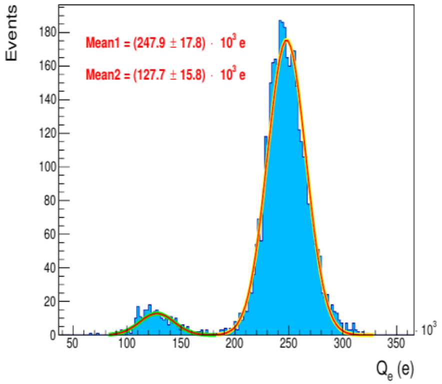

Extraction of RC and Gain maps from X-rays

Use of the method for the extraction of ERAM GAIN and RC

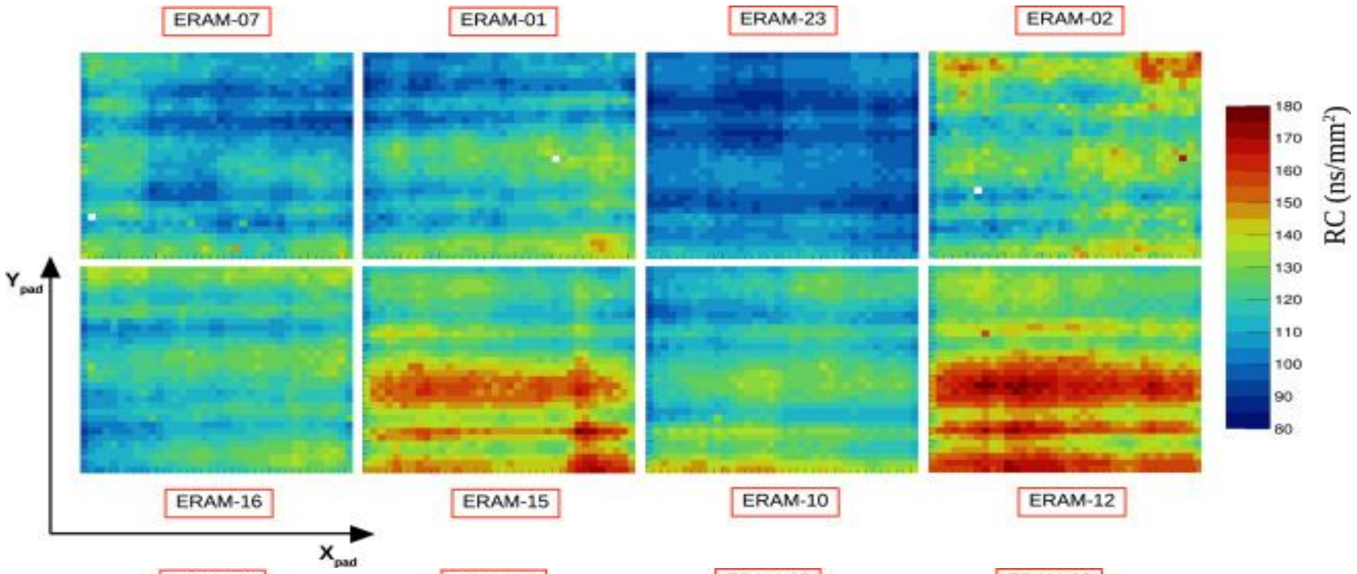

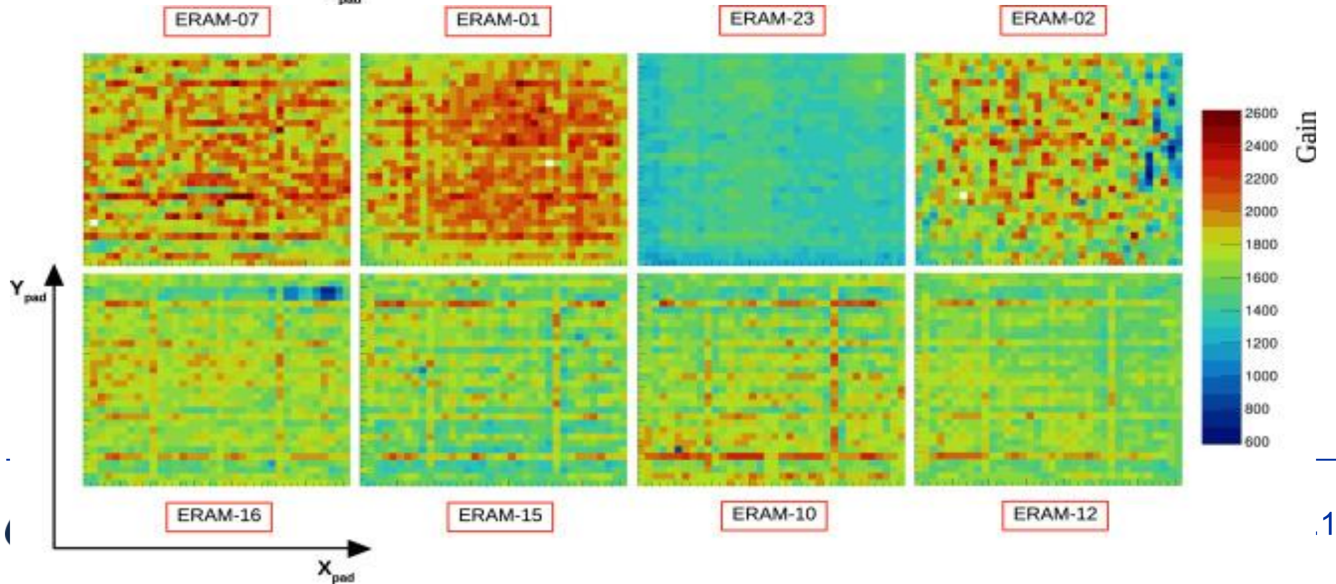

Converted X-ray impact point position is also fitted
→**accurate maps of Gain and RC**

Use for detailed studies of charge diffusion and ERAM response at fine PAD position level

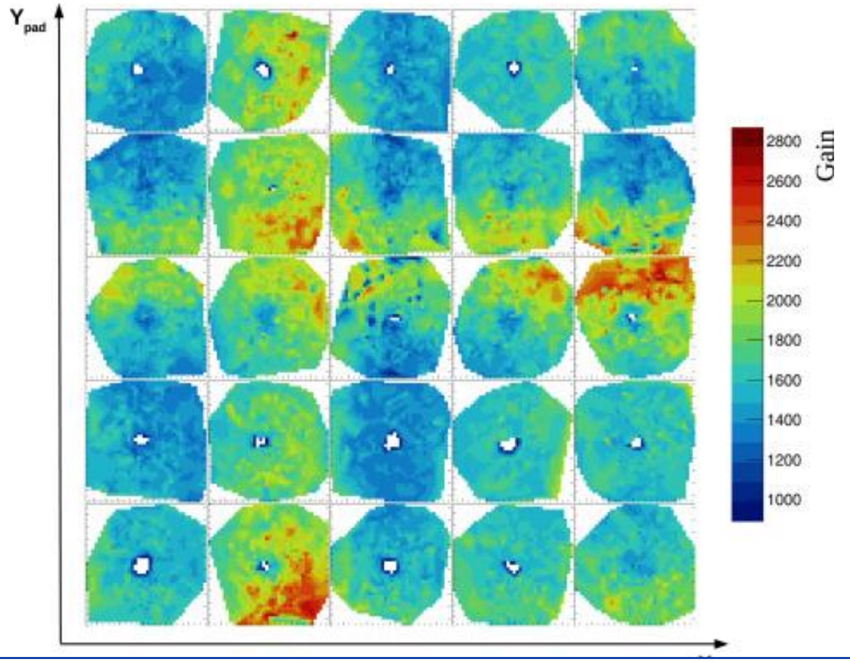

Indications are that the **lower resistivity** the **better the performance** (eg space resolution)

Reconstructing Q along tracks

For the reconstruction of the charge along the tracks two methods

- **Waveform Sum (WS)**
- **Crossed Pad (XP)**

Compare the performance of the two methods for dE/dx extraction

Reconstructing Q along tracks: Waveform Sum

Simple method based on
Sum of waveforms(t) (WS)
over pads in a cluster

OK for almost H & V tracks

Q missing for inclined tracks

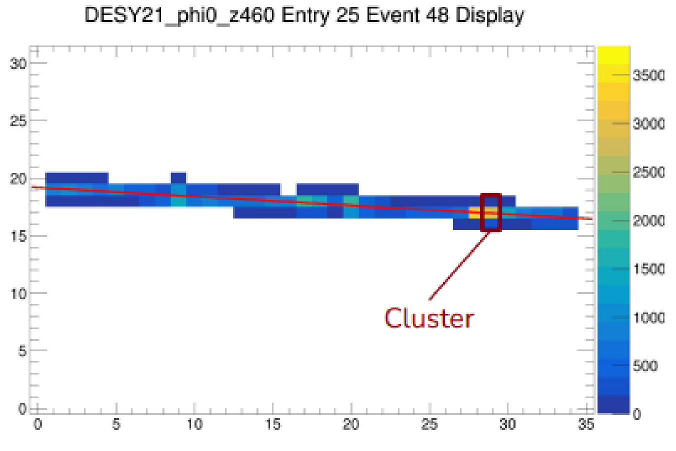

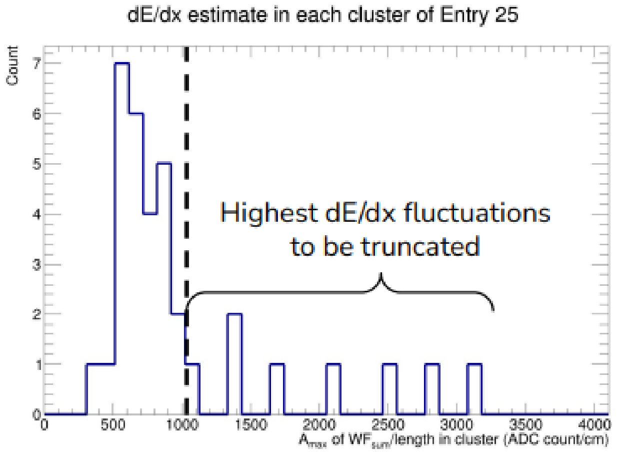

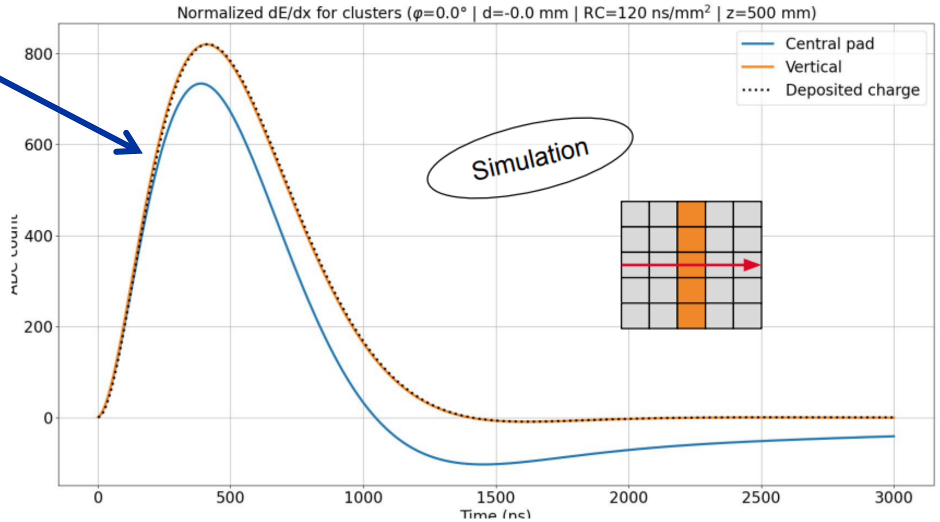

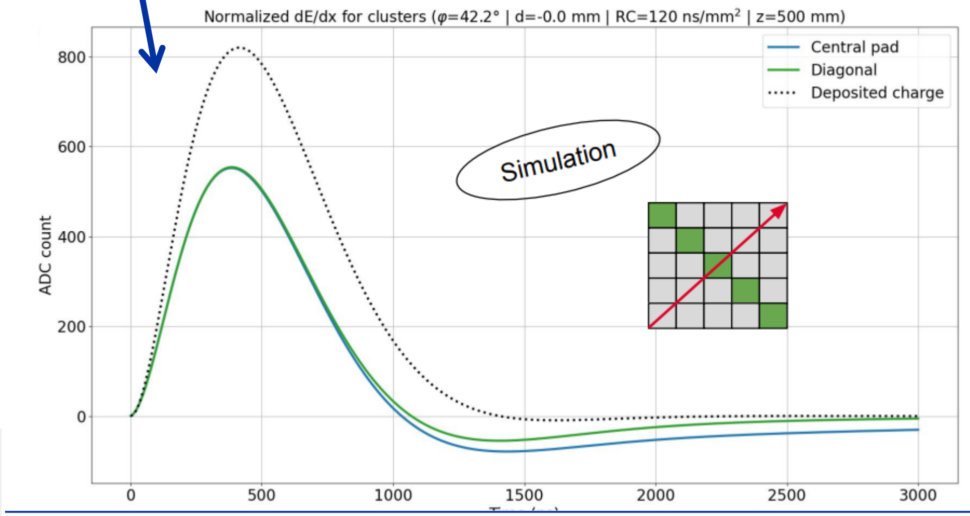

1. Clusterize the pads into slices and sum the waveforms in each slice to get dE

2. Get the track length in each cluster to get dx

3. Truncate the clusters with the highest dE/dx (top 30%) to get rid of fluctuations

just like for vertical TPCs!

4. Get the mean over remaining estimates dE/dx

Reconstructing Q along tracks: Crossed Pad (XP)

1) Reconstruct tracks and consider only pads crossed (XP) by the track (primary pads)
2) Reconstruct original (ion induced) charge (Q) for each XP (given the track parameters there) by Q = A x (Q/A) – where A is recorded amplitude on XP and rescaling ratio (Q/A) from Look Up tables (LUT)

LUTs build from model: original Q is distributed linearly over the segment for each XP so that solutions of diffusion equations can be used

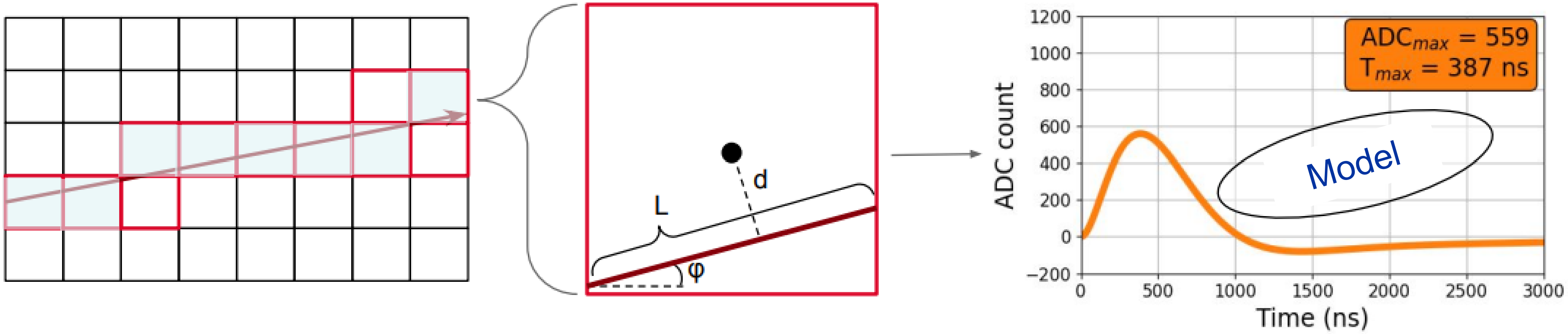

1) No clustering => potentially more accurate method because reconstructing full induced charge on primary pads
2) «dilution of ion signal» on a XP pad, due to charge spread over the pad is correctly taken into account
3) «longitudinal correlation» among adjacent XP pads, due to charge spread along track direction is accounted for
4) Fast method though based on model templates (long time is to generate LUTs …)

Reconstructing Q along tracks: Crossed Pad (XP)

Building the rescaling ratio Q/A ratio 4D LUTs via model

4D Look-Up Table (**LUT**):

- Angle **φ**: 200 steps [0°, 90°]
- Impact parameter: 200 steps [-7.3, +7.3] mm
- Drift distance: 21 steps [0, 1] m
- RC: 21 steps [50, 150] ns/mm²

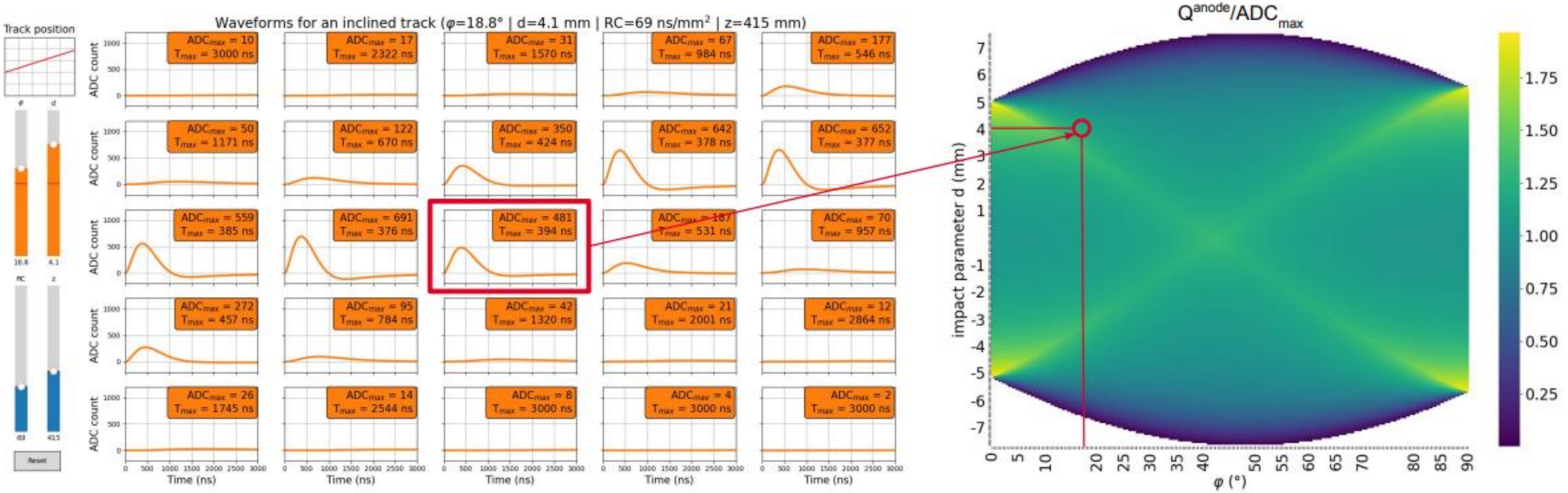

dE/dx preliminary results: (WS) and (XP) methods

dE/dx (4GeV electrons) – comparison of WF and XP methods on Test Beam data (DESY)

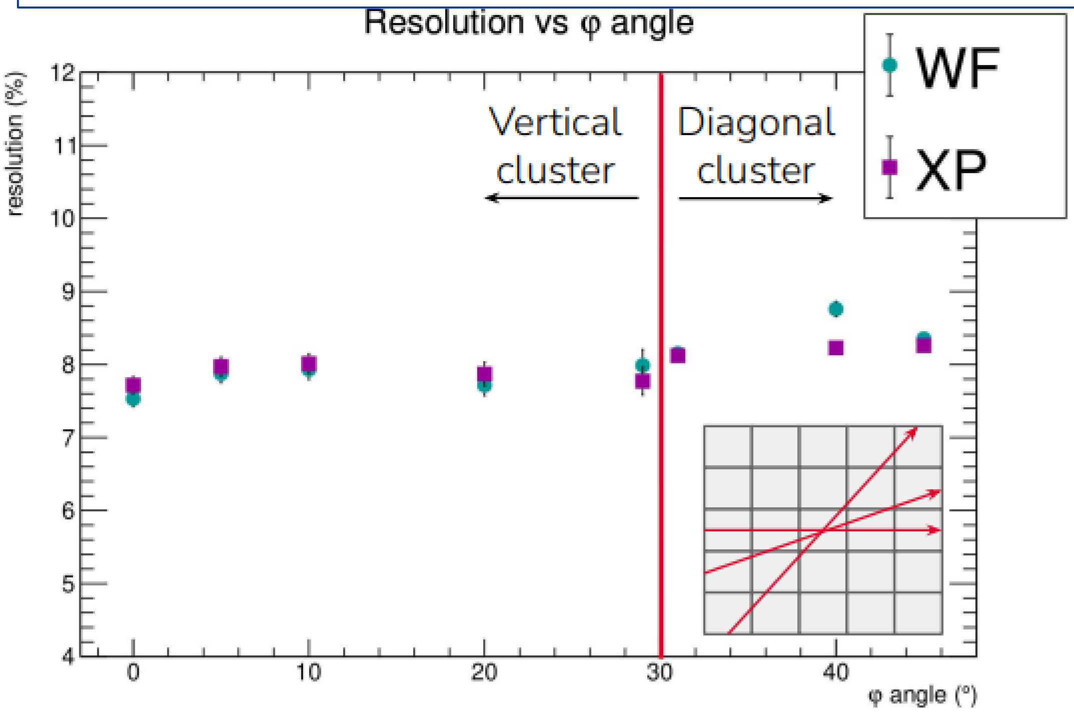

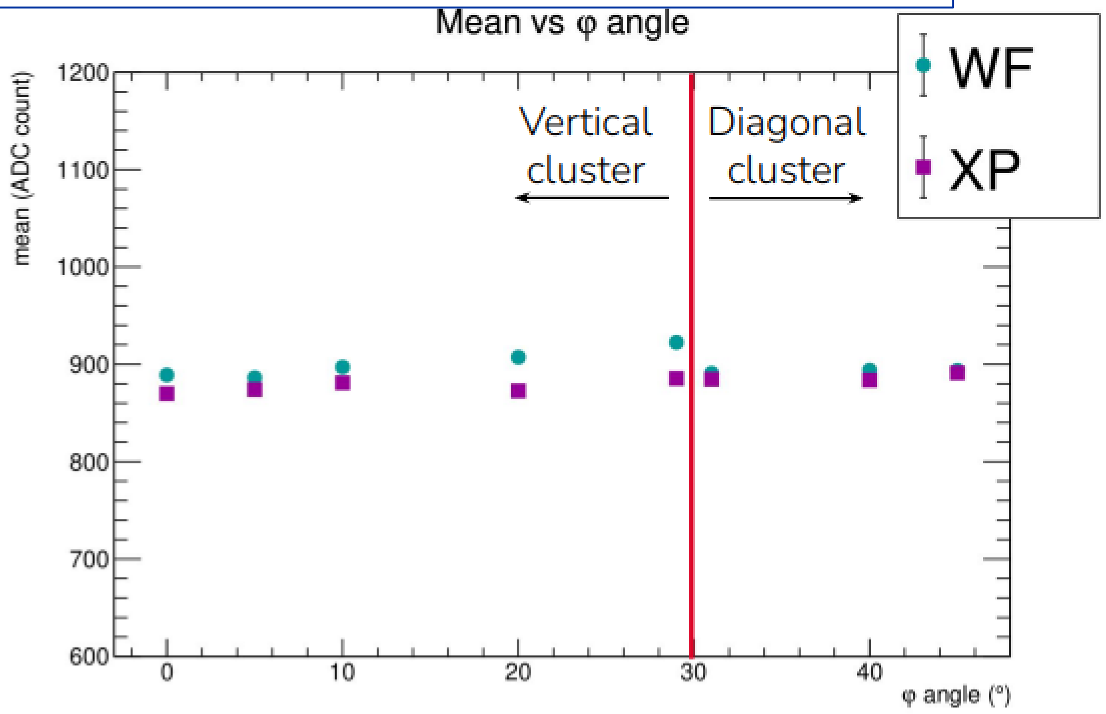

- Resolution σ/μ ~ 8% and stable
- XP gives better results at diagonal angle

- Flat distribution of dE/dx across φ for XP
- Slight sink with WF_{sum} for diagonal clusters

dE/dx preliminary results: (XP) method

dE/dx via XP method on Test Beam data (CERN PS T10)

- Resolution < 6.5% (except low stat)
- e^+ stable < 5%

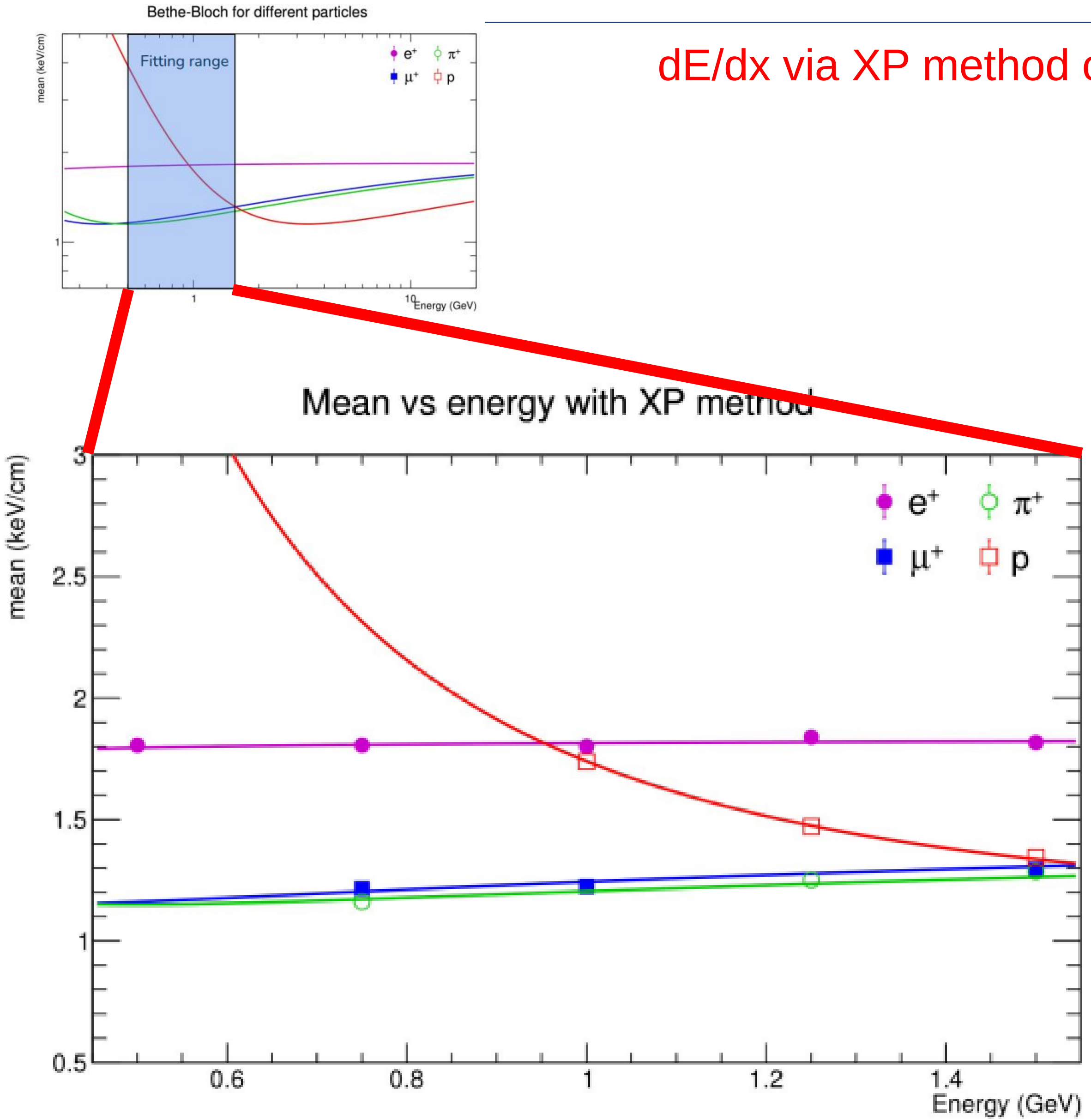

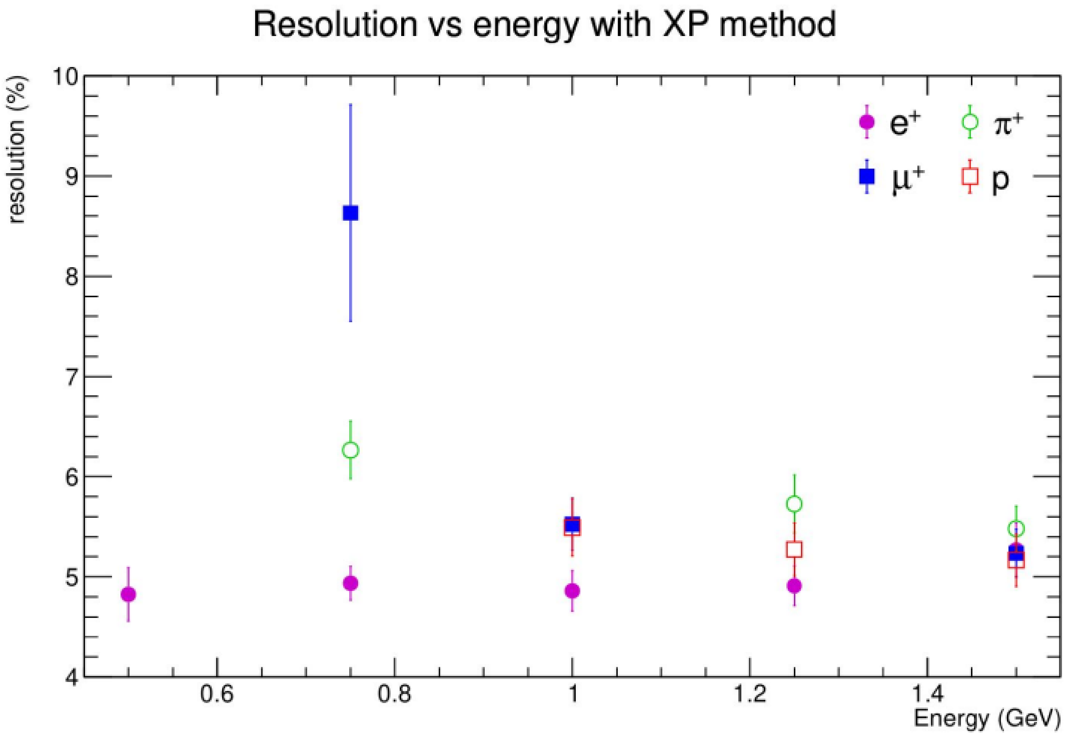

PID preliminary results (XP) vs (WS)

e/μ separation @ 1.5 GeV – Test Beam data (CERN PS T10)

Short tracks (~40cm)

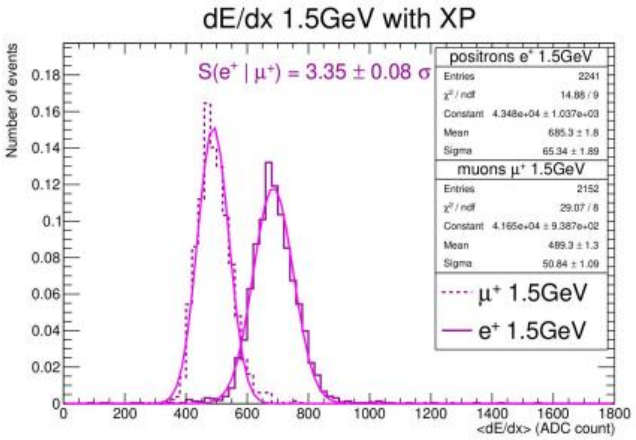

Separation power

	WF	XP
μ^+-π^+	0.01 (0.03)	0.08 (0.03)
p-π^+	0.42 (0.03)	0.45 (0.03)
p-μ^+	0.4 (0.03)	0.37 (0.03)
e^+-π^+	3.62 (0.07)	3.42 (0.07)
e^+-μ^+	3.58 (0.07)	3.34 (0.07)
e^+-p	3.11 (0.06)	2.91 (0.07)

$$S(e^+,\mu^+) = \frac{|\mu_{e^+} - \mu_{\mu^+}|}{\sqrt{\left(\sigma^2_{e^+} + \sigma^2_{\mu^+}\right)/2}}$$

- μ^+ & e^+ split by more than 3σ

Long tracks (~160cm)

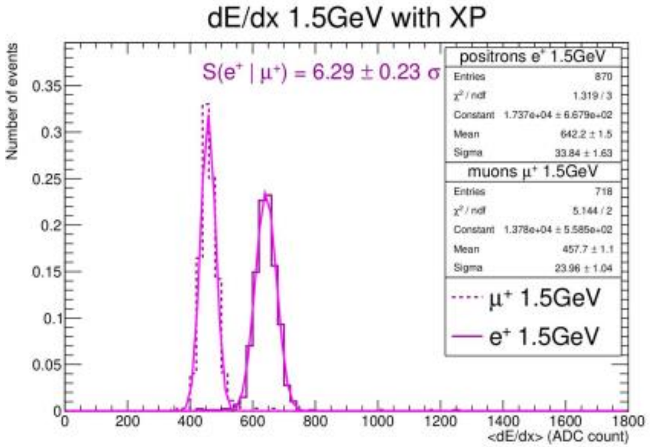

Separation power

	WF	XP
μ^+-π^+	0.1 (0.06)	0.13 (0.06)
p-π^+	0.86 (0.06)	0.84 (0.07)
p-μ^+	0.74 (0.06)	0.72 (0.07)
e^+-π^+	6.91 (0.2)	6.32 (0.22)
e^+-μ^+	6.66 (0.2)	6.29 (0.23)
e^+-p	5.8 (0.16)	5.64 (0.21)

$$S(e^+,\mu^+) = \frac{|\mu_{e^+} - \mu_{\mu^+}|}{\sqrt{\left(\sigma^2_{e^+} + \sigma^2_{\mu^+}\right)/2}}$$

- μ^+ & e^+ split by more than 6σ

Reconstructing tracks

For the reconstruction of the tracks

Log(Q) methods

Full Waveform fit Method

Reconstructing tracks, trajectory fitting: an example

LogQ Method based on clustering & Log[Qprimary /Qsecondary]

- logQ method to reconstruct position in each cluster
- Helix fit performed on those reconstructed positions

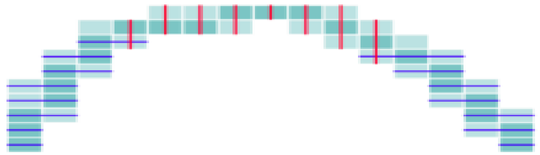

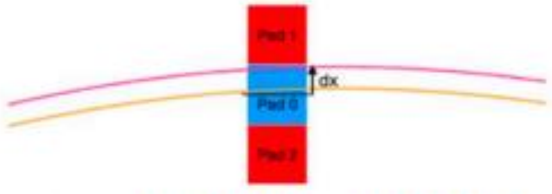

Full Waveform fit Method – based on model & no clustering

1) Use all the pads associated to a track (Q_{max} values) to define a (v,u) local frame

2) Distribute "arbitrary" point charges along v axis separated by Δv (5mm)
the Q per each point is a free parameter

3) Diffusion model to predict the waveform generated by point charges in surrounding pads

4) Move all points along the u axis to minimize the chi-square difference between measured waveforms and templates → extract the coordinates

$$\chi^2 = \sum_{i(pad)} \sum_{j(timebin)} \frac{(Q_{i,j}^{obs} - Q_{i,j}^{Dixit})^2}{\sigma_{i,j}^2}$$

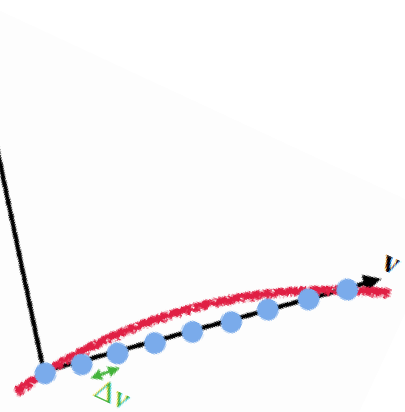

Spatial resolution: the importance of the QA

Top HAT was equipped with ERAMs with larger RC variation w.r.t. Bottom

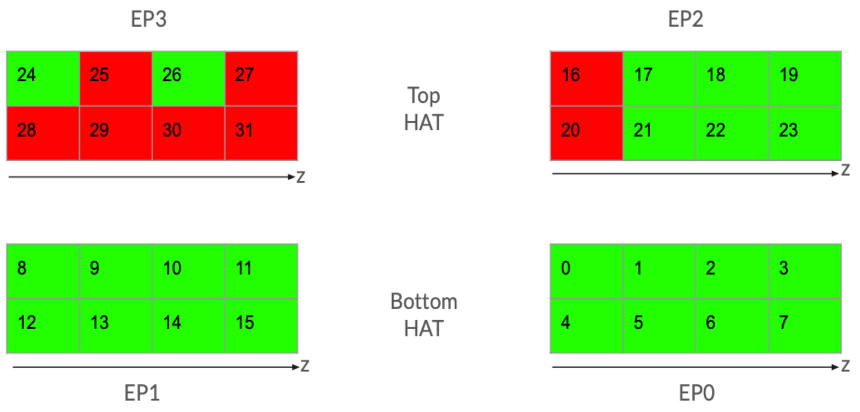

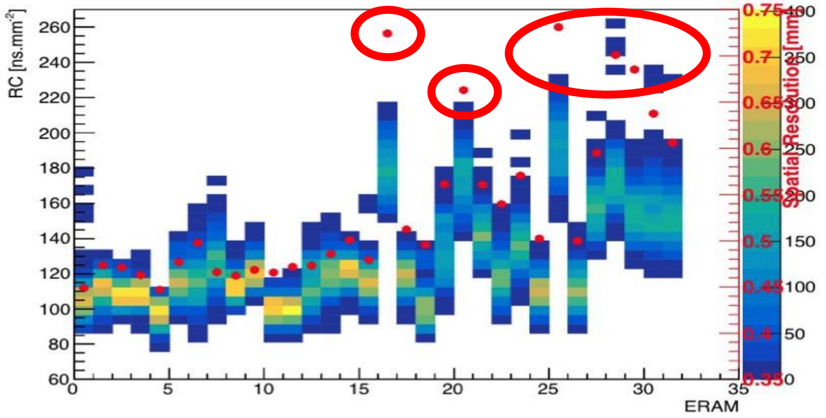

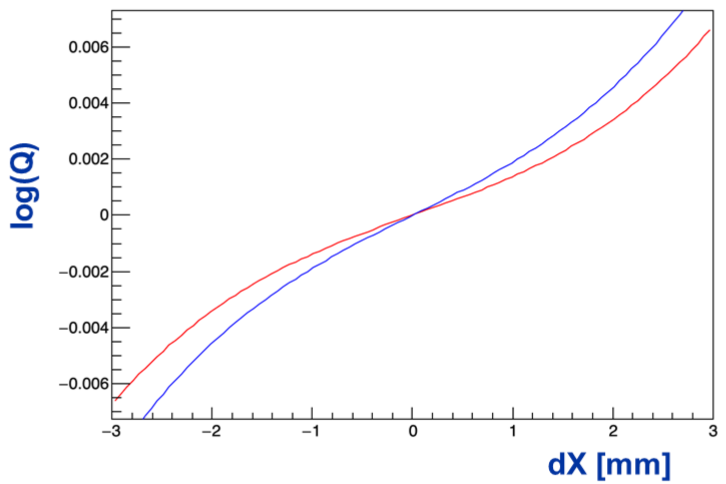

High RC → less charge spreading "flatter curve"

Low RC → more charge spreading "steeper curve"

dX: distance from the center of the cluster and the real position

Non negligible RC variation among the same Endplate of the TPC

Need to tune the log(Q) parametrization → ERAM dependent….

Spatial resolution after reparameterization

Work in progress, preliminary

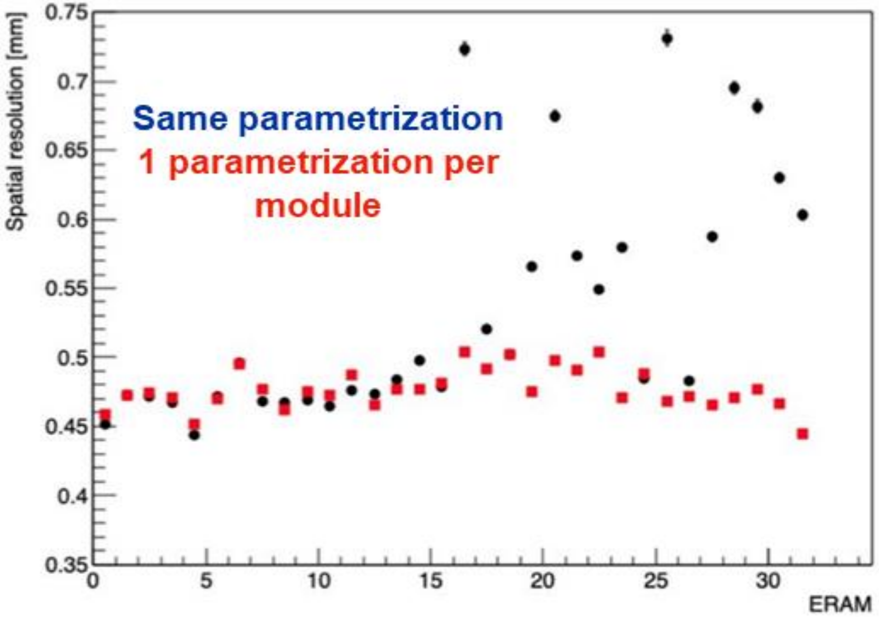

With **the new parametrization** all modules have similar performances in terms of spatial resolution

σ ≈ 0.45 mm

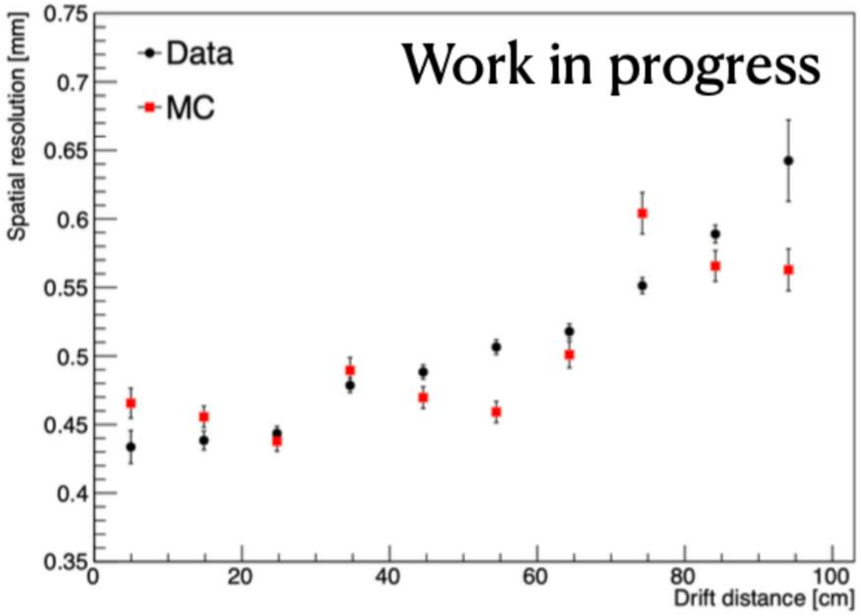

Reconstructing tracks: momentum resolution

ϕ = 5.7°

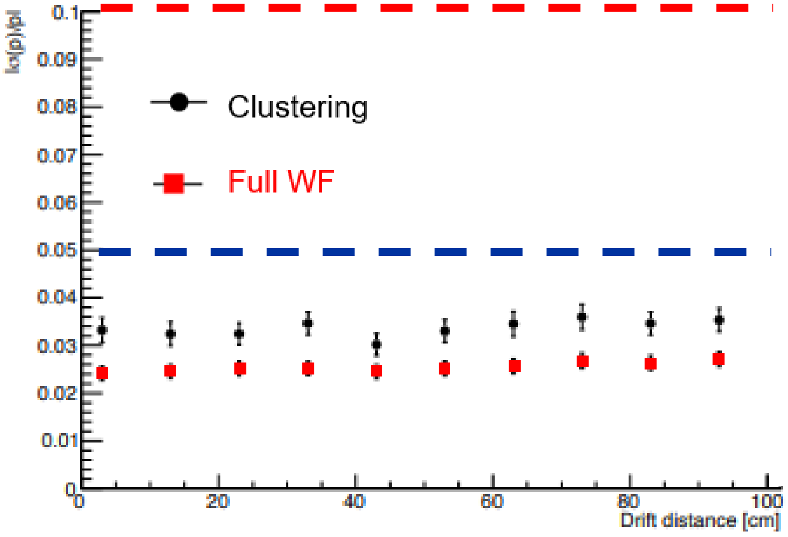

ϕ = 45°

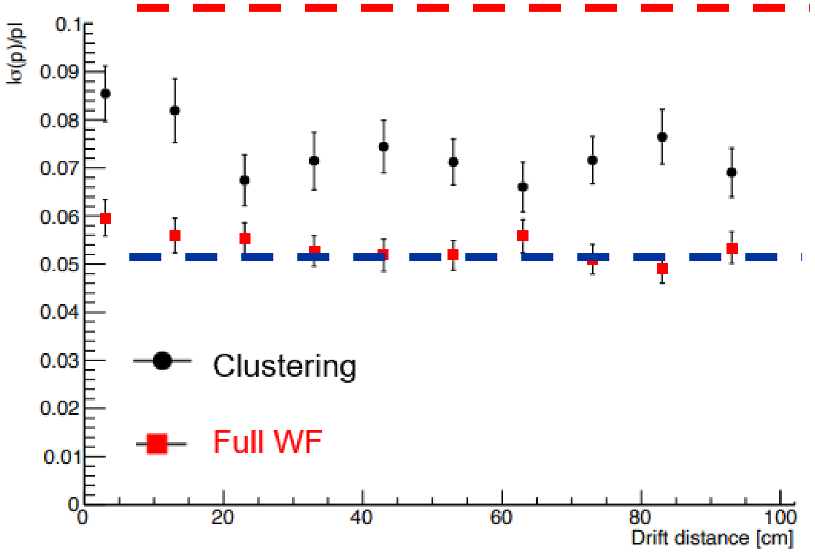

ϕ = 84.3°

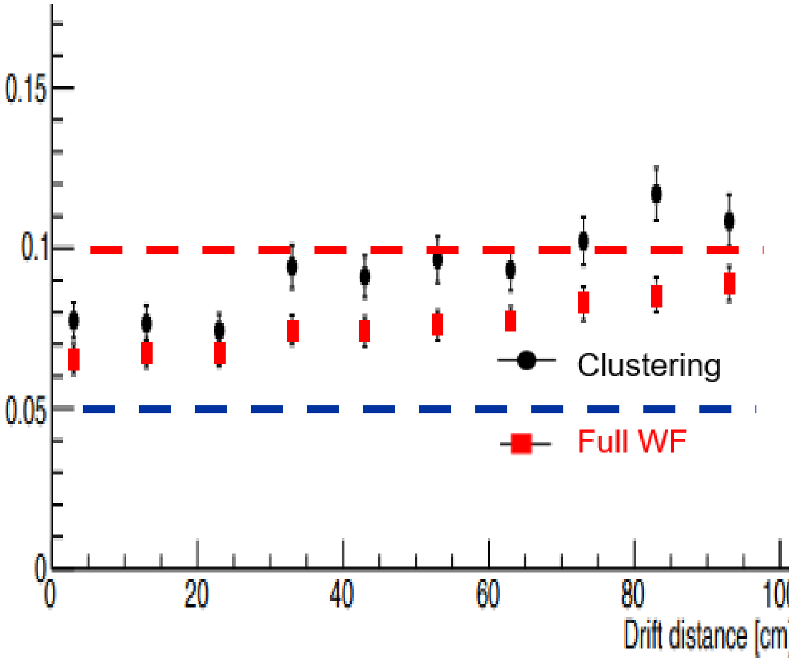

σ_p/p momentum resolution as a function of track drift distance: simulated 700 MeV/c muons

Event display, full ND280 detector!

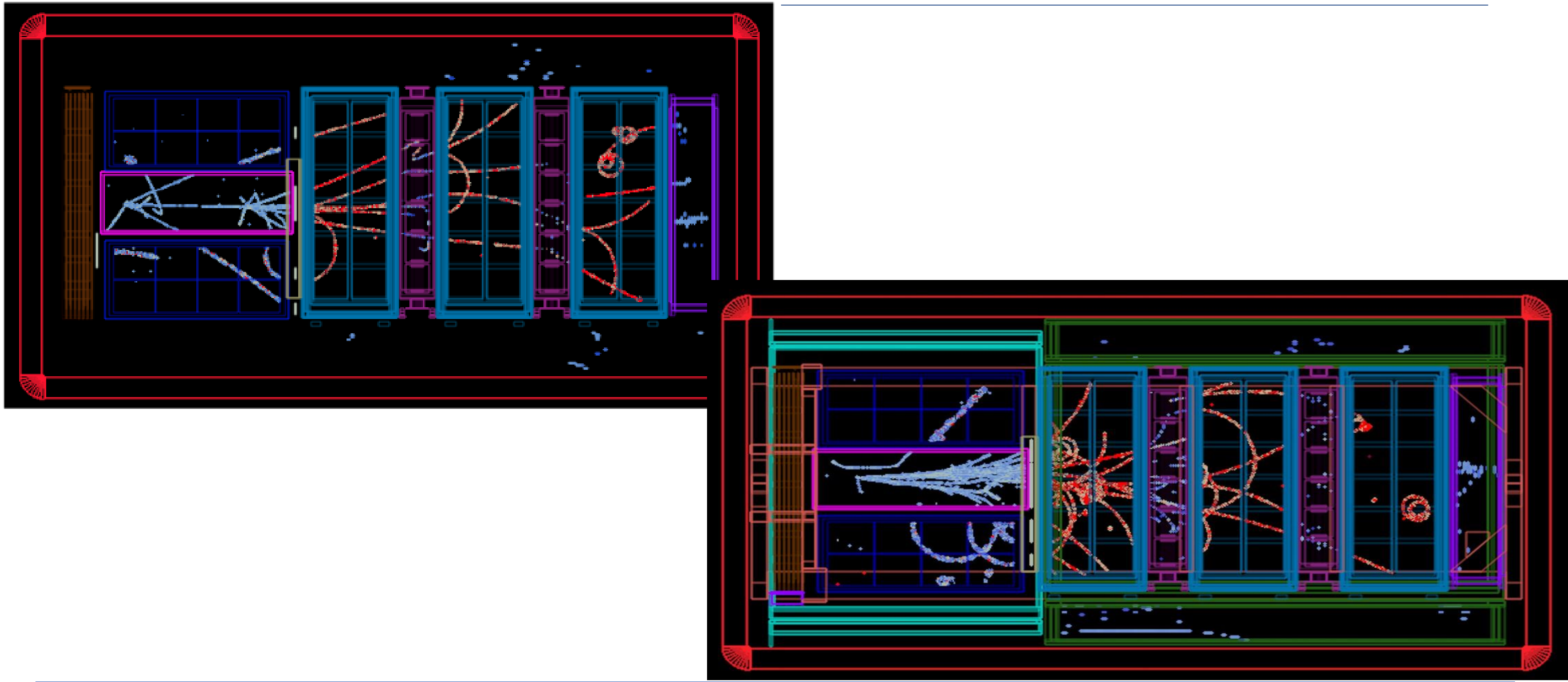

Conclusions

Two new TPCs have been just installed in ND280 at JPARC

- Very stable operations in commissioning and technical runs
- Firs Neutrino Data taking just completed, restarting now !

Resistive MM with encapsulated anode **ERAM**

- First time use of an encapsulated resistive Micromegas in a High Energy running experiment
- Low resistivity & optimal charge spread & no sparks effects
- Series production allowed several detailed studies
- The ERAM technology is complex and delicate to produce as are all the resistive MPGDs. The expertise and excellent partnership with the CERN/PCB workshop enabled a high yield (~80%) of high-quality production
- New algorithms for square pads exploiting detailed response model under development
- Detector performance, still preliminary but very promising!

Conclusions

Two new TPCs have been just installed in ND280 at JPARC

- Very stable operations in commissioning and technical runs
- Firs Neutrino Data taking just completed, restarting now !

Thanks!

Resistive MM with encapsulated anode **ERAM**

- First time use of an encapsulated resistive Micromegas in in a High Energy running experiment
- Low resistivity & optimal charge spread & no sparks effects
- Series production allowed several detailed studies
- The ERAM technology is complex and delicate to produce as are all the resistive MPGDs. The expertise and excellent partnership with the CERN/PCB workshop enabled a high yield (~80%) of high-quality production
- New algorithms for square pads exploiting detailed response model under development
- Detector performance, still preliminary but very promising!

Spare

Just in Case

- The goal of Long Baseline neutrino experiments:

✓ Remaining problems: CP symmetry, Mass ordering, Octant of θ_{23}

✓ Precise measurements of $\theta_{23}, |\Delta m^2{}_{31}| \, (\sim |\Delta m^2{}_{32}|)$

Muon neutrino disappearance ($\nu_\mu \to \nu_\mu$) :

$$P(\nu_\mu \to \nu_\mu) \approx 1 - (\cos^2 \theta_{13} \sin^2 2\theta_{23}) \sin^2\left(\Delta m^2_{32} \frac{L}{4E_\nu}\right)$$

Sensitive to:

$\theta_{23}, \left|\Delta m^2{}_{31}\right| \left(\sim \left|\Delta m^2{}_{32}\right| \right)$

Electron neutrino appearance ($\nu_\mu \to \nu_e$) :

$$P(\nu_\mu \to \nu_e) \approx \sin^2 \theta_{23} \sin^2 2\theta_{13} \sin^2\left(\frac{\Delta m^2_{32} L}{4E_\nu}\right)\left(1 + \frac{2a}{\Delta m^2_{31}}(1 - 2\sin^2\theta_{13})\right)$$

$$- \sin 2\theta_{12} \sin 2\theta_{23} \sin 2\theta_{13} \cos\theta_{13} \sin\delta \sin^2\left(\frac{\Delta m^2_{32} L}{4E_\nu}\right) \sin\left(\frac{\Delta m^2_{21} L}{4E_\nu}\right)$$

Sensitive to:

$\theta_{13}, \delta_{CP}, \theta_{23}$, and

Mass ordering $\Delta m^2{}_{31}$

- $P(\bar{\nu}_\mu \to \bar{\nu}_e)$: **δ turns into – δ and a to -a ("a" matter effect term)**

Reconstructing tracks: trajectory fitting

LogQ Method based on clustering & Log[Qprimary /Qsecondary]

- logQ method to reconstruct position in each cluster
- Helix fit performed on those reconstructed positions

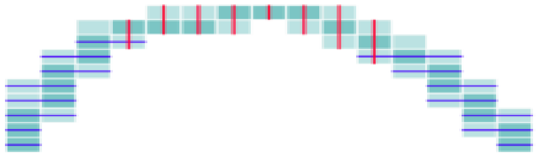

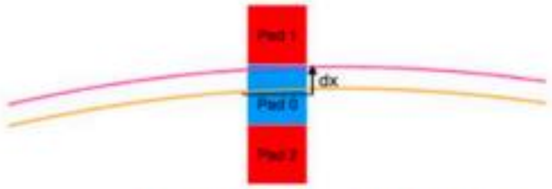

$$dx = f(\log(Q_1/Q_0) \text{ or } \log(Q_2/Q_1))$$

Full Waveform fit Method – based on model & no clustering

1) Use all the pads associated to a track (Qmax values) to define a (v,u) local frame

2) Distribute “arbitrary” point charges along v axis separated by Δv (5mm)
the Q per each point is a free parameter

3) Diffusion model to predict the waveform generated by point charges in surrounding pads

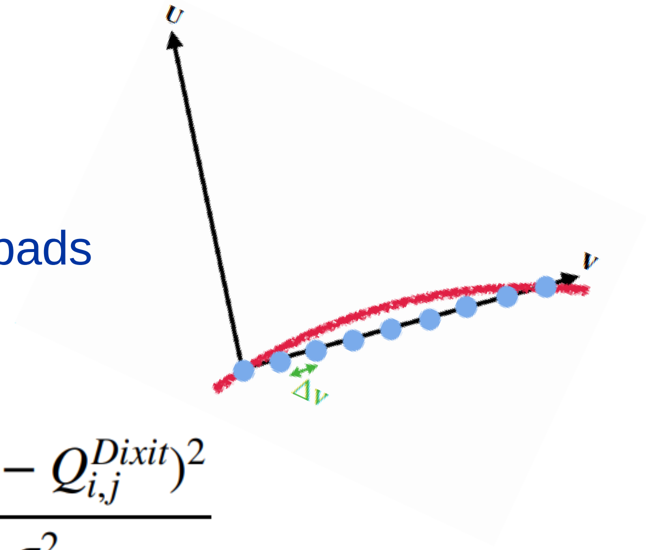

4) Move all points along the u axis to minimize the chi-square difference between measured waveforms and templates
RungeKutta method to fit (u0, du/dv, q/p, t_0, dv/dt)

$$\chi^2 = \sum_{i(pad)} \sum_{j(timebin)} \frac{(Q_{i,j}^{obs} - Q_{i,j}^{Dixit})^2}{\sigma_{i,j}^2}$$

GAIN, RC

Figure 28: Comparison of gain extracted using the waveform sum and simultaneous fit methods for all the analyzed ERAMs.

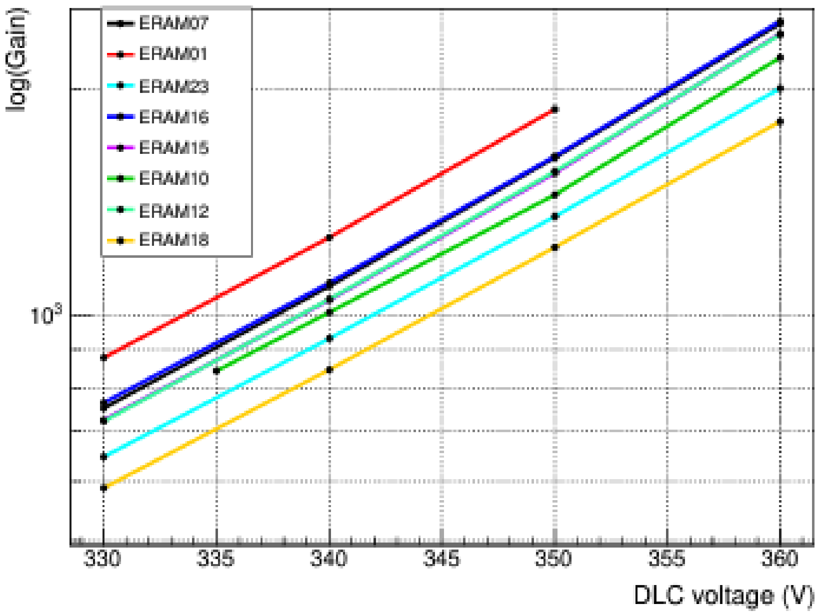

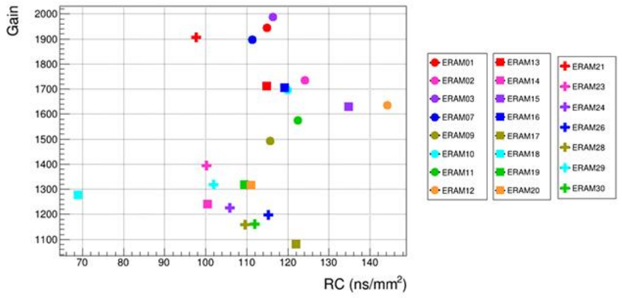

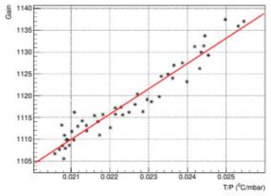

Figure 37: Effect of T/P on the gain of one pad. The lowest value of (T,P) recorded during the scan was (19.8 °C, 959.5 mbar) and the highest value was (24.5 °C, 963.7 mbar).

Figure 29: Dependence of mean *RC* on mean gain of all the analyzed ERAMs.

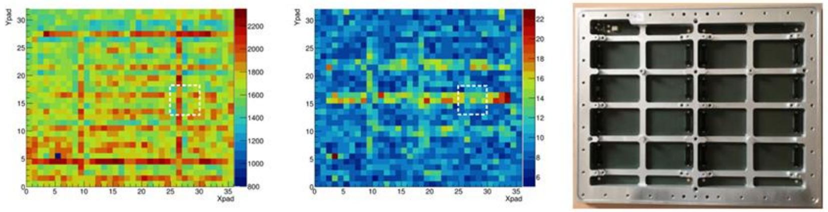

Figure 30: Left: 2D map of the relative gain in ADC of the ERAM-10 module; Middle: 2D map of the energy resolution in % of the ERAM-10 module; Right: PCB top layer: the grey area are 20-35 μm thick copper + 50 μm soldermask while the cross hatched area is made of copper mesh only.

Readout PCB	Original T2K-TPC	HA-TPC V1 + ARC FEE	HA-TPC V2 + final FEE V1	HA-TPC V2 + final FEE V2
Size	34 × 36 cm²	34 × 42 cm²	34 × 42 cm²	34 × 42 cm²
Pads	48 × 36 cm²	32 × 36 cm²	32 × 36 cm²	32 × 36 cm²
Pad size	6,85 × 9,65 mm²	10,09 × 11,18 mm²	10,09 × 11,18 mm²	10,09 × 11,18 mm²
Number of pads	1728	1152	1152	1152

Detailed R measurement (dedicated probe)

A dedicated probe has been built to perform a fine measurement of the surface resistivity.

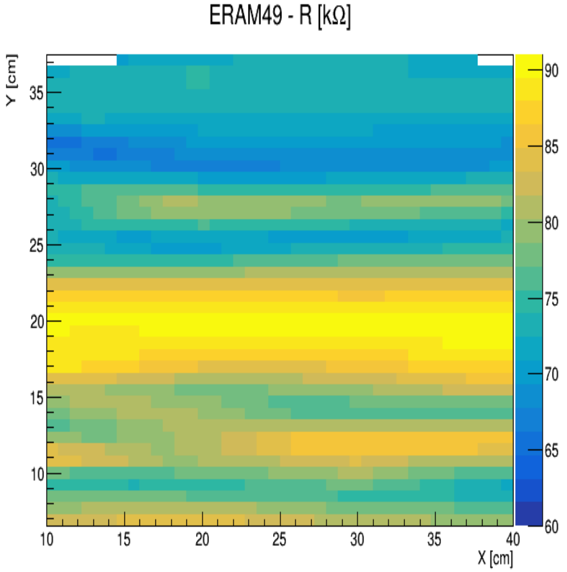

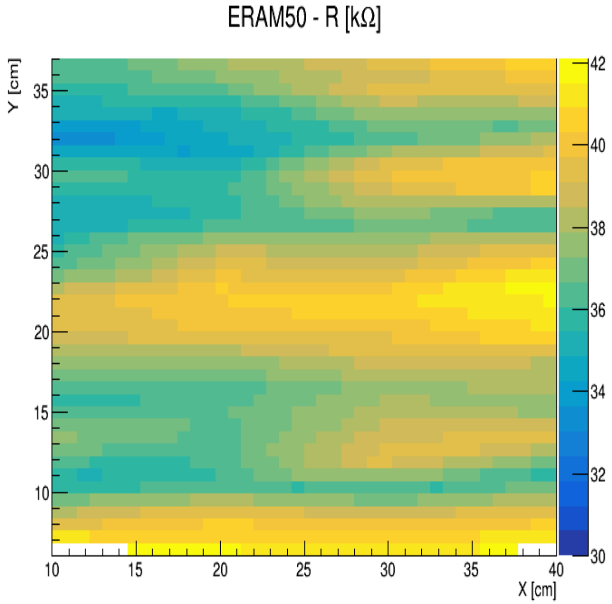

Will be soon complemented with the comparison with the data extracted from X-ray analysis

R **inhomogeneities** in the sputtering are clearly visible in the direction perpendicular to the drum rotation axis.

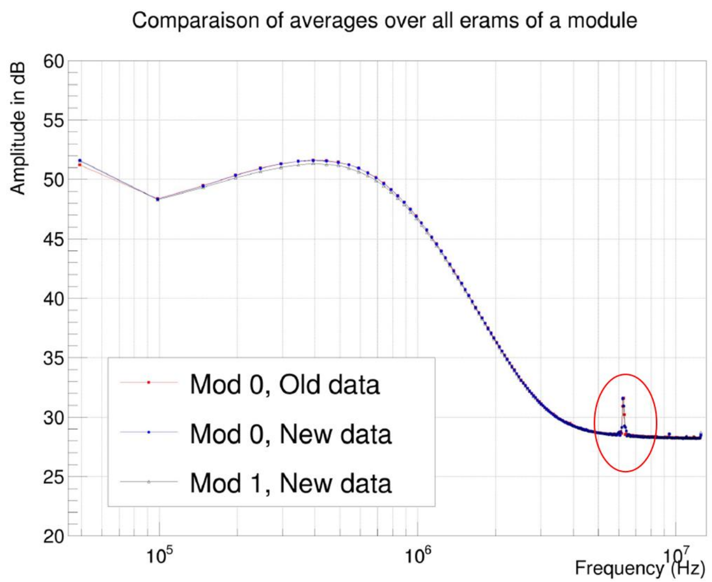

- Here are the averages over a full module (excluding Eram 27 for module 0)
- The old and new data for the module 0 are identical (but at very low frequency)
- The modules 0 and 1 are very, very close
  Module 1 is slightly less noisy

20/06/24 S. Hassani, J.F.Laporte 6

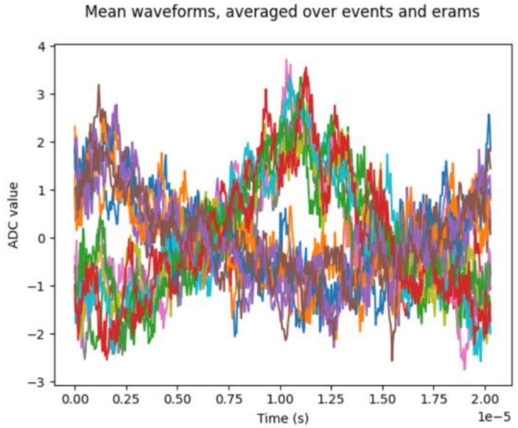

Figure 5.3: Mean waveforms of few pads in the ERAMs, averages over all events

As is clear from the Fig. 5.3, there is two typologies of the mean waveform.
It has been shown that these two types correspond to two populations of pads positioned on the ERAMs as shown on Fig. 5.4.

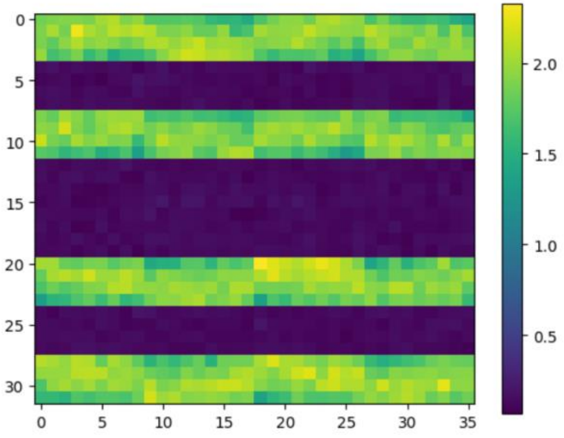

- The term 6.1, identified as the low-frequency fitting of the deterministic contribution (Section 5.3.4, Fig. 5.6). The form of the equation ensures that the mean is 0. Additionally, A_{max} controls the maximum amplitude, and t_{max} determines its position.
- The term 6.2, represents the high-frequency adjustment of the deterministic contribution (Section 5.3.5, Fig. 5.6) is represented by a simple $cos(f_n)$ with a frequency of $\frac{f_s}{4}$. The amplitude is adjusted using the parameter A.

$$S(t_b) = A_{\max}\left(1 - \frac{\pi}{2}\left|\sin\left(\frac{\pi(t_b - t_{\max})}{t_w}\right)\right|\right) \quad (6.1)$$

$$+ A\cos\left(2\pi\frac{f_s}{4}t_b + \pi\right) \quad (6.2)$$

$$+ \sum_f I(f)\,|H(i2\pi f)|\cos(\omega t_b + \phi_H + \phi_{\boldsymbol{R}}) \quad (6.3)$$

$$+ \mathcal{N}(0,\sigma) \quad (6.4)$$

- The term 6.3, describe the AFTER chip contribution (Section 5.2), which is the response of the electronics to the random current:

$$\mathrm{I}(t) = \sum_f I(f)\cos(\omega t + \phi_{\boldsymbol{R}})$$

because for a signal such as :

$$\mathrm{I}(t) = I_0\cos(\omega t)$$

the electronic response is by definition of the Transfer Function:

$$S_{elx}(t) = I_0\,|H(i2\pi f)|\cos(\omega t + \phi_{\boldsymbol{H}})$$

where $|H(s = i2\pi f)$ and Φ_H are the norm and the phase of the transfer function (cf Fig. 3.2).

- The term 6.4, we refer to the white noise (Section 5.4), which is represented by Gaussian distribution added for each time bin.

Conclusions

Two new TPCs have been just installed in ND280 at JPARC

- Very stable operations in commissioning and technical runs
- Firs Neutrino Data taking just completed, restarting in October 2024

Field cages

- High ratio active/passive volume
- Highly effective insulation & E field uniformity
- Composite material technology exploited at the limit of the technology

Resistive MM with encapsulated anode

- Low resistivity & optimal charge spread & no sparks effects
- Series production allowed several detailed studies
- The ERAM technology is complex and delicate to produce as are all the resistive MPGDs. The expertise and excellent partnership with the CERN/PCB workshop enabled a high yield (~80%) of high-quality production
- New algorithms for square pads exploiting detailed response model under development

HATPC: features, challenges, constrains and solutions

Mechanics and Electric Field uniformity

- Min dead space & max active volume in the dipole magnet
  →Rectangular shape & thinnest walls & field shaping electrodes incorporated into the walls
- Electric field uniformity better than 10^{-3} @1cm from walls
  → Mechanical accuracy: inner surfaces planarity & parallelism ~ O(0.2mm/m)
  → Shaping Electrode design: Field and Mirror copper strip layers on two sides of a Kapton foil
- Low material budget walls
  → lightweight & lowest Z & robust (self supporting)

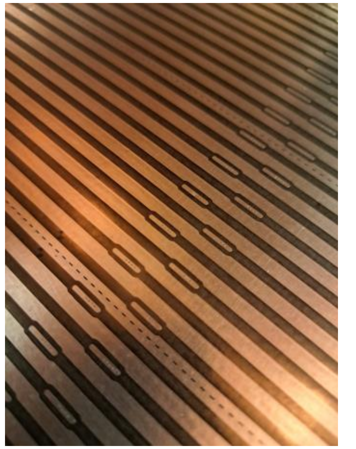

Electrical insulation Constrains

- HV insulation mantle R > 1TOhm and volume resistivity, HV
  →geometry: several cm paths for charge from -HV strips to GND shielding (cathode flanges)
  →insulating materials: very high resistivity & dielectric strength

HATPC: features, challenges, constrains and solutions

Building process: hand lay-up of composite materials on a Mould & polymerization in autoclave at high Pressure

- Autoclave dimensions
  → Field Cage comprising two halves (symmetrical flanges at central cathode position)
- Hand layup & large dimensions
  → several hours per process step → very long pot life for epoxy resin
- Mechanical accuracy of geometry → resin curing at low T < O(40ºC)

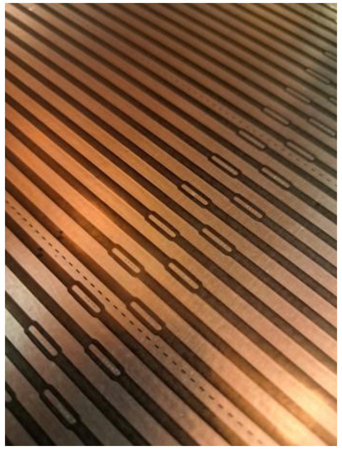

Materials of choice

- lamination materials: Aramid polymers for peels (Twaron) and for honeycomb (Nomex paper)
- epoxy resin limited choice: Resoltech 1054 combined with quality control against contaminants (moisture, …)
- high insulation layers: Kapton
- box skeleton material: high quality laminated G10

The ND280 experiment: High Angle TPC highlights

- Field Cage (FC)
  - Assembly and layout
  - Production
  - Characterization and Quality Assessment
    - Mechanical
    - Electrical

- Encapsulated Resistive Anode Micromegas (ERAMS)
  - Production of 50 sensors
  - Characterization
  - Detector response, signal and impact on reconstruction

- Impact on HATPC performance

Field Cage: walls stack up layout

Inner surface

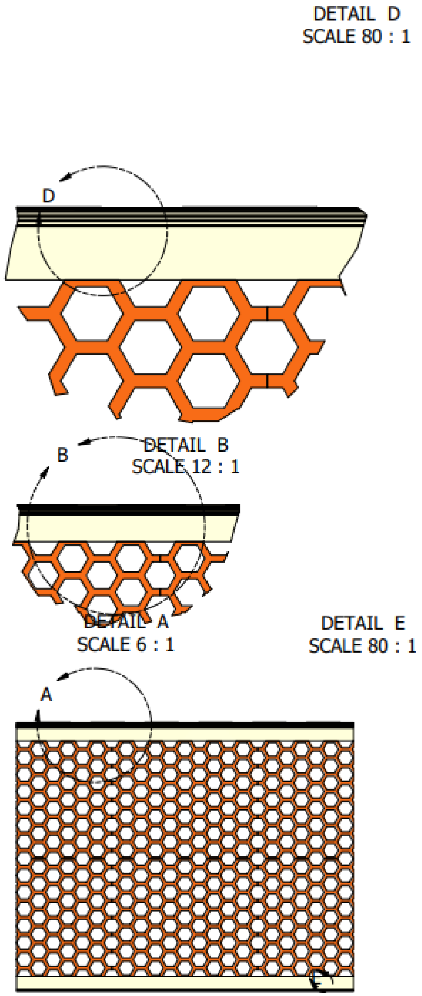

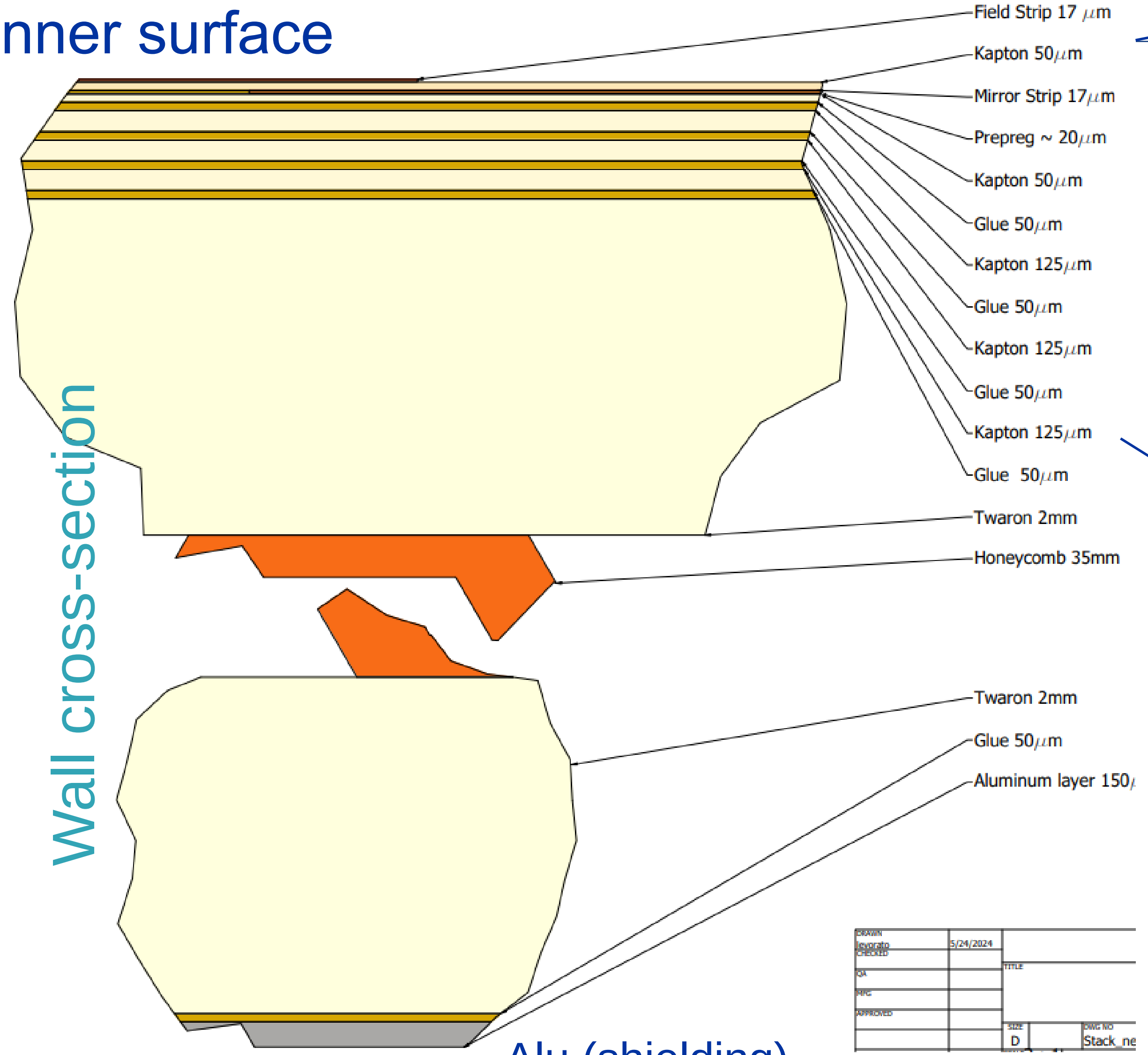

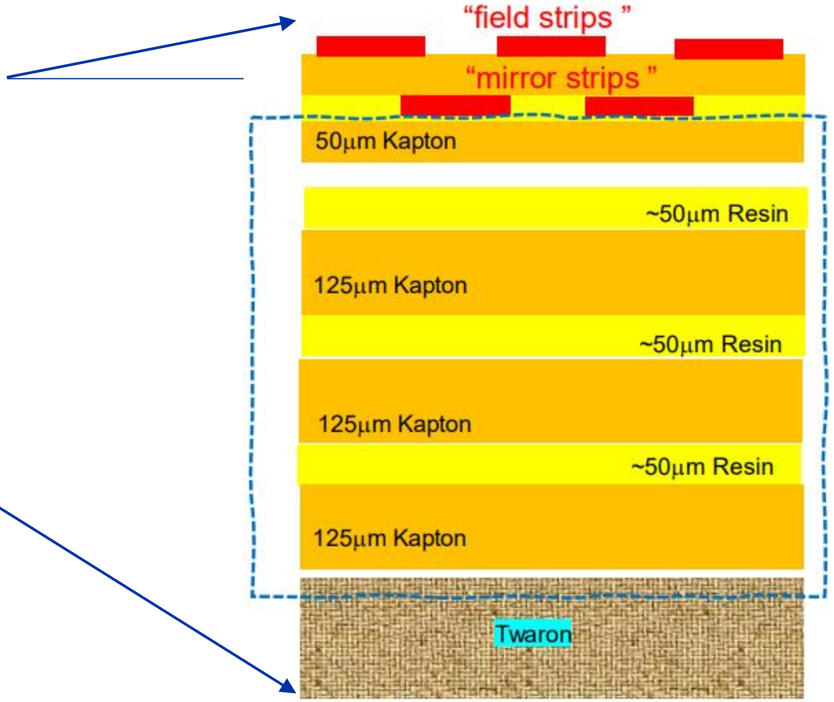

Wall thickness
~ 40 mm
~ 2% radiation length

Alu (shielding)

Outer surface

Field cage mechanical details

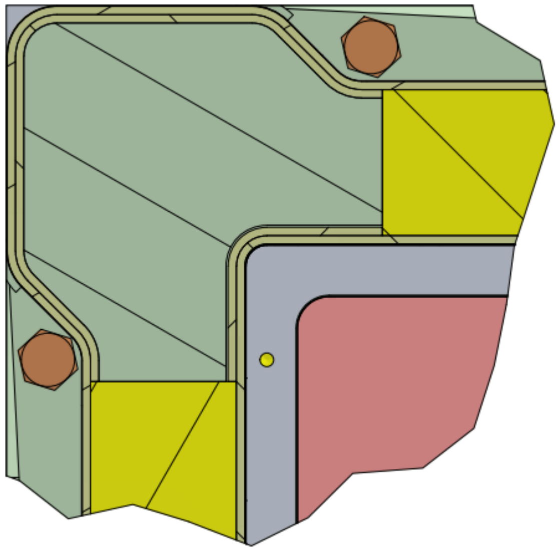

DETAIL C
SCALE 2 : 1

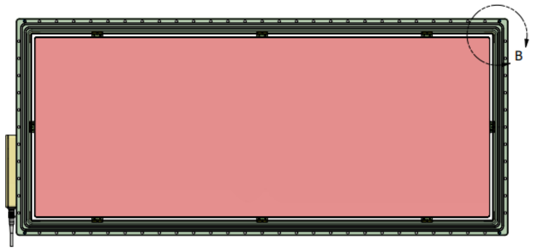

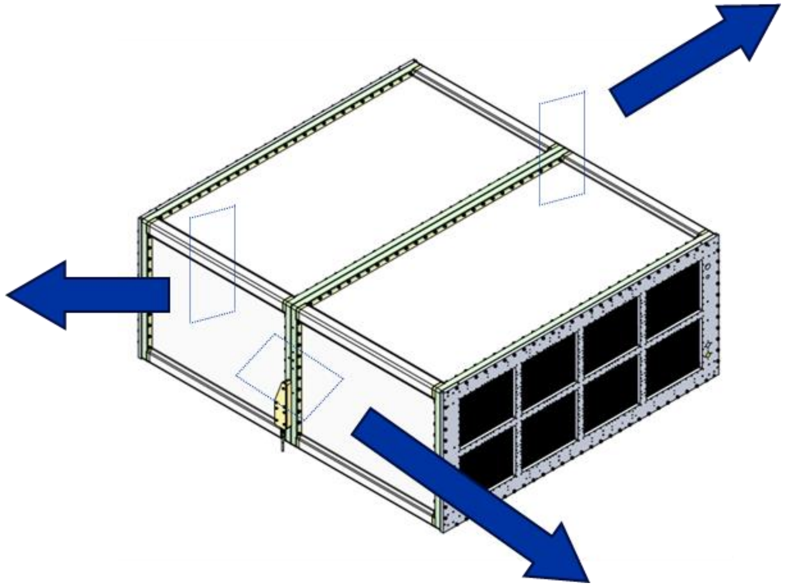

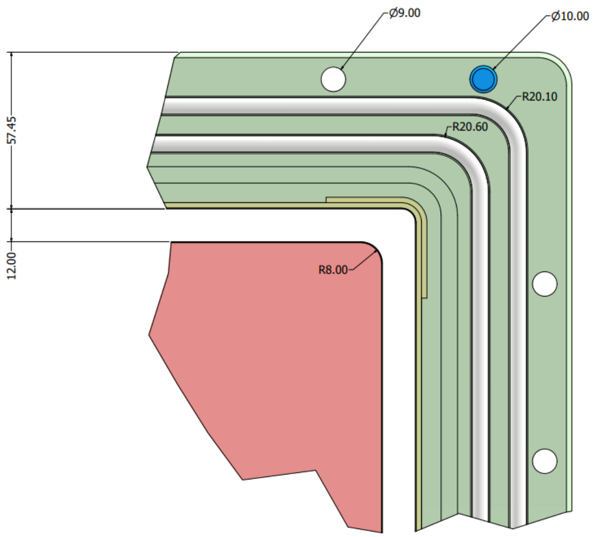

DETAIL B
SCALE 2 : 1

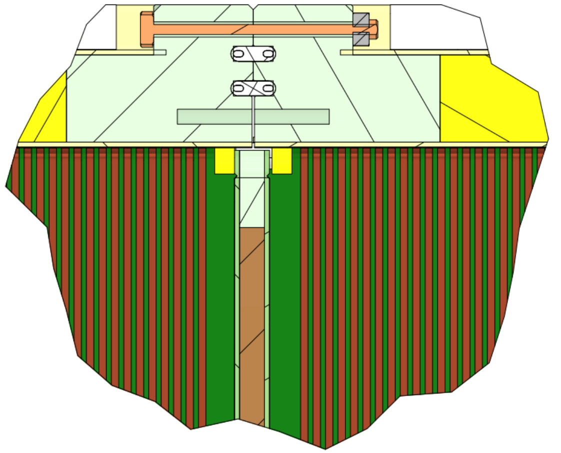

DETAIL B
SCALE 2 : 1

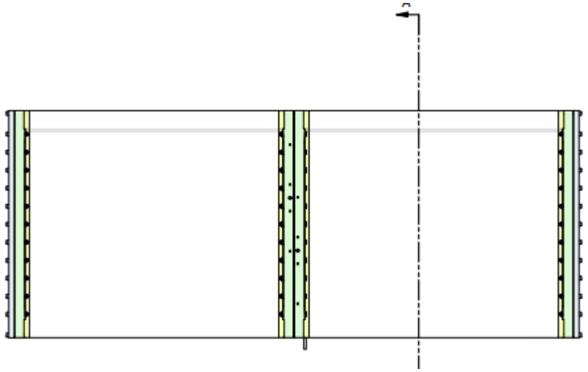

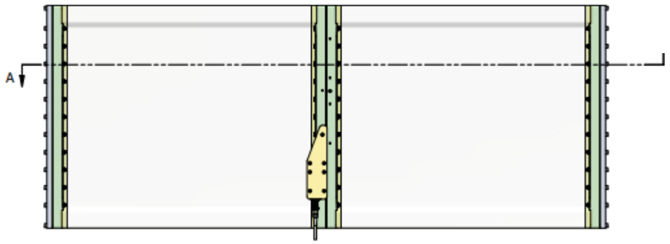

Field cage mechanical details: charge path to gnd

Flange thickness (5cm) too small for degrading -30kV to GND over a flat surface

Three deep grooves
for extending the path from HV to GND
for charge moving on surface and with gas
flanges

~ 7cm thick labirinth
~14 cm path lenght

→ voltage drop / path length < 3kV/cm

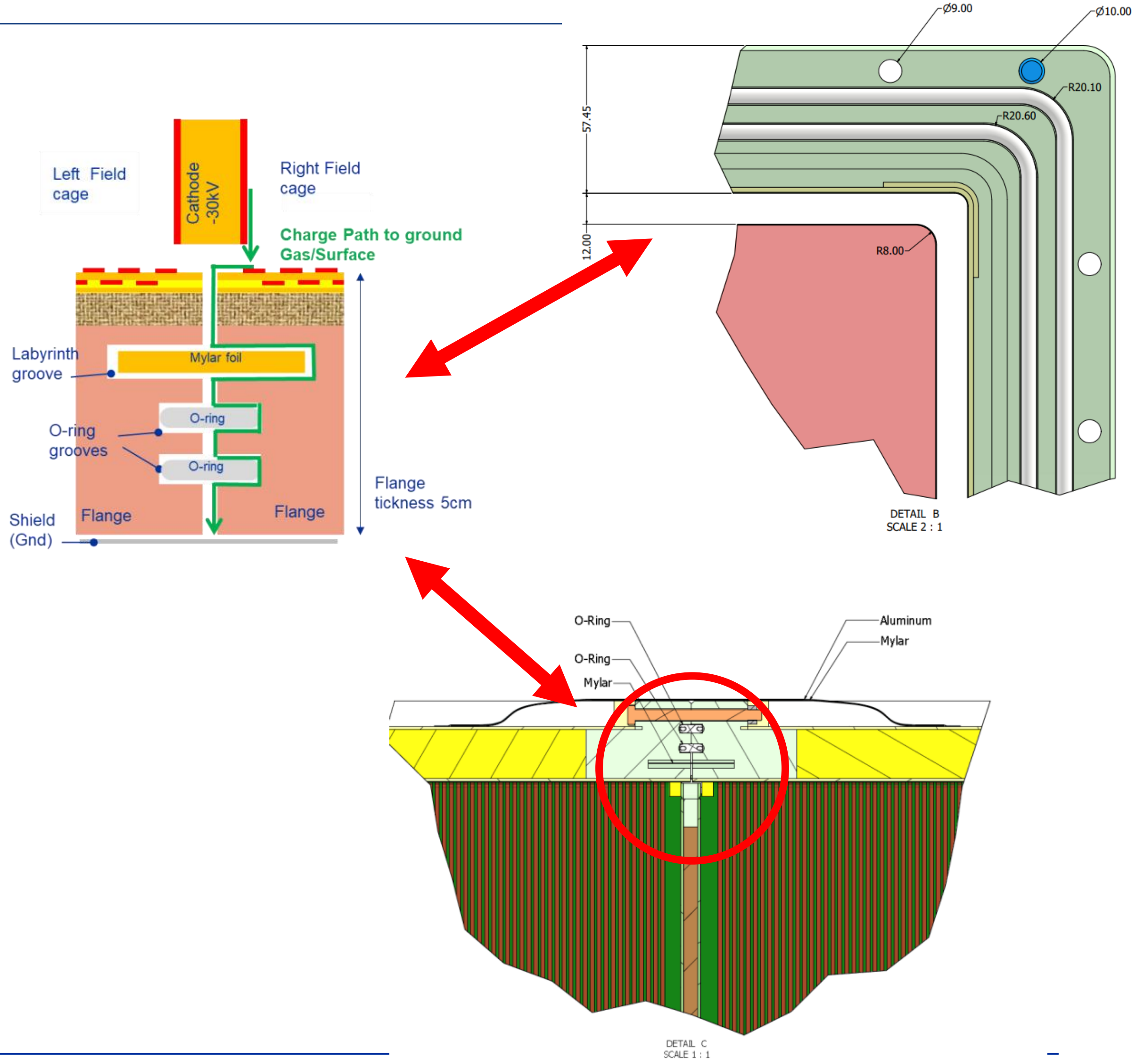

The ND280 experiment: High Angle TPC highlights

- Field Cage (FC)
  - Assembly and layout
  - Production
  - Characterization and Quality Assessment
    - Mechanical
    - Electrical

- Encapsulated Resistive Anode Micromegas (ERAMS)
  - Production of 50 sensors
  - Characterization
  - Detector response, signal and impact on reconstruction

- Impact on HATPC performance

Field Cage building, assembling and characterization

Production at NEXUS company (Barcelona) ~ 10 weeks
Validation, QC, electrical and mechanical assembly at CERN ~ 4 weeks

Mould building (INFN)

Mold features
- 1cm thick Alu walls
- Anodyzd. Surfaces
- Waviness compl. iso1302 N8
- Surfaces ⊥ and ∥ better than 80μm/m
- Mount / unmount geom. reproducibility with high precision

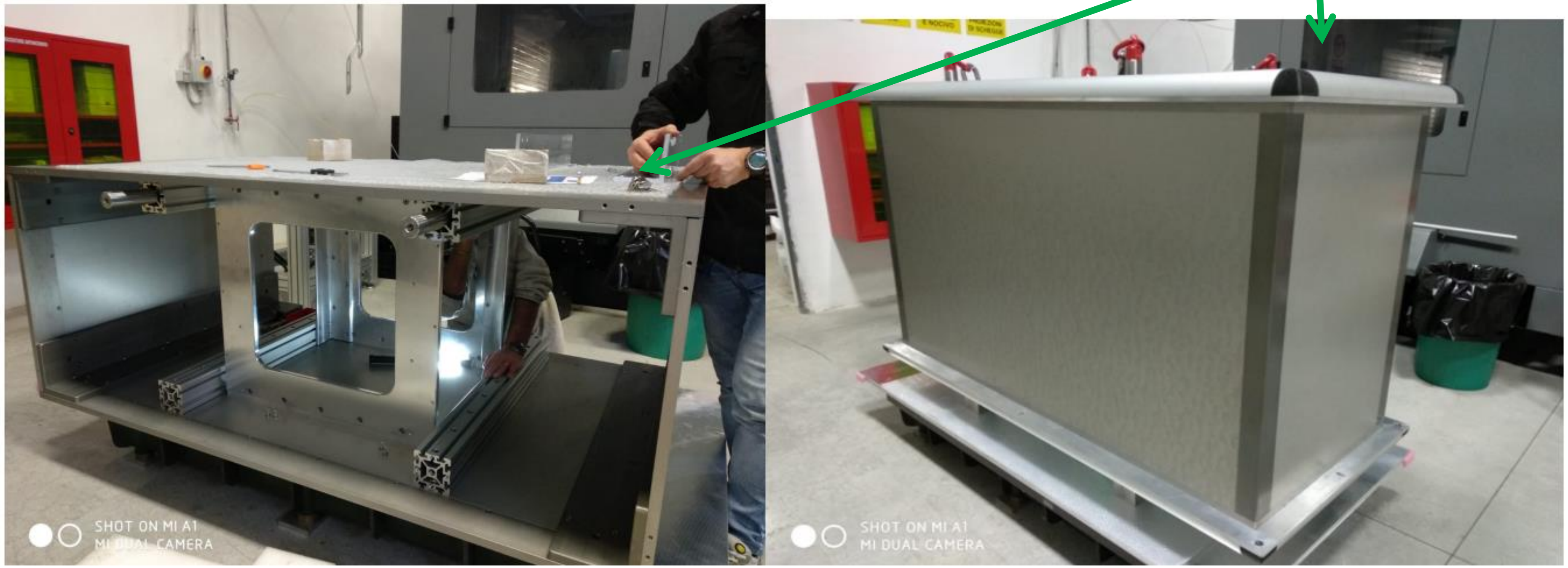

Field Cage building, assembling & characterization at NEXUS Kapton Layer

Production at NEXUS company (Barcelona) ~ 10 weeks
Validation, QC, electrical and mechanical assembly at CERN ~ 4 weeks

5 m perimeter x 1m height (drift length)

- Mold preparation
- Inner Vacuum bag
- Strip Foil positioning

- Thick corners w/ Kapton tape
- Electrical tests on surfaces
- Resin samples electrical Tests

Strip foil (by CERN) alignment and lamination of 3 Kapton layers

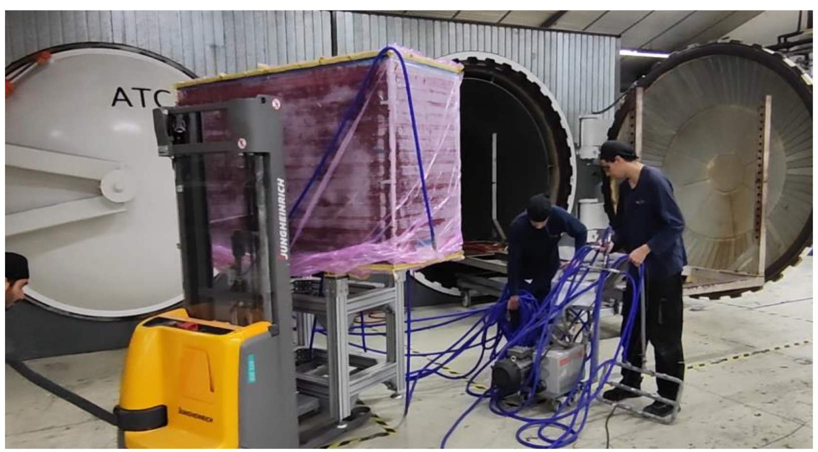

- Kapton lamination
- Curing at 40C (fast)
- Electrical tests on surfaces and resin samples after curing

Field Cage building, assembling & characterization at NEXUS
Kapton Layer and inner Twaron

Inner Twaron peel lamination

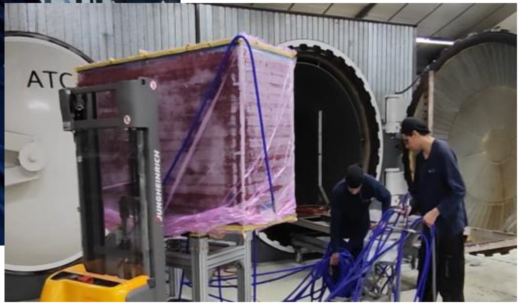

- First Twaron layer lamination
- Curing at 40C (fast) in autoclave

Electrical tests

- Resin sample
- Inner Twaron layer

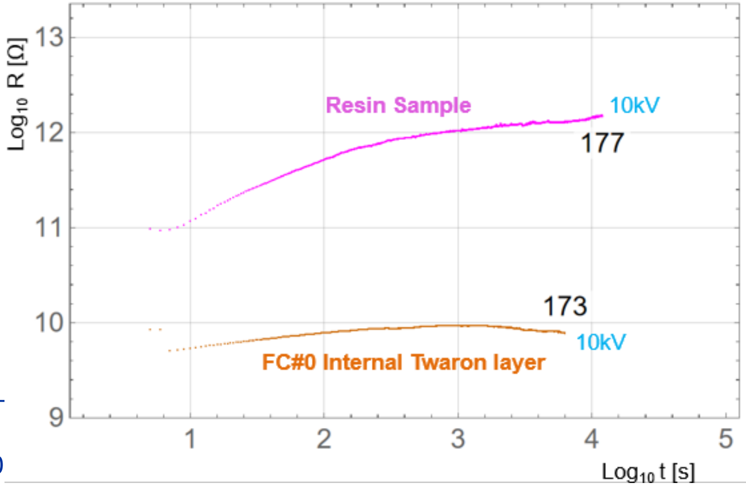

Quality controls – Resistivity of early Layers

1) Resistance between mold and 40x45cm2 electrode
-> volume resistivity of layers

2) Surface resistivity
of last layer Twaron

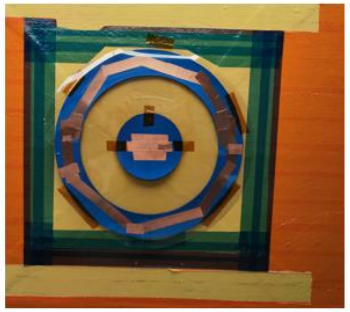

3) Resistance between two 6x80cm2 electrodes
-> mix of surface and volume resistivity

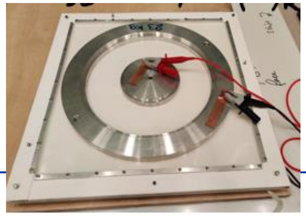

Resin sample
(Resoltech Epoxy)

1) various methods and electrode types (optimizing contact)
→ consistent measurements

2) Resin sample ρ_S ~ 10 TΩ/□
→ very good

Field Cage building, assembling & characterization at NEXUS
Kapton Layer + inner Twaron + G10 Skeleton

Gluing G10 "skeleton"

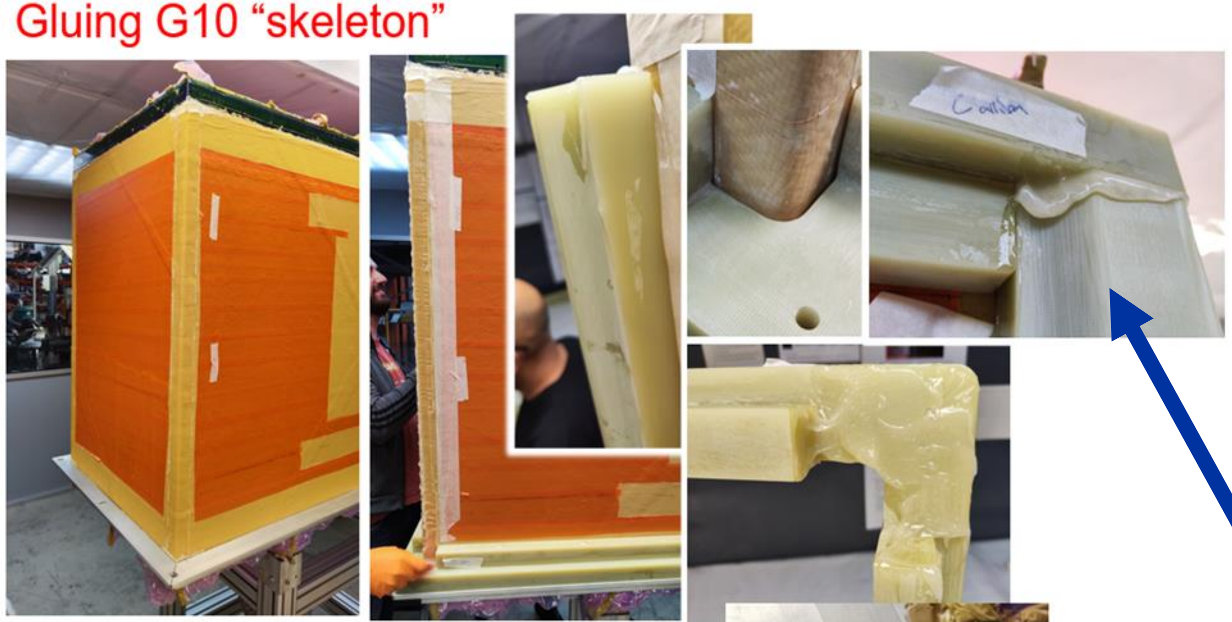

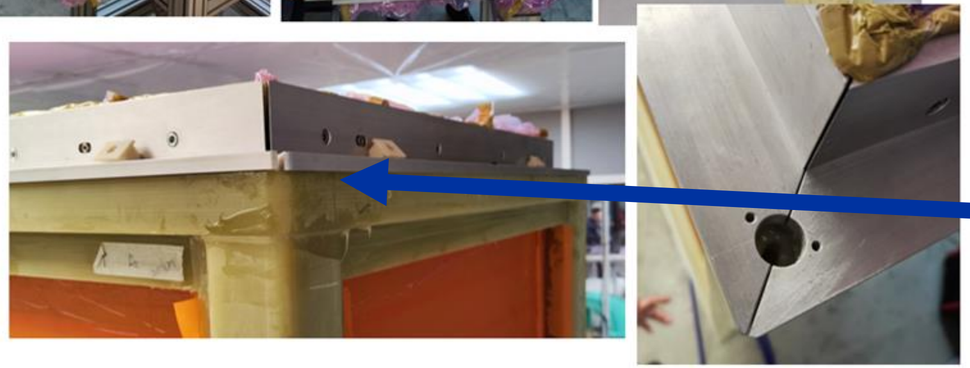

Gluing G10 structural skeleton and casting resin on flanges for ensuring gas tightness

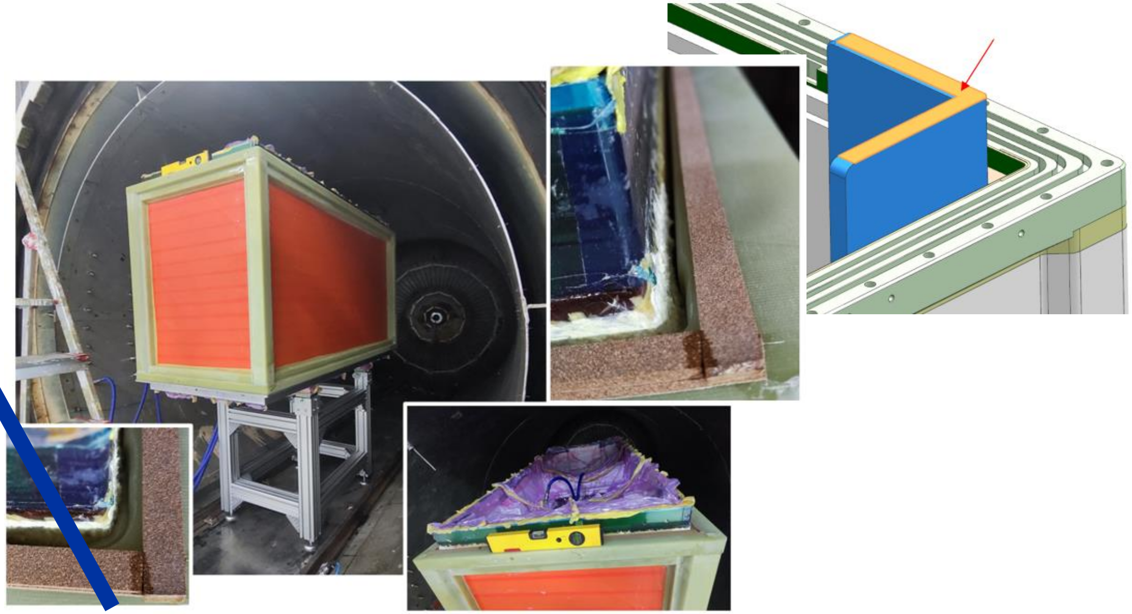

Flanges & Bars by ORVIM company (TV, Italy)

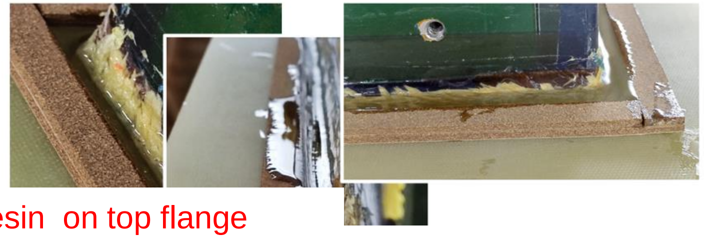

- G10 skeleton gluing
- Curing 40C in clean room

- Casting low viscosity resin on top flange
  →sealing flange to laminated layers
- Autoclave curing at 40C

Field Cage building, assembling & characterization at NEXUS
Kapton Layer + inner Twaron + G10 Skeleton + HC + Ext Twaron

- Gluing Nomex Honeycomb
- Curing at 40C in oven


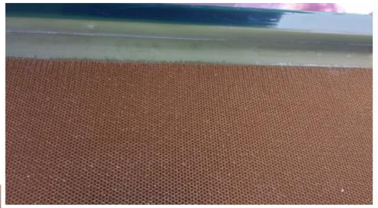


- Flipping the box top-bottom
- Resin casting on second flange
- Curing at 40C in autoclave
- Second Twaron peel lamination
- Curing at 40C in autoclave

Outer Twaron peel lamination

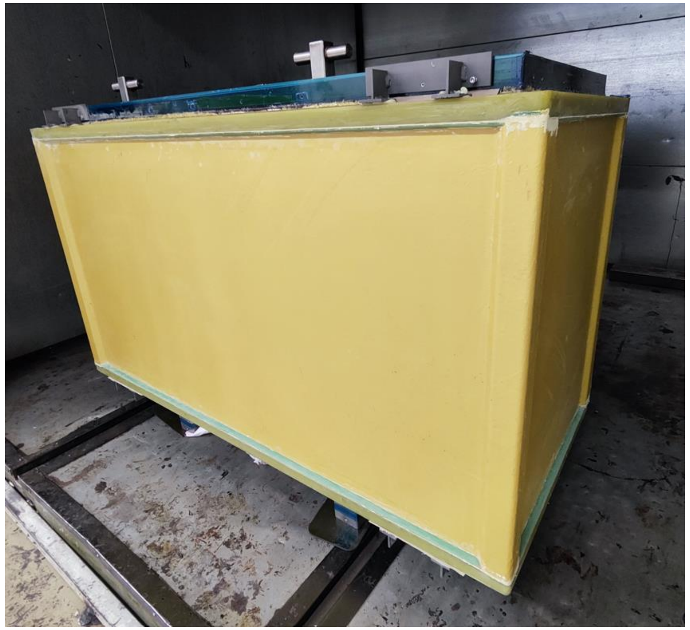

Post-curing at 40C in oven (lasting as long as possible)

Field Cage machining and final QC at Nexus

Precision machining of cathode and anode flanges and surfaces finishing

Back to NEXUS company for

- Mould removal
- Very fine polishing of flanges
- Correction of defects (eg bubbles)

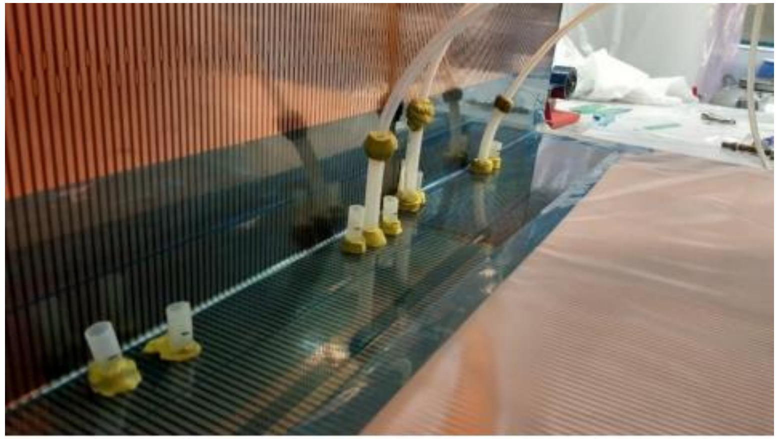

Shipment to CERN

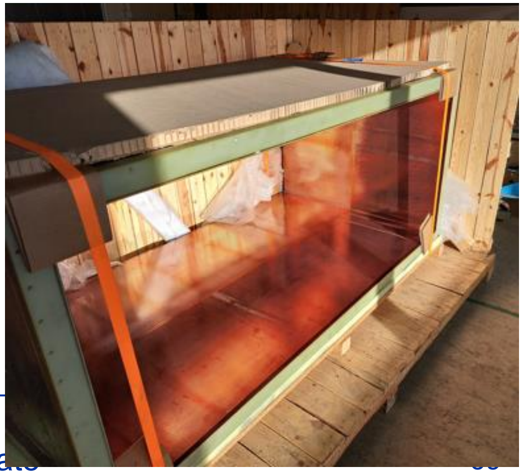

The ND280 experiment: High Angle TPC highlights

- Field Cage (FC)
  - Assembly and layout
  - Production
  - Characterization and Quality Assessment
    - Mechanical
    - Electrical

- Encapsulated Resistive Anode Micromegas (ERAMS)
  - Production of 50 sensors
  - Characterization
  - Detector response, signal and impact on reconstruction

- Impact on HATPC performance

Field Cage assembling, characterization at CERN

Vertical assembly of
two Field Cages into HATPC

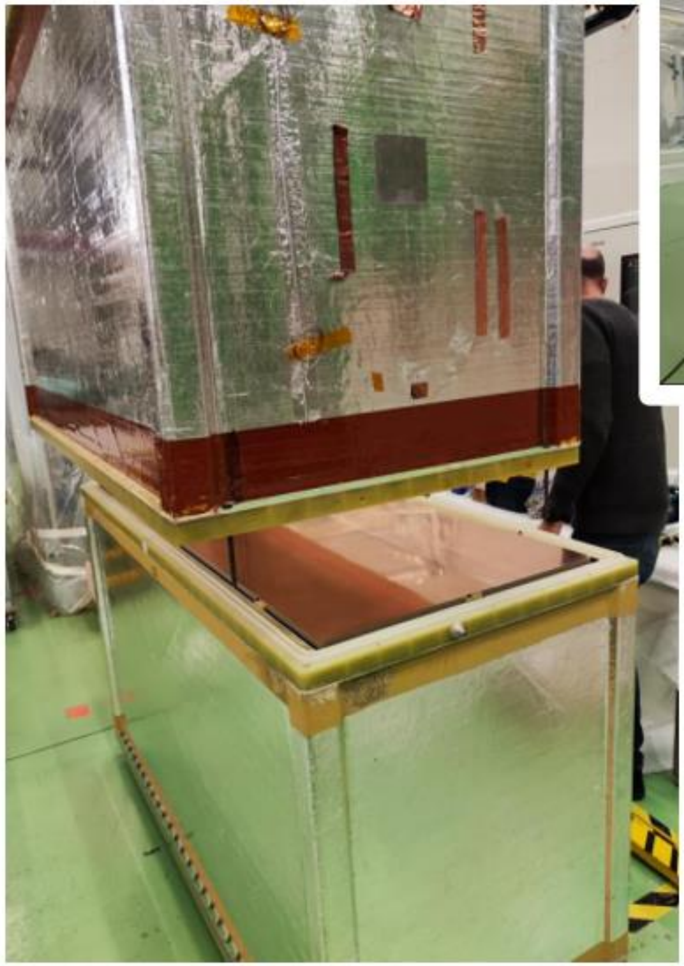

Cathode assembly

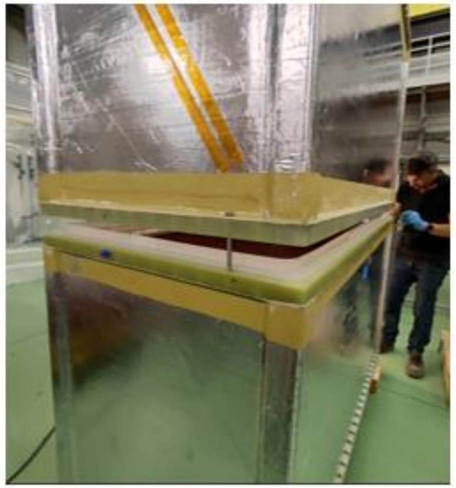

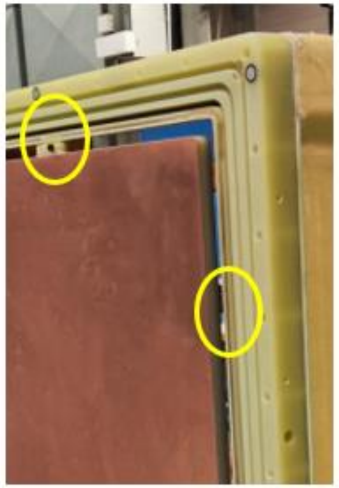

Cathode assembly

High Voltage feedtrough
external connection

Connection of last strips to cathode
and to high voltage feedtrough

High voltage tests after assembly

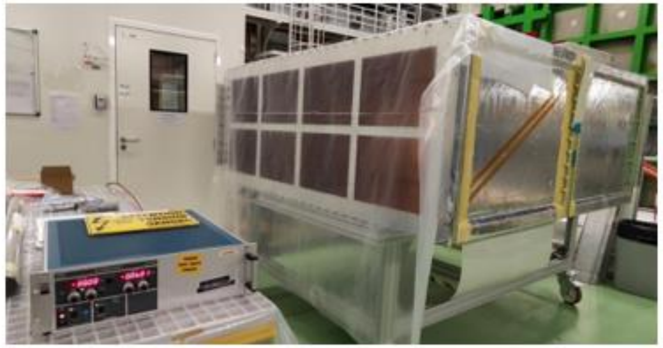

Field Cage assembling, characterization at CERN

1) **He leak tested**
sniffer (air + 30mbar of He)

2) Tested against gas density changes
- He Over-pressure (+20mbar)
- Air Under-pressure (-20mbar)

Gas leakages qualification

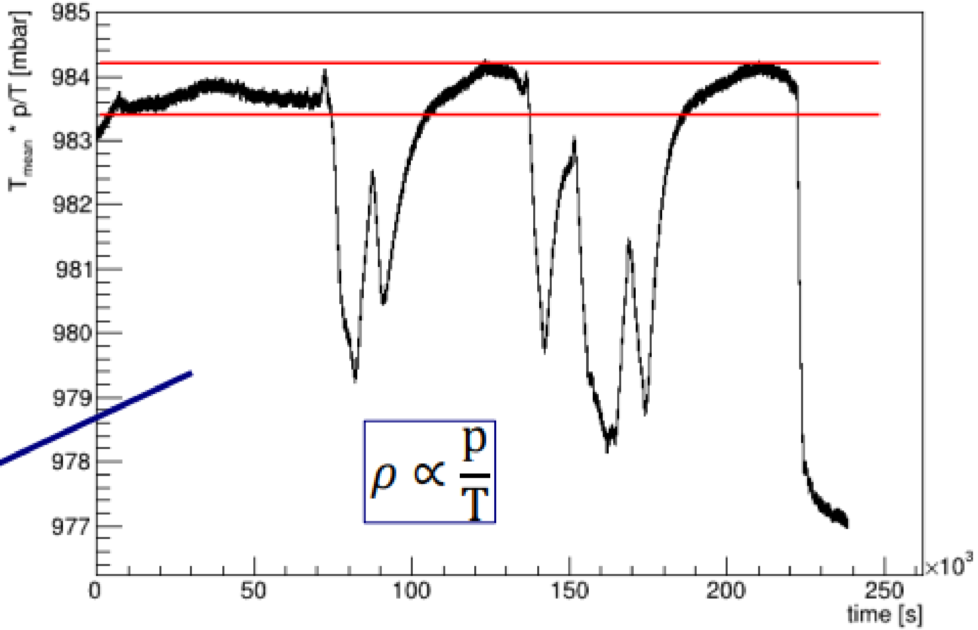

Several T,P,RH sensors
Inside FC

BME280 – T_{cage}, P, RH
IR sensor - T_{gas}
Thermocouple and Pt100
Voltage divider current meas.

Gas density corrected
for Volume variation (due to Pin - Pout)

$$= \frac{Pin(t)}{Tin(t)/Tin(0)}\left(1-\frac{\Delta V}{V0}\right)(\mathrm{Pin}-\mathrm{Pout})$$

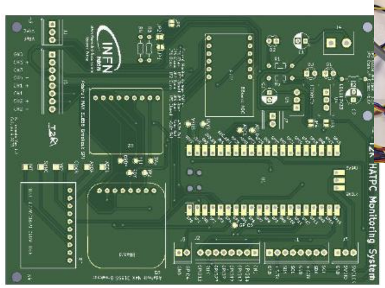

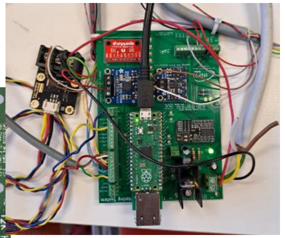

=> Overall Leak < 10^{-3} mbar L / s

Field Cage assembling, characterization at CERN

Mechanical qualification

Comparison with FEM models in fair agreement with
- load tests
- deformation vs pressure

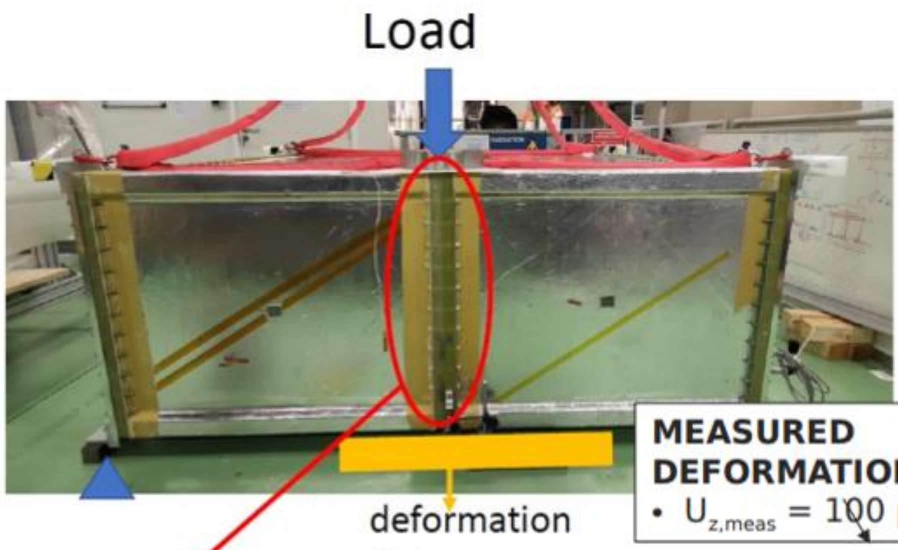

G10 screws
(No metal near cathode)

MEASURED DEFORMATION
- $U_{z,meas}$ = 100 µm

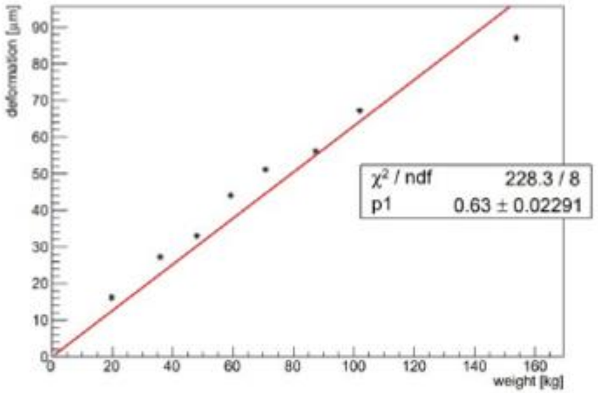

Load test performed up to 160 kg

Around $\sim 0.6 \frac{\mu m}{kg}$ of deformation w.r.t. horizontal position

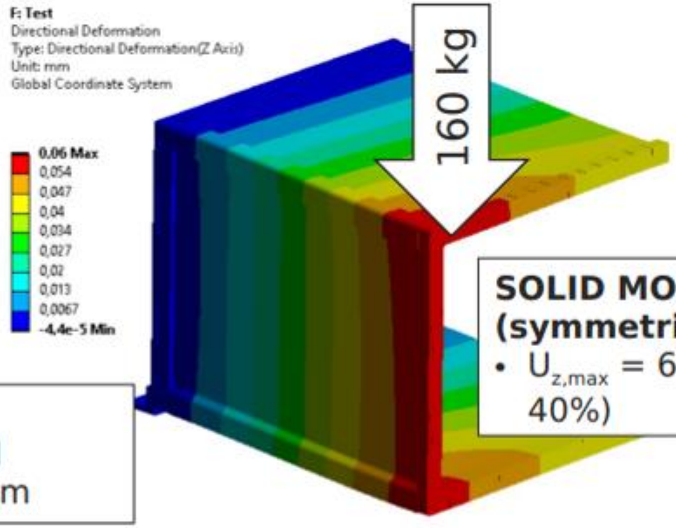

SOLID MODEL (symmetric)
- $U_{z,max}$ = 60 µm (Δ = -40%)

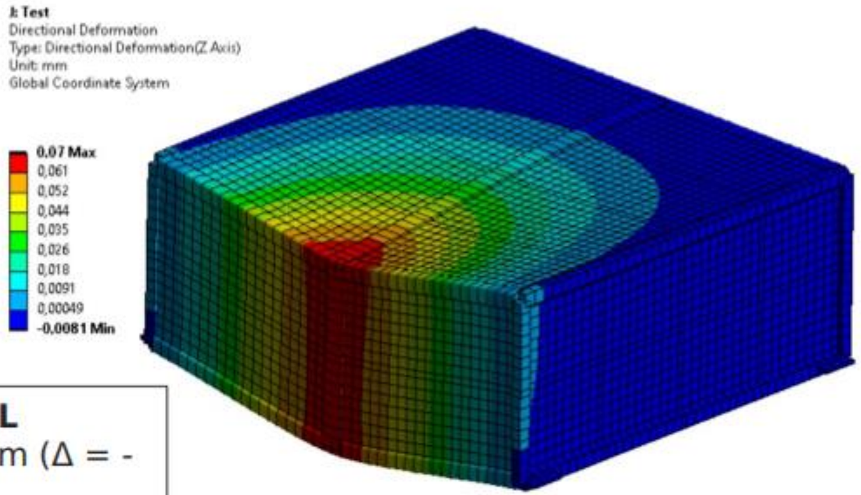

SHELL MODEL
- $U_{z,max}$ = 70 µm (Δ = -30%)

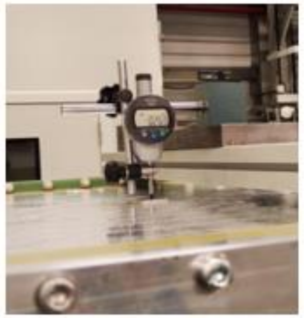

Field Cage assembling, characterization at CERN

Mechanical qualification

Comparison with FEM models in fair agreement with
- load tests
- deformation vs pressure

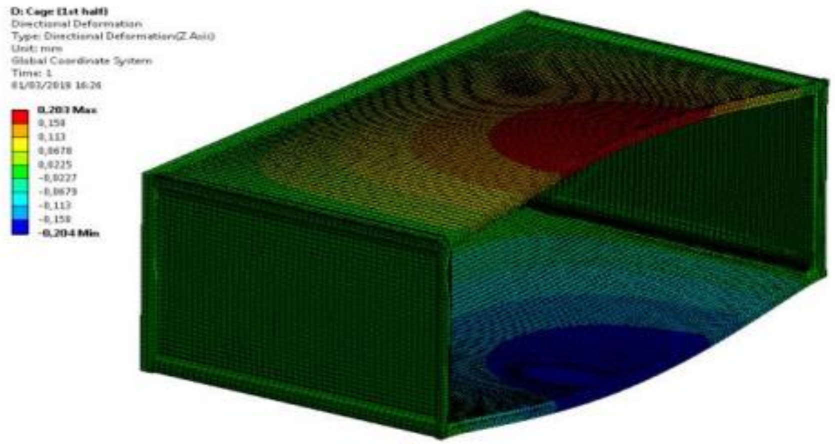

Max total deformation ~ 200 µm

Simulation:
Max deformation of large faces: $\sim 50\,\frac{\mu m}{mbar}$

Max total deformation ~ 60 µm

Data:
Max deformation of large faces: $\sim 50\,\frac{\mu m}{mbar}$

Max deformation of small faces: $\sim 8\,\frac{\mu m}{mbar}$

Almost linear in the studied pressure range

Field Cage assembling, metrology at Nexus

Tolerances and specifications at a level better than 300μm/m for planes parallelism and orthogonality and better than ISO1302-N8 for waviness are respected with few localized acceptable exceptions

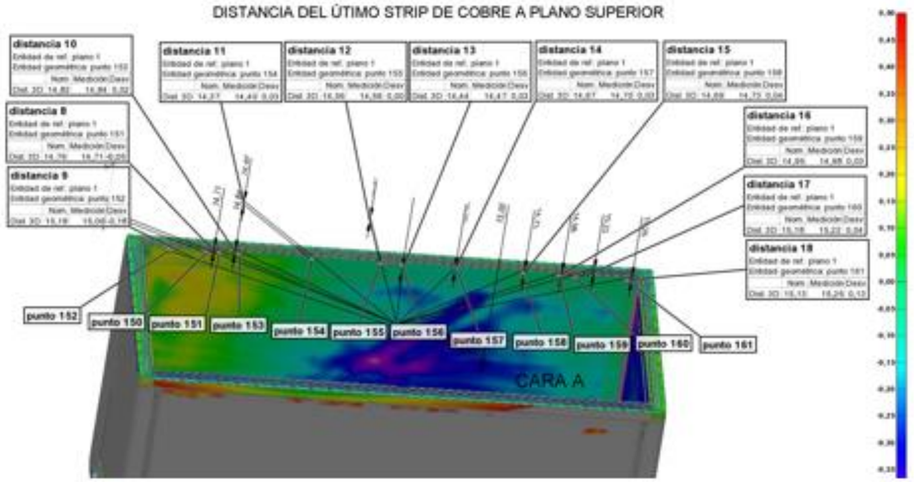

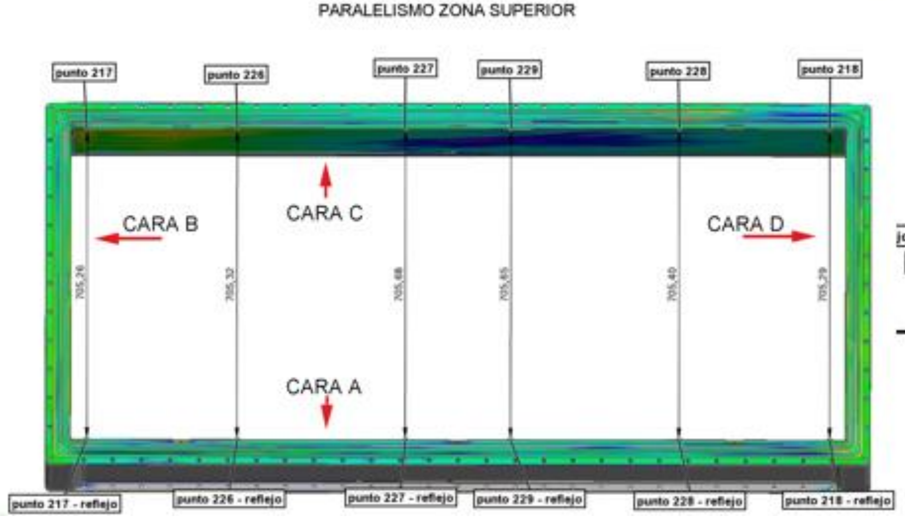

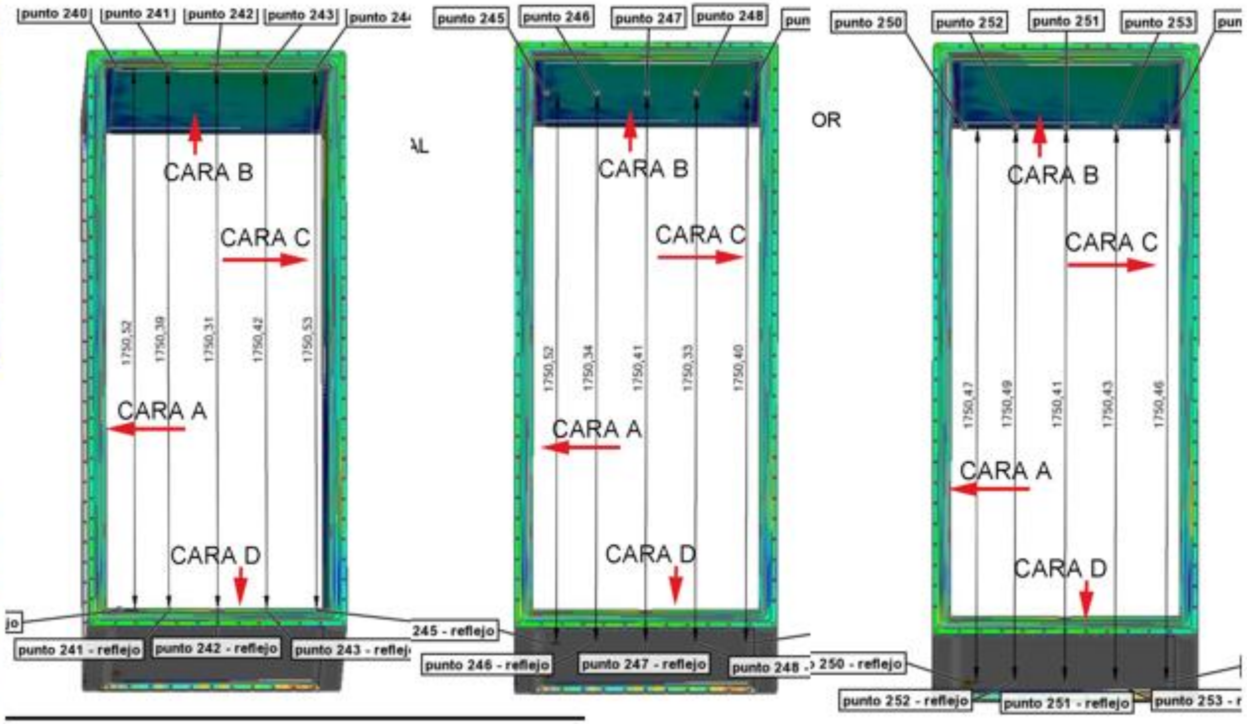

Reached limits of composite material technique
Large dimensions and hand lay-up

Field Cage assembling, metrology at CERN

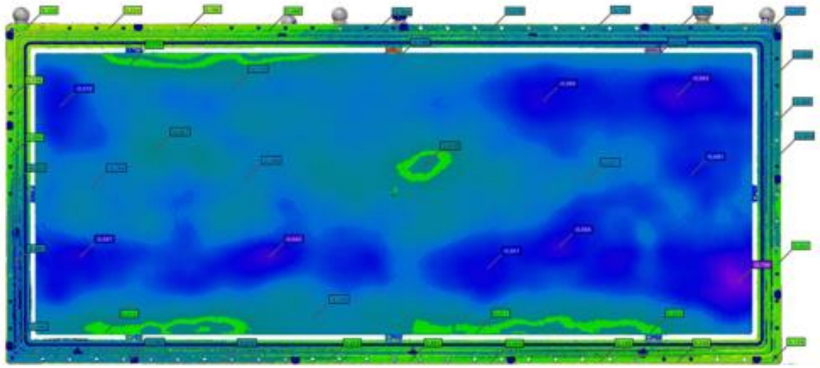

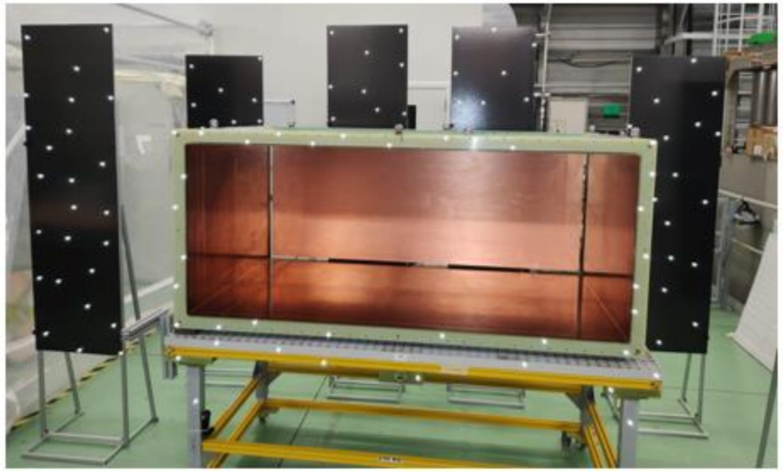

Metrology at CERN Bottom–HATPC (2023)
(Two separate cages and cathode)

Metrology at CERN Top–HATPC
(2024, single whole TPC 3D metrology)

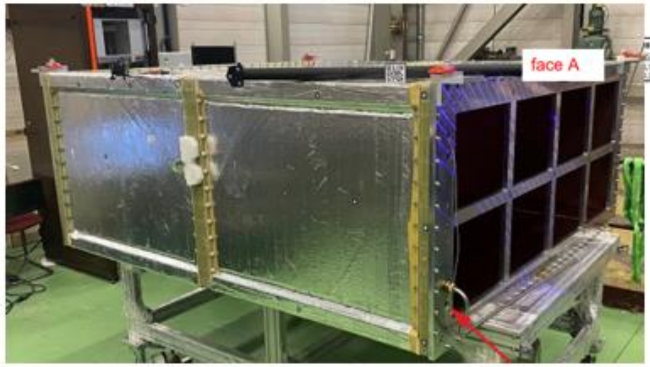

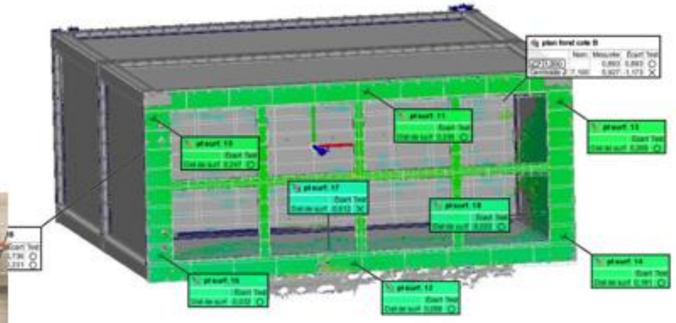

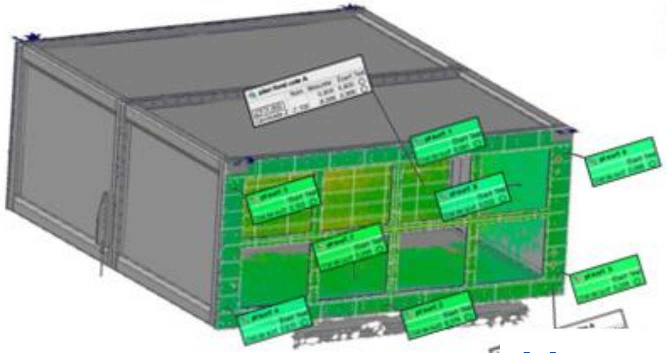

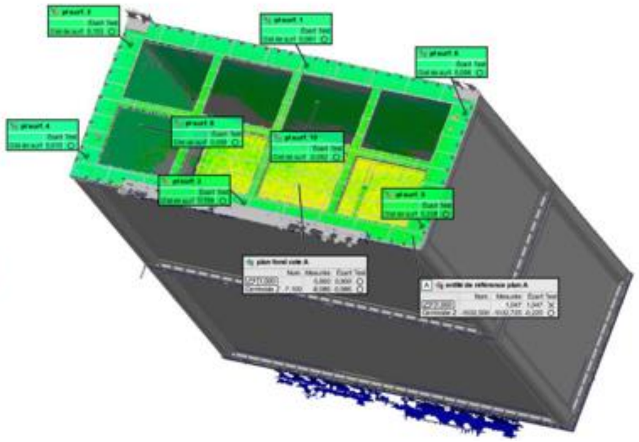

Measured internal geometry after assembly agrees with nominal CAD with pull better than 300μm with few localized, acceptable exceptions

Field Cage assembling, ERAM installation

Assembly the 16 ERAMs in Clean room for each TPC

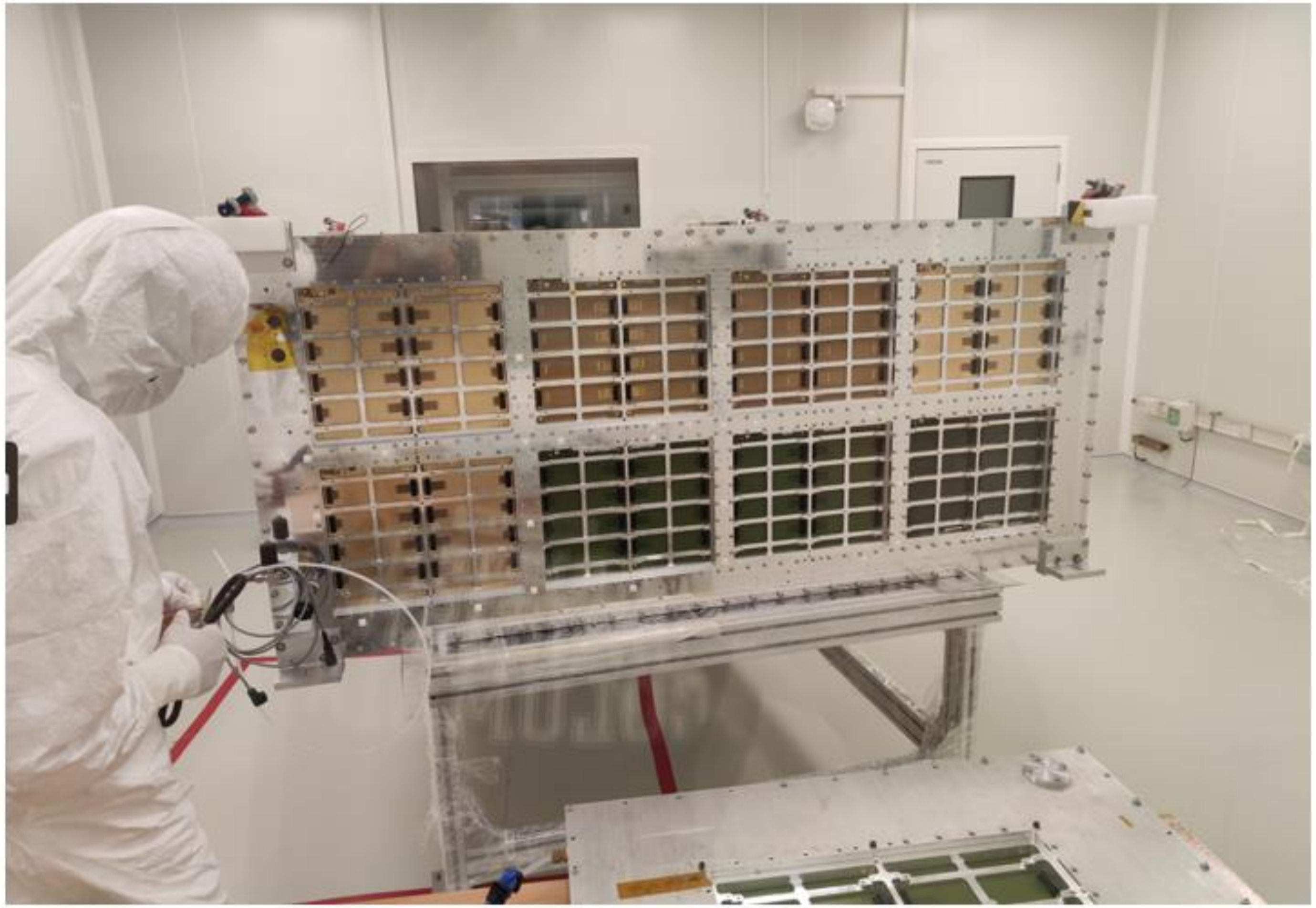

Grey tent area in front of Clean Room
large entrance for enhanced clean conditions

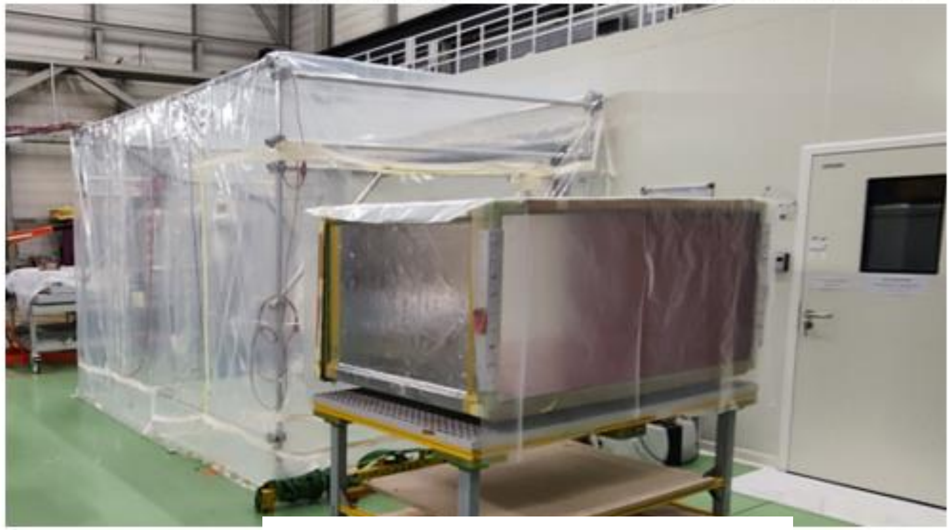

ERAMs: avoid dust

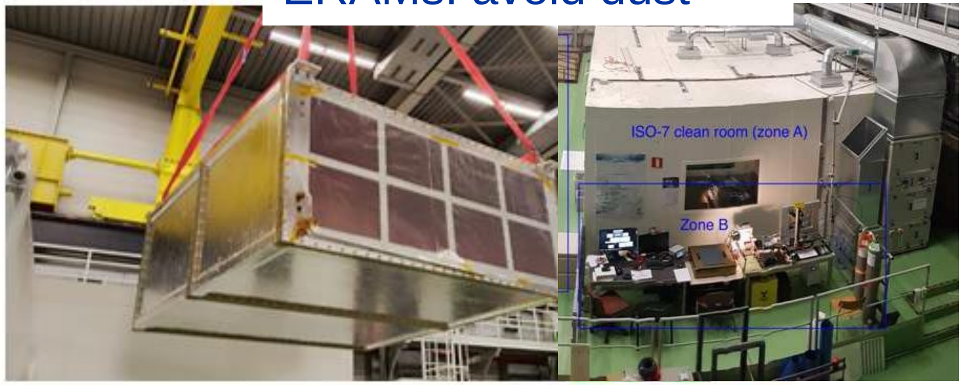

Field Cage assembling, commissioning with cosmics

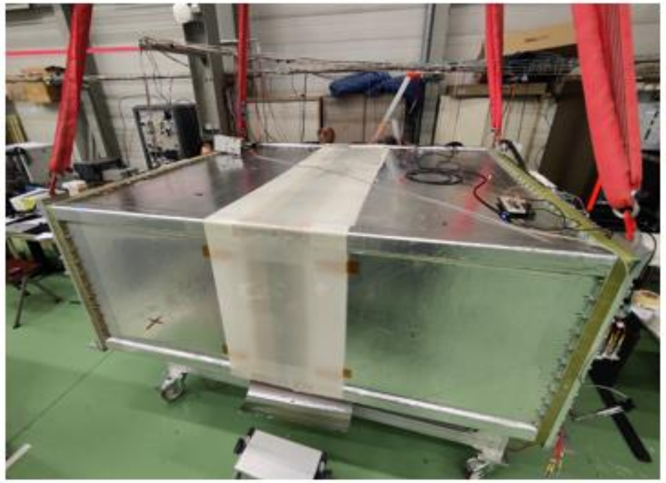

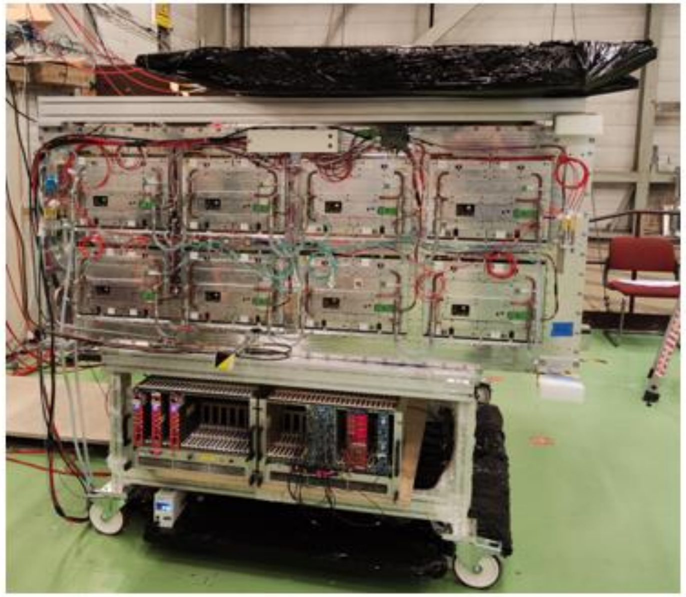

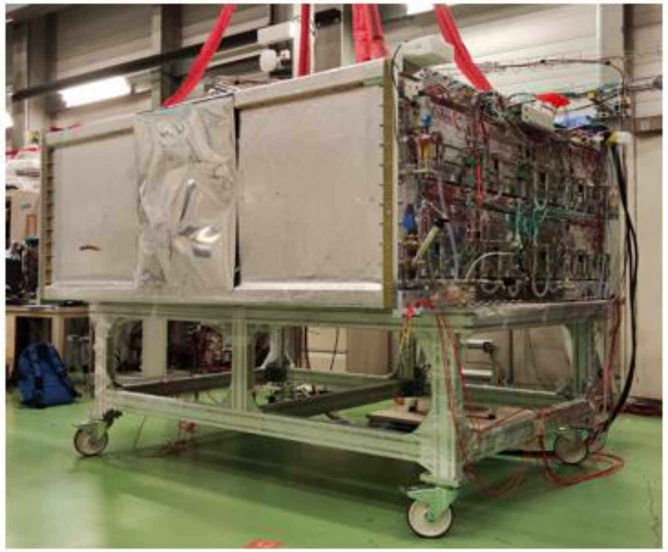

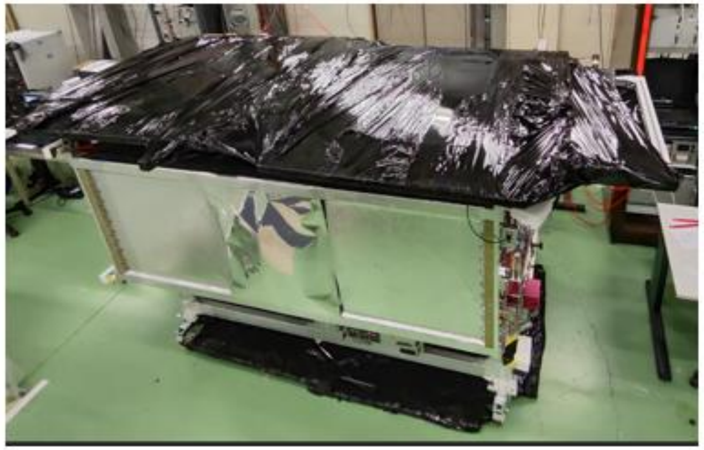

Cosmic shower evwnt

Projection on Anode End Plate 2

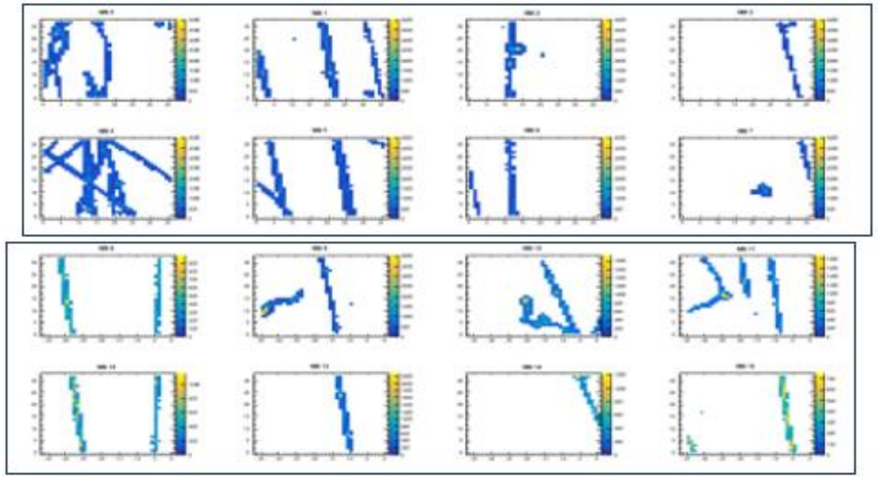

Projection on Anode End Plate 1

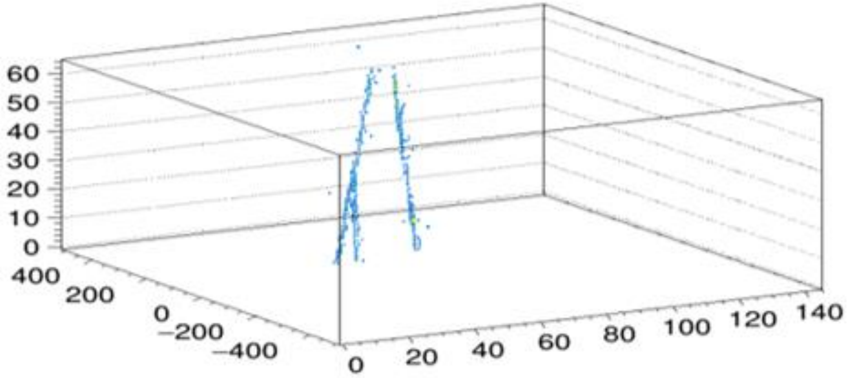

Cosmic tracks interaction evwnt

Field Cage assembling, commissioning: gas contamination at CERN

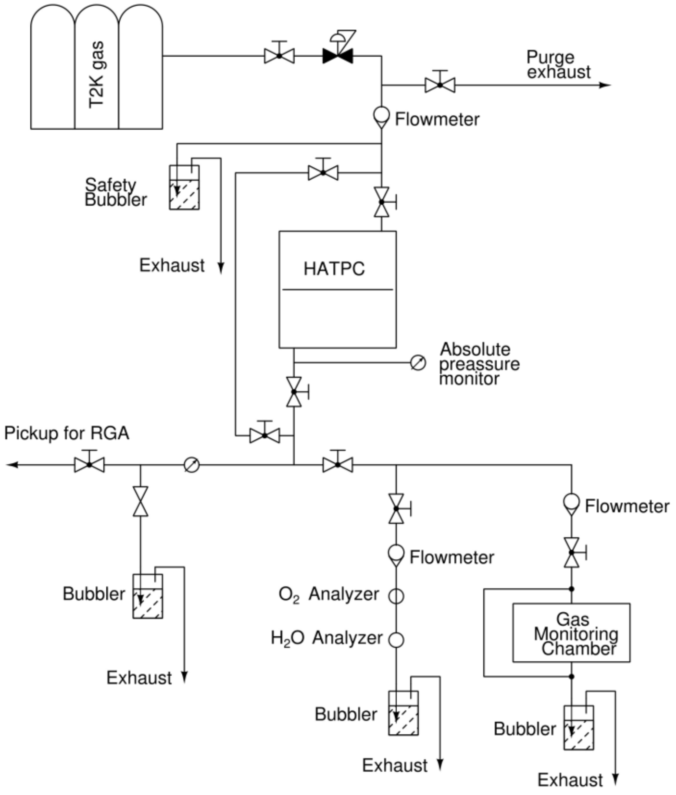

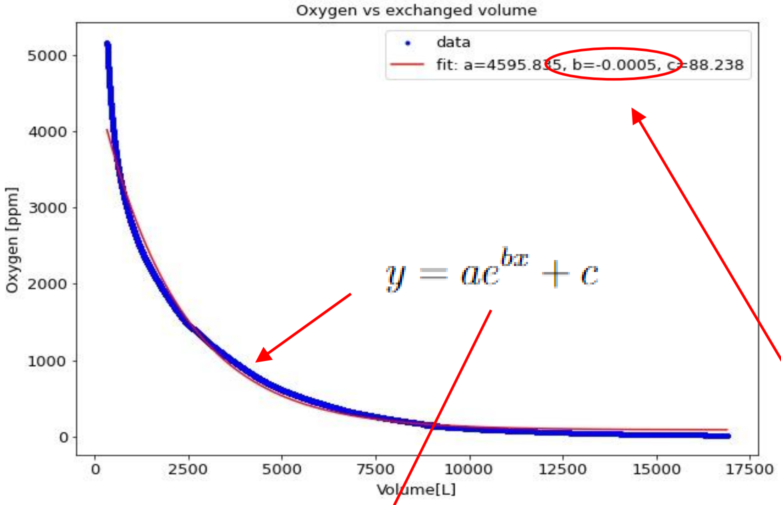

$$y = ae^{bx} + c$$

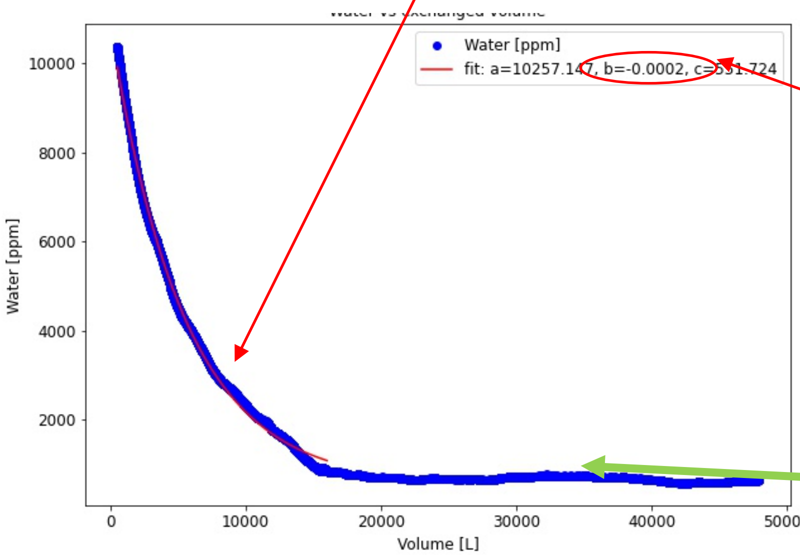

Water and Oxygen contamination evolution

Large amount of water uptake by Kapton: 2% in mass, with respect to dry Kapton, ~ about 70 g → purging time ~ a couple of months

Different dragging coefficient ? Under investigation

$$\frac{dc(t)}{dt} + \frac{f}{V}c(t) = \delta$$

δ water desorption from walls → 0.06 g/day water removal / desorption (long)

Field Cage assembling, commissioning: gas contamination at J-PARC

New gas system (CERN)
Overall recirculation flow ~ 500 l/h per TPC with overall few % fresh gas injection

Gas contamination from Field Cage O_2 and H_2O

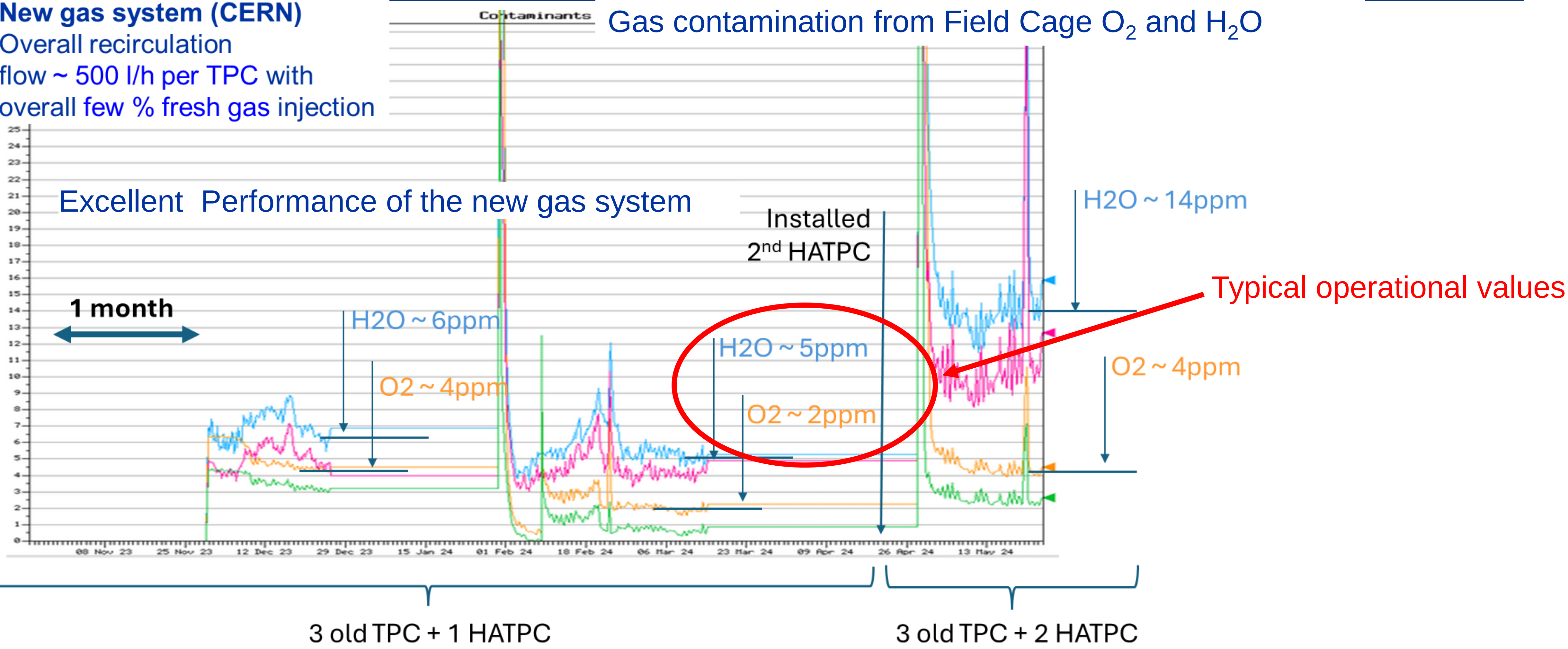

Field Cage assembling, commissioning: drift velocity measurement

Drift velocity

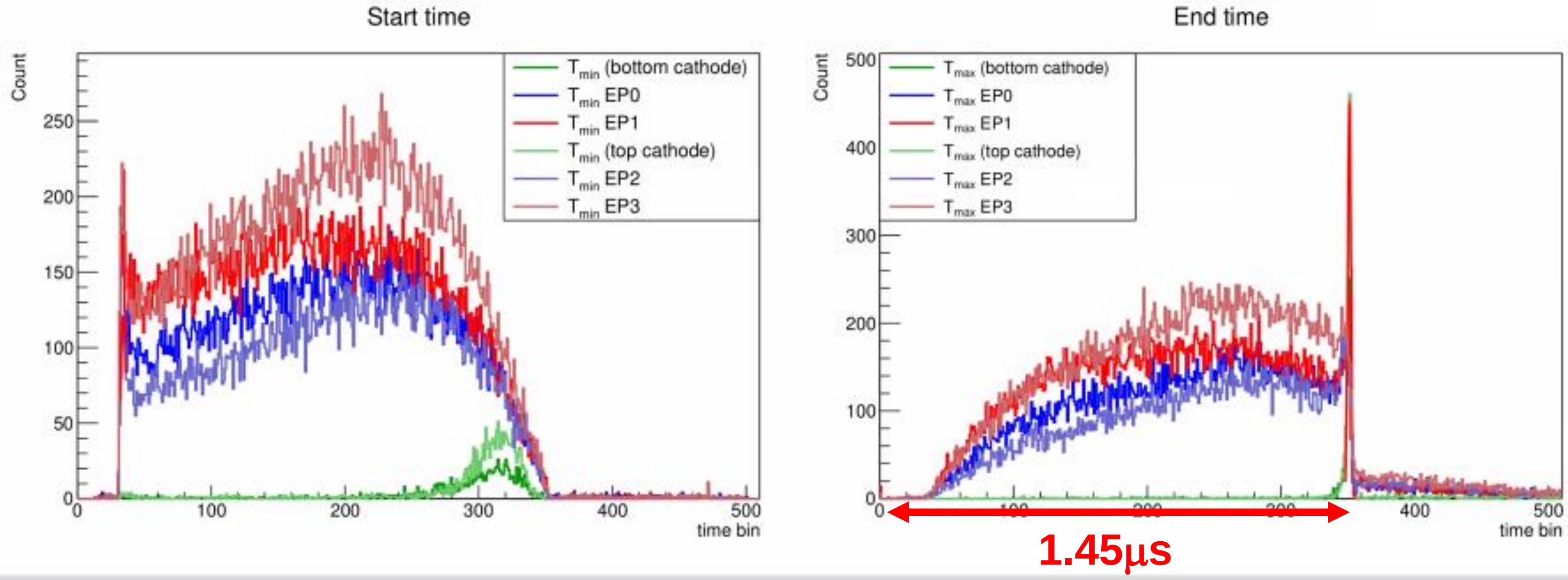

Gas contamination H_2O ~ 10 ppm H_2O @ J-PARC All TPCs

Drift velocity in bottom HATPC: 7.769 ± 0.005 cm/μs

Drift velocity in top HATPC: 7.772 ± 0.005 cm/μs

Perfect agreement with expectations (Magboltz)

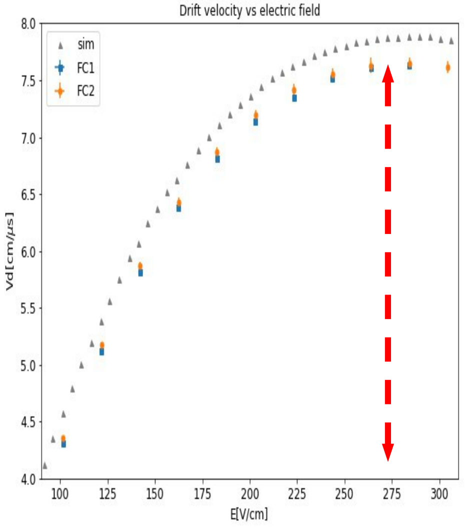

Gas contamination from Field Cage – O_2 and H_2O included 500 ppm H_2O @ CERN Bottom TPC

Thanks to CERN

We would like to express our gratitude for the continuous and extremely valuable support from CERN

Burkard Schmidt, Roberto Guida, Frederic Merlet and colleagues → Gas system EP-DT/ED-DT-FS

Davide Tommasini, Roland Piccin, Sebastien Clement, Cedric Urscheler → Polymer lab/TE-MSC

Rui de Olivera, Olivier Pizzirusso→ EP-DT-EF

Eraldo Oliveri, Djunes Janssen→ EP-DT-DD

Francesco Lanni, Lluis Secundino Miralles Verge Albert DE ROECK, Filippo Resnati → Neutrino Platform

Ahmed Cherif, Jean Philipphe Rigaudt → Metrology/TE-MSC-SMT

Antje BEHRENS, Jean Christophe Gayde → BE-GM-ESA

Mauro Taborelli, Colette Charvet, Marcel Himmerlich → TE-VSC-SCC

Paolo Chiggiato → TE-VSC

Patrick Muffat, Loredana ZENI Toberer, Laurence Planque, Stephanie Krattinger, Elsa Clerc→ SCE-SSC-LS

Thanks to CERN

We would like to express our gratitude for the continuous and extremely valuable support from CERN

Burkard Schmidt, Roberto Guida, Frederic Merlet and colleagues → Gas system EP-DT/ED-DT-FS

Davide Tommasini, Roland Piccin, Sebastien Clement, Cedric Urscheler → Polymer lab/TE-MSC

Rui de Olivera, Olivier Pizzirusso→ EP-DT-EF

Eraldo Oliveri, Djunes Janssen→ EP-DT-DD

Francesco Lanni, Lluis Secundino Miralles Verge Albert DE ROECK, Filippo Resnati → Neutrino Platform

Ahmed Cherif, Jean Philipphe Rigaudt → Metrology/TE-MSC-SMT

Antje BEHRENS, Jean Christophe Gayde → BE-GM-ESA

Mauro Taborelli, Colette Charvet, Marcel Himmerlich → TE-VSC-SCC

Paolo Chiggiato → TE-VSC

Patrick Muffat, Loredana ZENI Toberer, Laurence Planque, Stephanie Krattinger, Elsa Clerc→ SCE-SSC-LS

Thanks to INFN support at CERN and the CEA ANTENNA colleagues

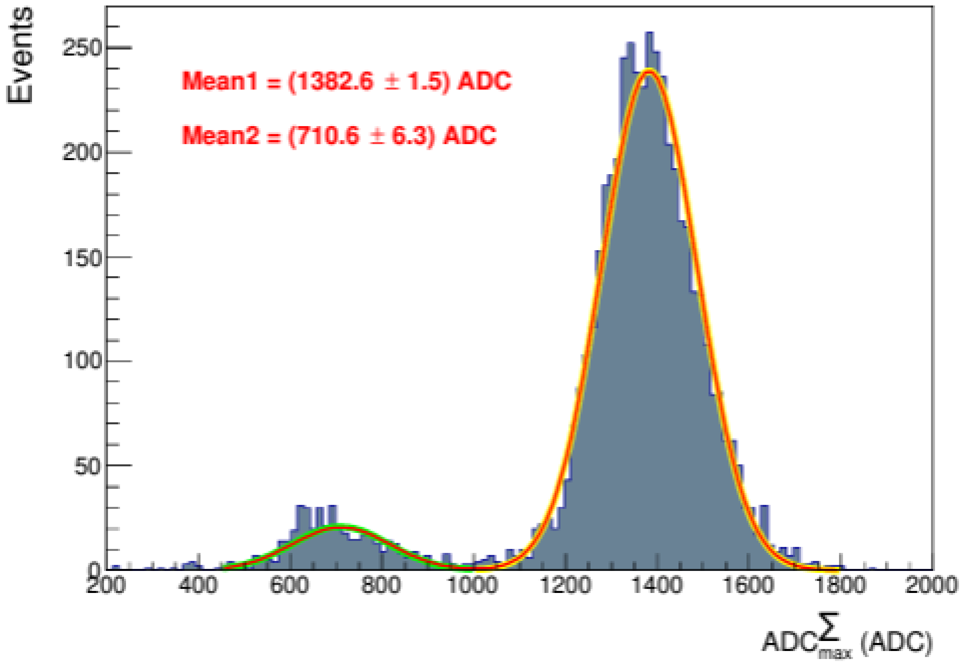
Events
Mean1 = (1382.6 ± 1.5) ADC
Mean2 = (710.6 ± 6.3) ADC
250
200
150
100
50
0
200
400
600
800
1000
1200
1400
1600
1800
2000
ADC$^{\Sigma}_{max}$ (ADC)

Near Detector impact on Oscillation Analysis

- ND280 magnetized detector
- Select interactions in FGD and measure muon kinematics in the TPCs
- Separate samples based on number of reconstructed pions (CC0π, CC1π, CCNπ), protons, photons, etc
- Factor of ~3 reduction on the uncertainty on the event rates at the Far Detector

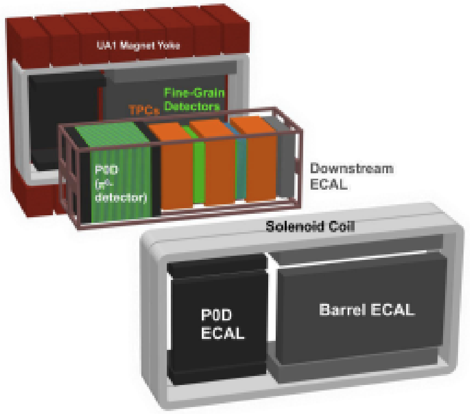

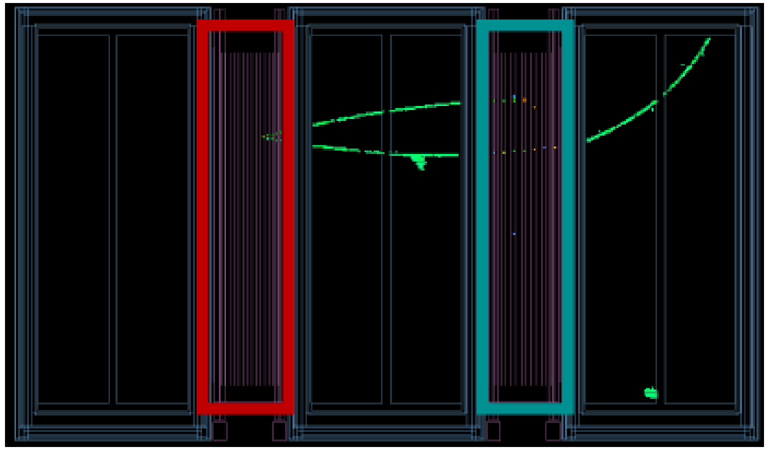

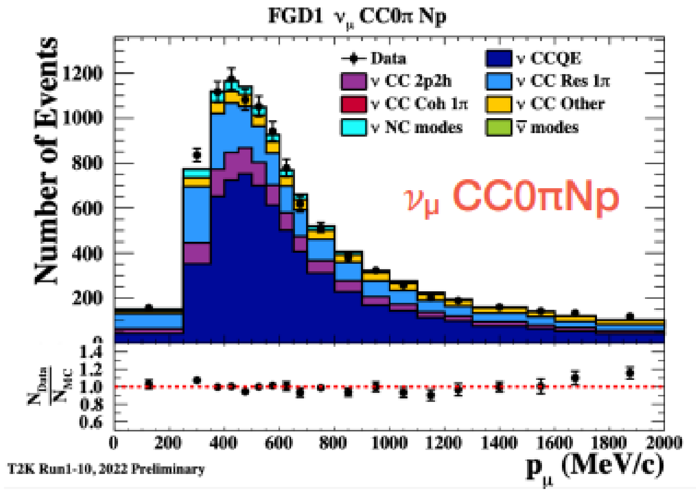

Sample	Pre-ND FIT error	Post-ND FIT error
FHC 1Rμ	11.1%	3.0%
RHC 1Rμ	11.3%	4.0%
FHC 1Re	13.0%	4.7 %
RHC 1Re	12.1%	5.9%
FHC 1Re 1d.e.	18.7%	14.3%

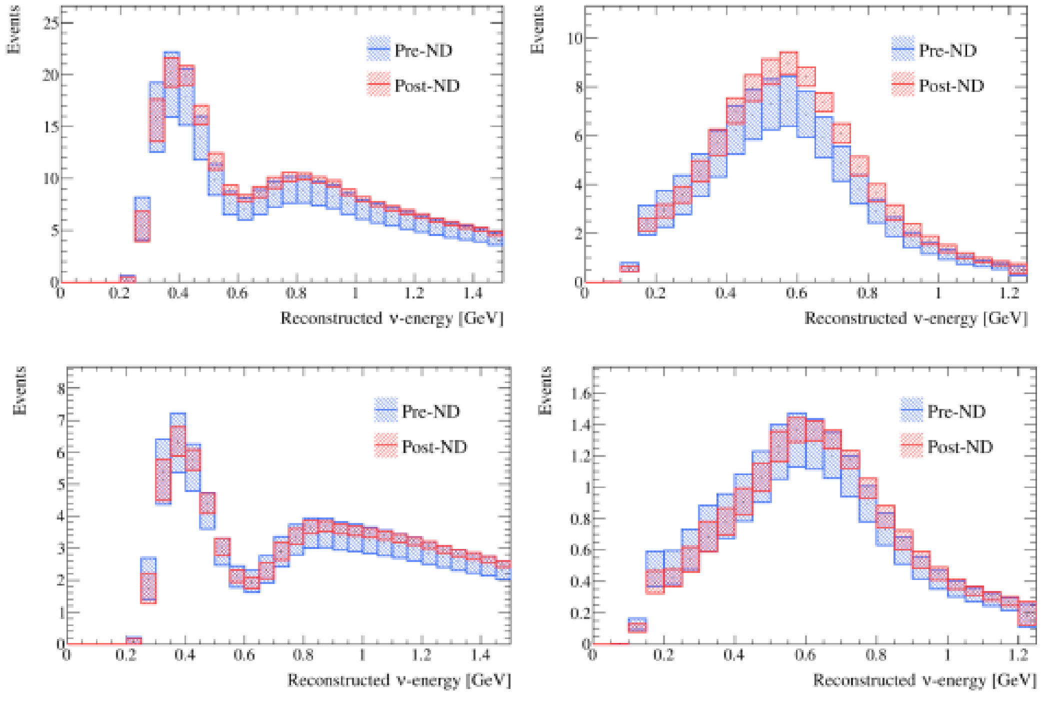

(d) $\bar{\nu}$-mode 1Rμ
(e) $\bar{\nu}$-mode 1Re

ND280 limitations

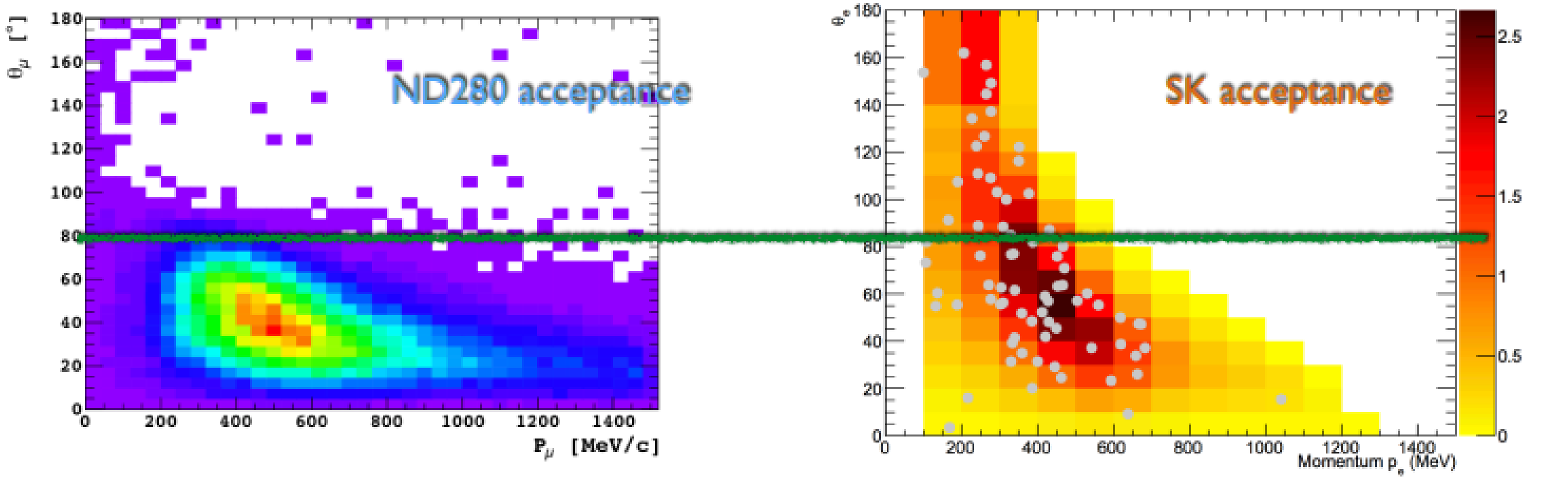

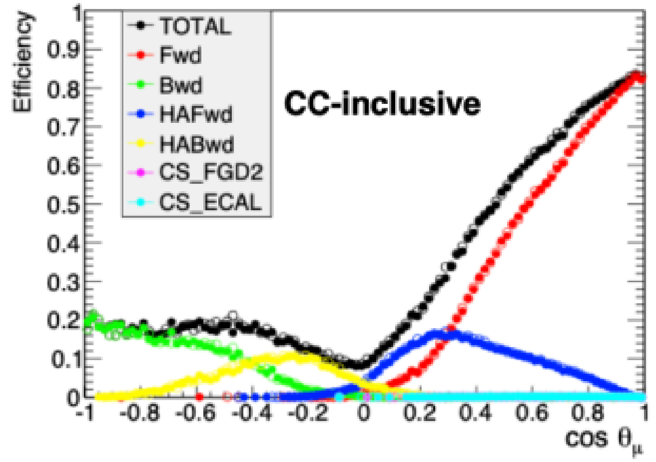

- Improve angular acceptance ν

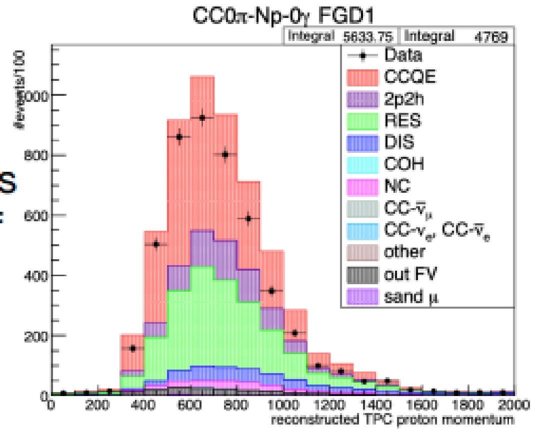

- Better reconstruction and usage of the hadronic part of the interactions!
  - Currently samples are selected according to their topology (0π, 1π, 1p, Nπ, …) but the kinematics of the hadrons is not used in any way in the constraint on flux and x-sec systematics → plenty of additional information to be exploited
  - This is due to both, a low efficiency from ND280 to reconstruct hadrons and the difficulties in modeling the x-sec systematics for the hadronic part
    - With the upgrade we plan to improve the efficiency to reconstruct hadronic part

ND280 Upgrade improvements

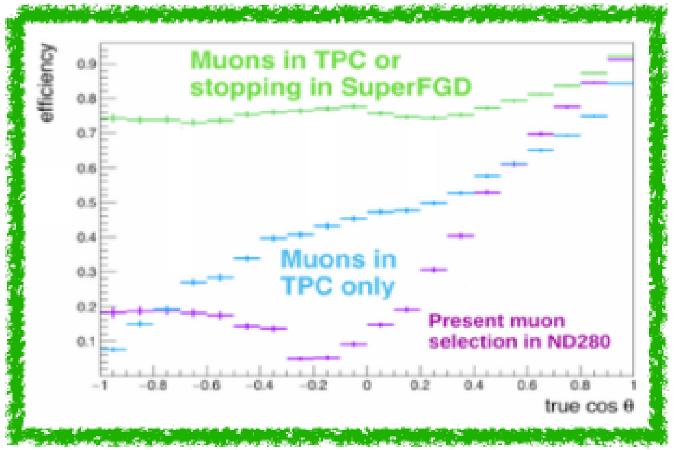

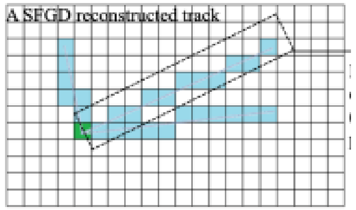

Protons → threshold down to 300 MeV/c
(>500/c MeV with current ND280)

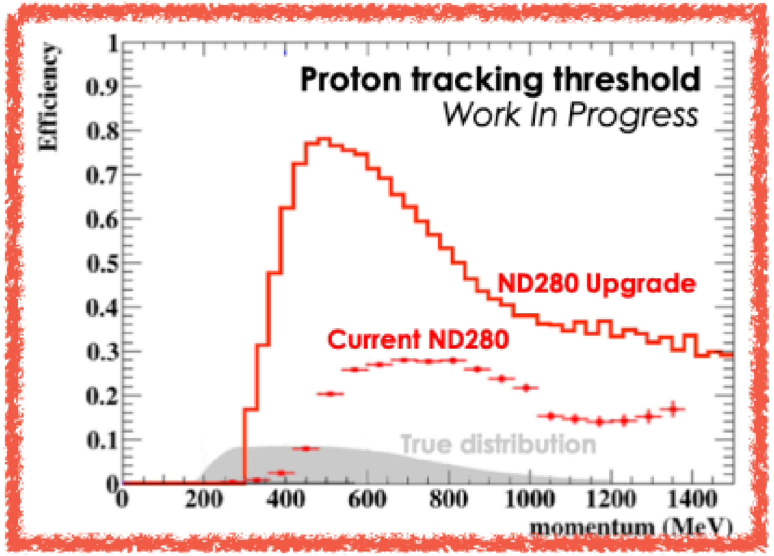

- High-Angle TPCs allow to reconstruct muons at any angle with respect to beam
- Super-FGD allow to fully reconstruct in 3D the tracks issued by ν interactions →lower threshold and excellent resolution to reconstruct protons at any angle
  - Improved PID performances thanks to the high granularity and light yield
- Neutrons will also be reconstructed by using time of flight between vertex of $\bar{\nu}$ interaction and the neutron re-interaction in the detector

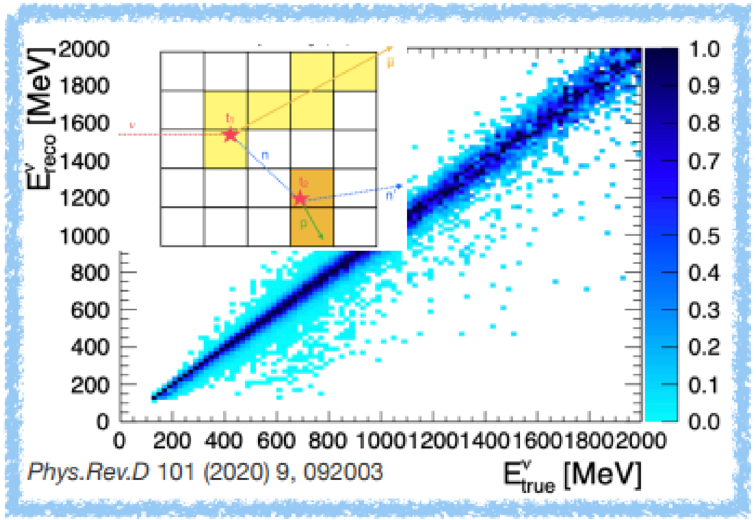

Phys.Rev.D 101 (2020) 9, 092003

Mantle resistance

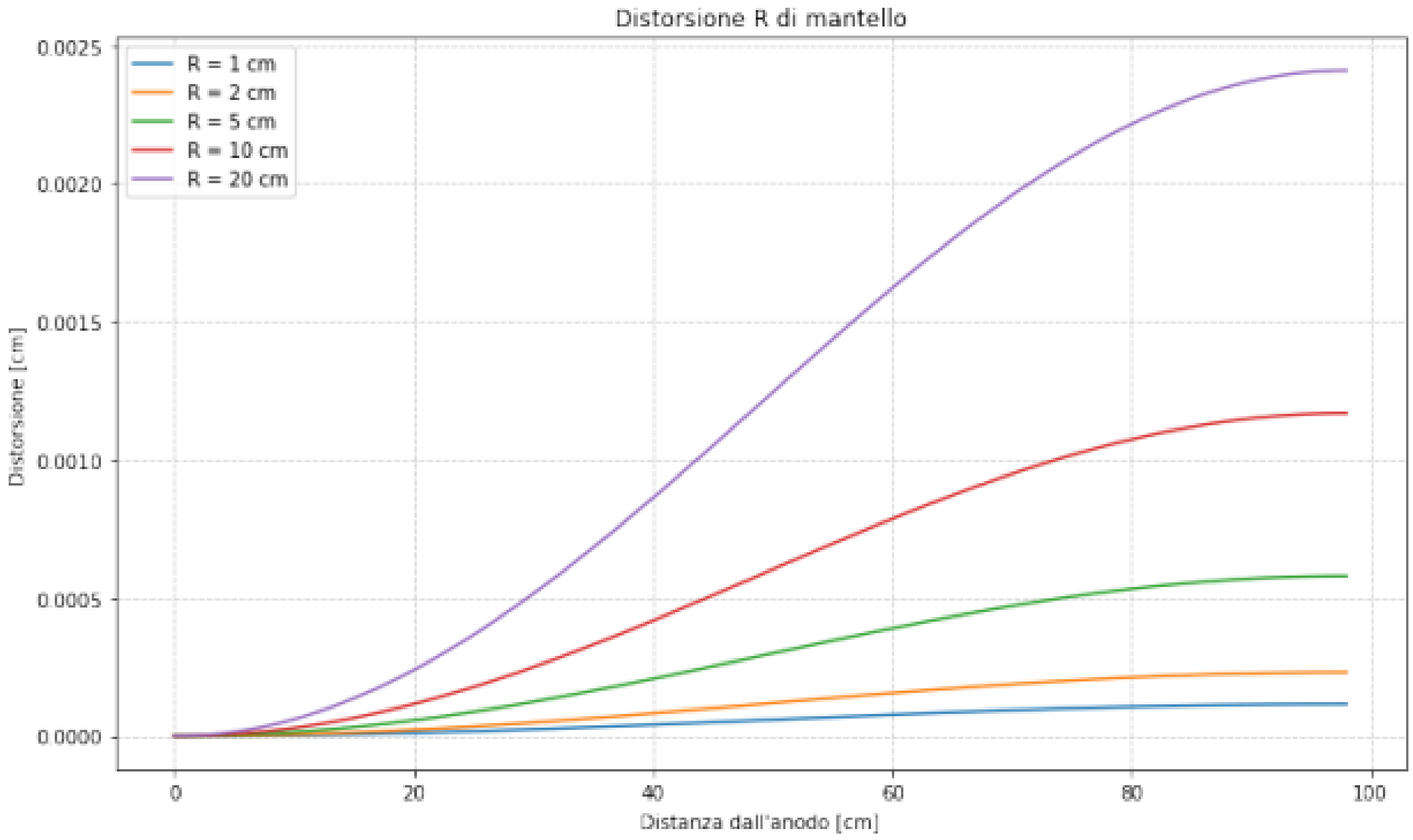

Figura 4.2: Spostamento lungo R del punto di arrivo di un elettrone causato da una resistenza R_{man} di un mantello isolante mille volte il valore della catena di resistori R. La distorsione é mostrata come funzione del punto di partenza z (Distanza dall'anodo).

ERAM Production - about 50 detectors

Crucial steps in production
(needed tuning)

1) Selecting DLC foil resistivity
- Large variations from DLC provider
- Value stable after annealing

2) Gluing steps by Pressing
- DLC to PCB
- Stiffener to DLC-PCB

X-rays Test Bench at CERN
was fundamental to

1) Qualify, characterize and calibrate all prototypes and series ERAMs

2) support the development of detailed ERAM response model

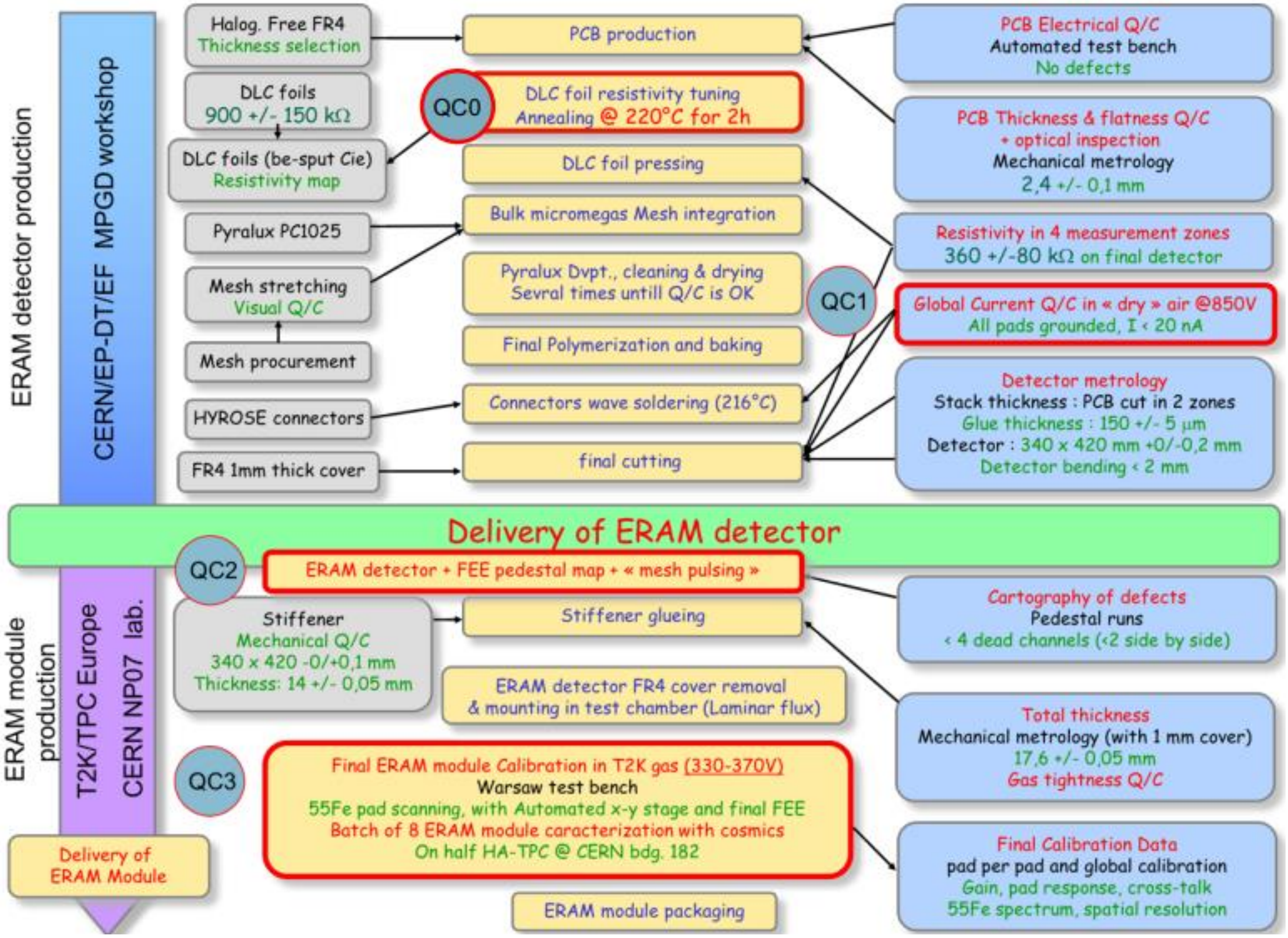

Field Cage assembling, characterization at CERN

Gas contamination from Field Cage – other contaminants

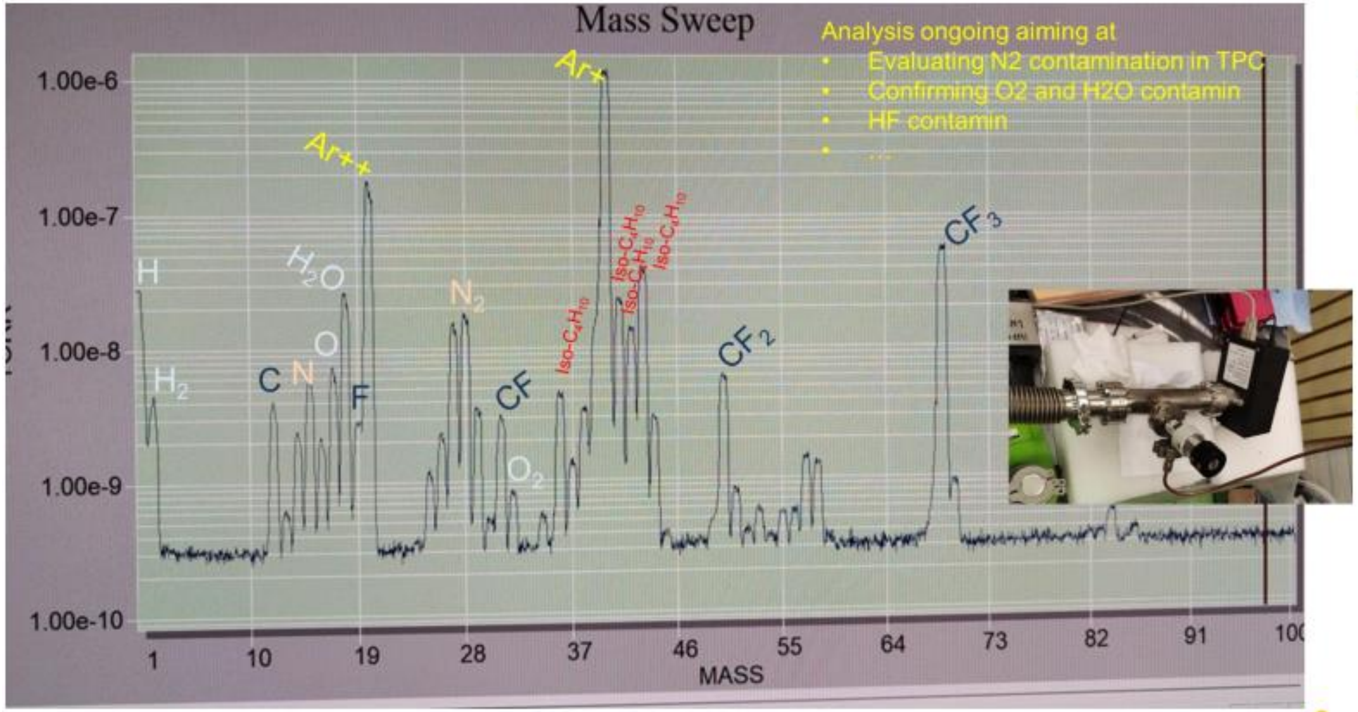

Analysis of gas composition during cosmics test in May

More accurate estimates ongoing

- N2 analysis
- HCl acid
- Evolution in time of components

Main componensts → multi-peaks consistent with ratios found in literature

- H2O (+ HO) contamination ~2% → consistent with other sensors (Vaisala)
- O2 peak below sensitivity → consistent with ppm level → need further checks
- No HF acid apparently (below Ar++)

ERAM Series Production experience

Effect of gas density on (gas) GAIN

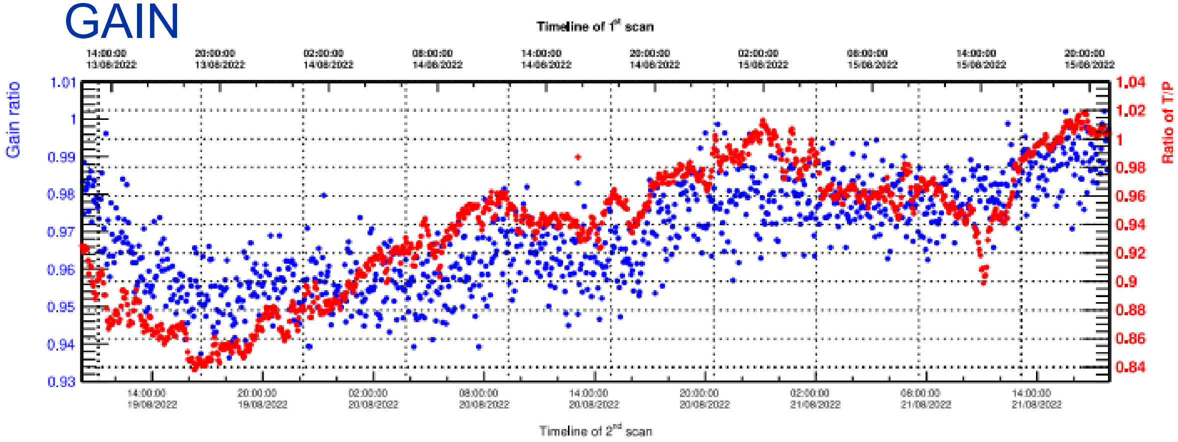

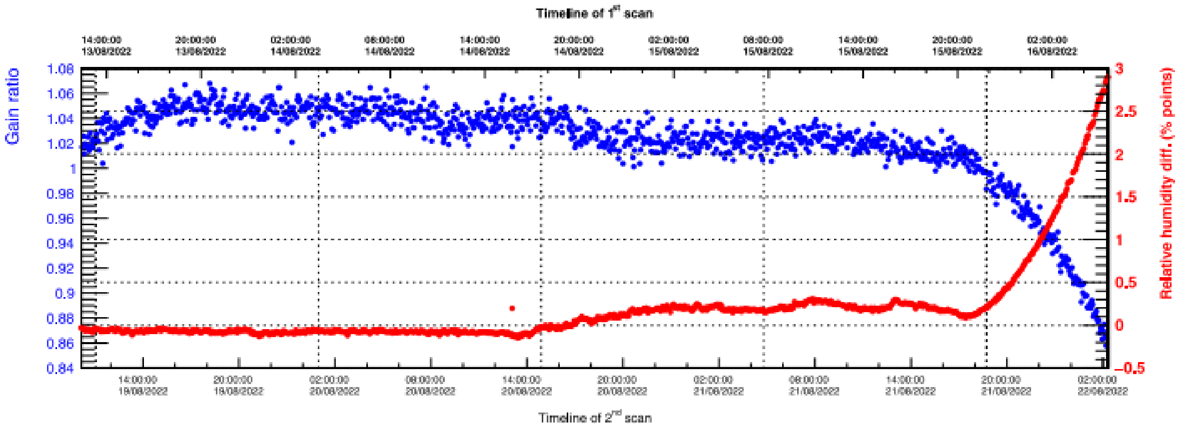

Effect of humidity on (gas) GAIN

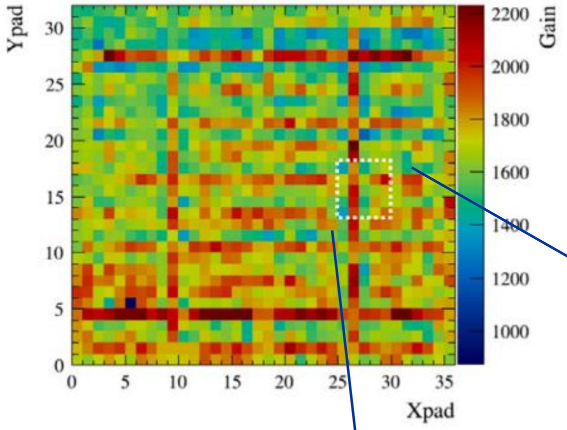

Fine grain scan

GAIN as a function of Pad positic

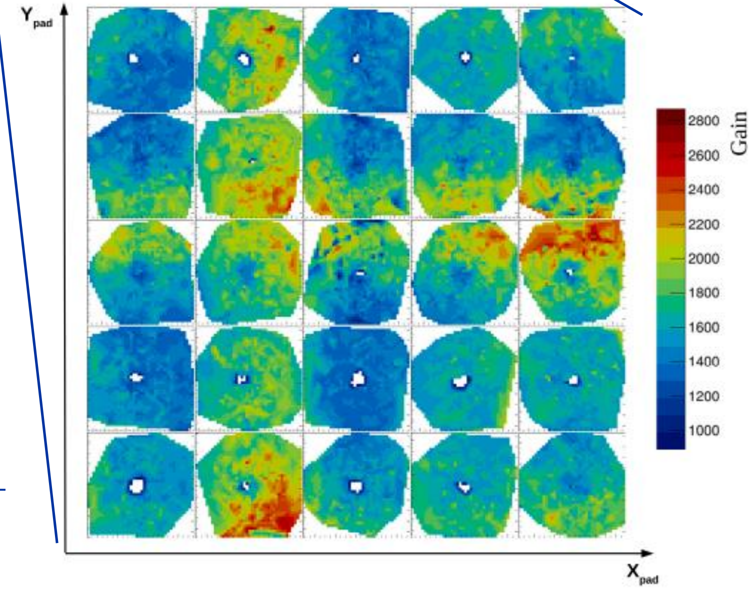

Reconstructing tracks dE/dx

dE/dx – comparison of SWF and XP methods on Test Beam data (4GeV electrons, DESY)

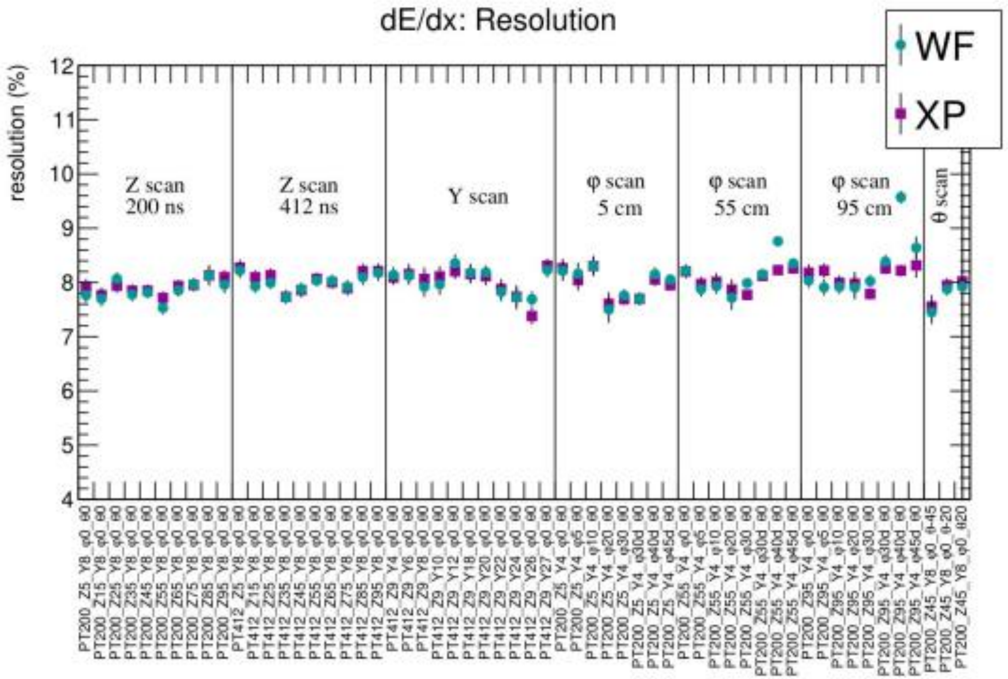

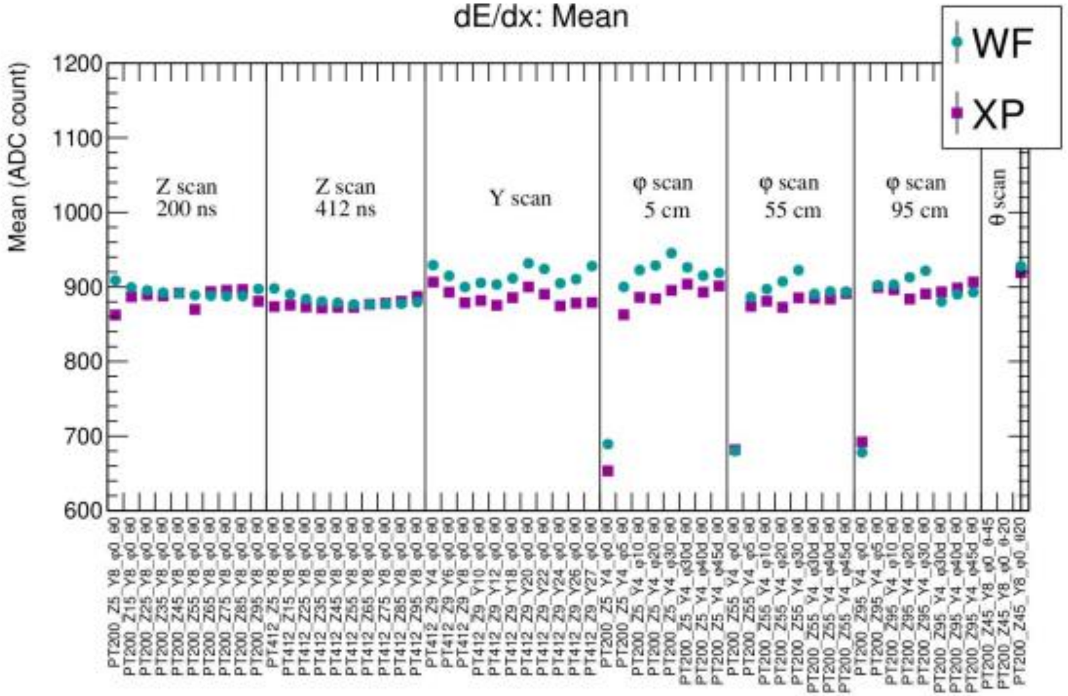

- Very good agreement overall
- Better resolution with XP with diagonal tracks

- Disagreement at small drift distance: reflects the track fitting quality
- Disagreement for Y scan: taken at small drift distance
- Disagreement for diagonal tracks: using only on correction function for WF_{sum} is not suitable

Reconstructing tracks – pattern recognition

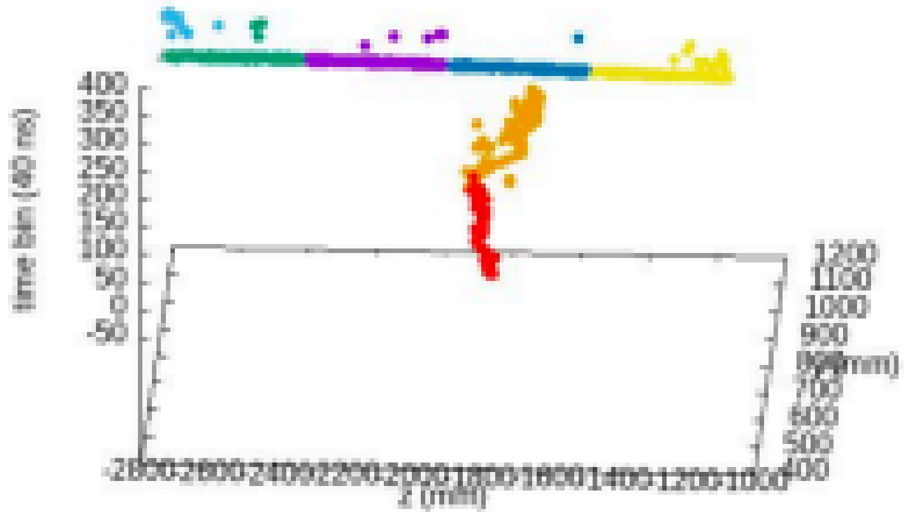

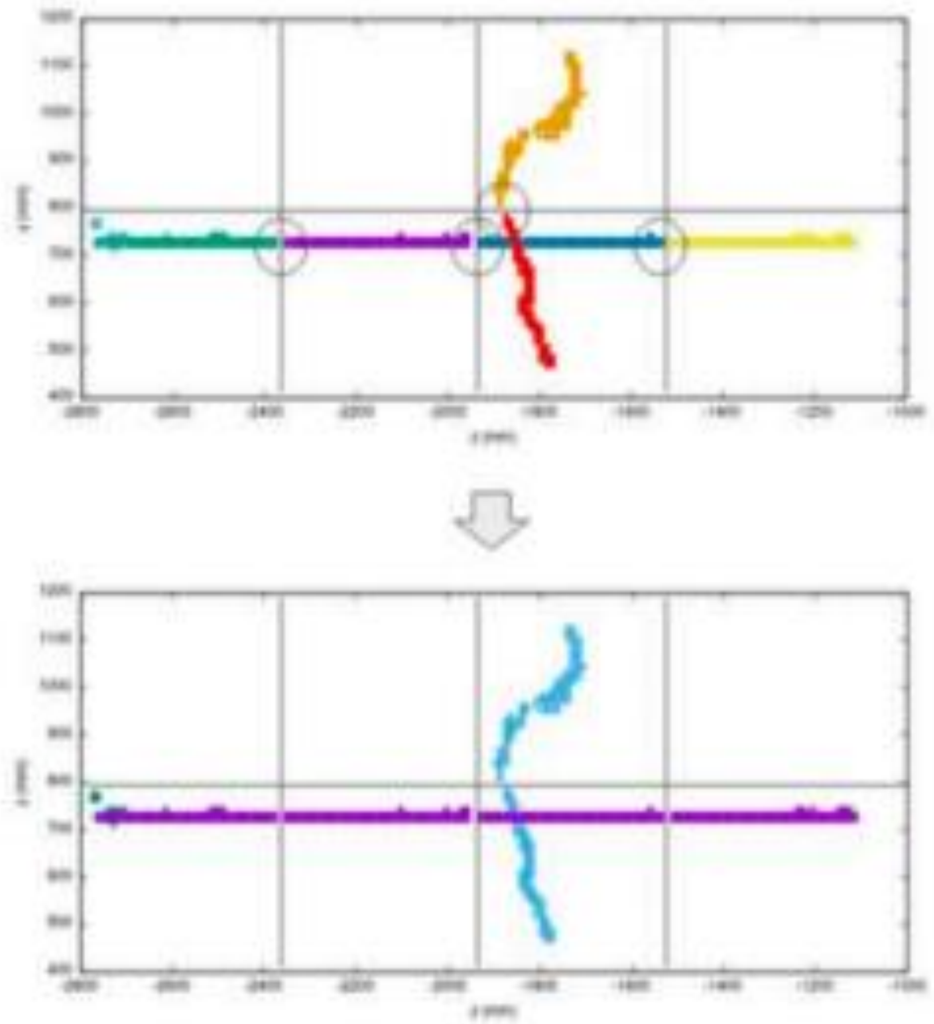

- Time and charge definition for each hit
- Waveform multipeak search in order to differentiate vertices and crossing trajectories
- Merging between different ERAMs and End Plates

Reconstructing tracks – trajectory fitting

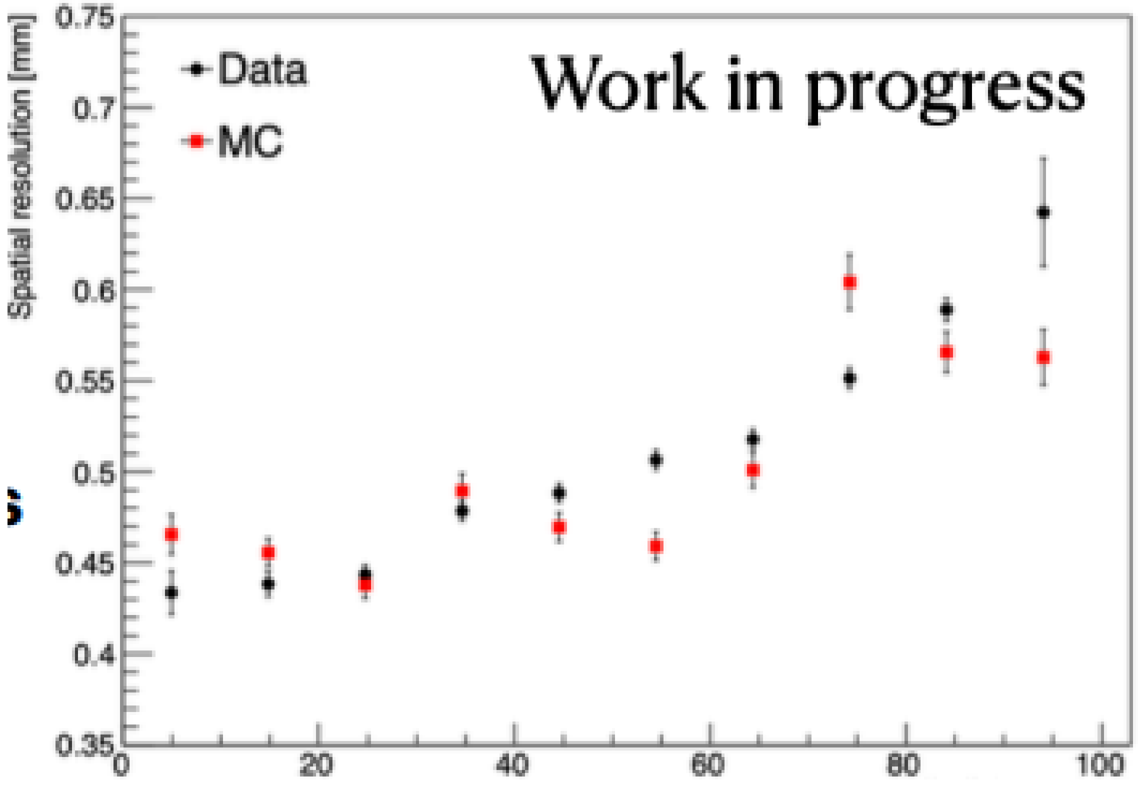

Spatial resolution ~500 μm with muons

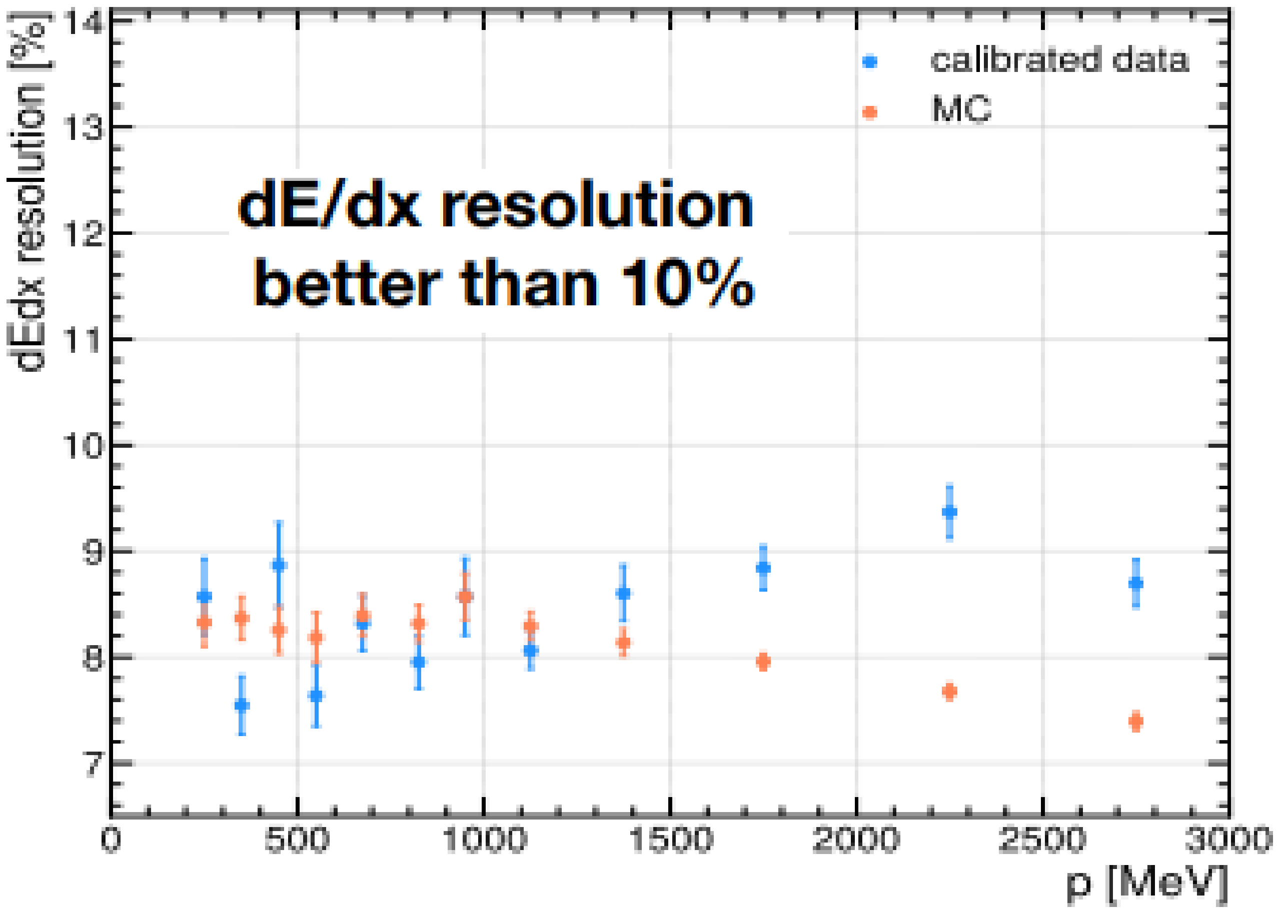

T2K gas properties

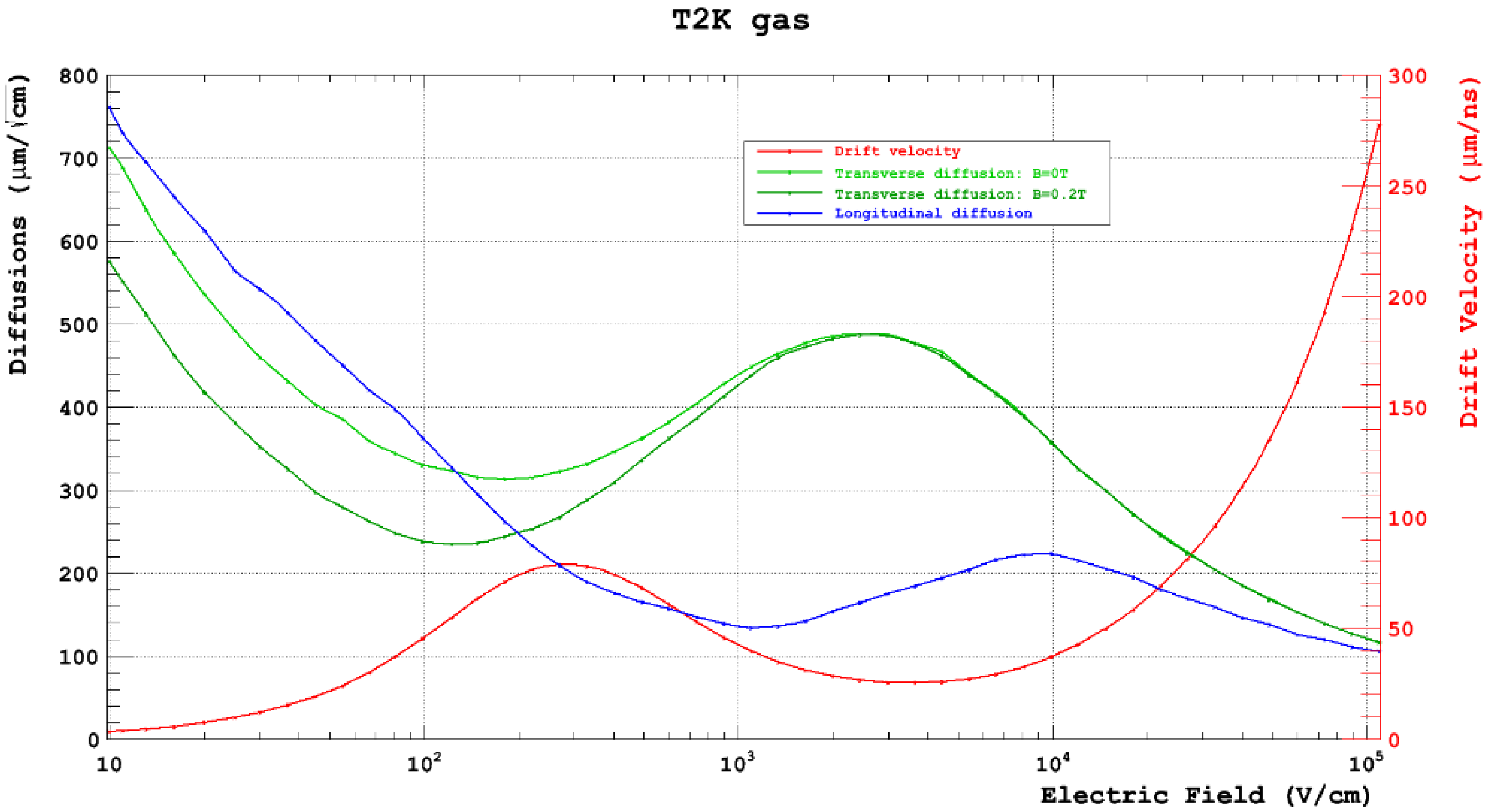

Ref: S. Joshi (Irfu/PhD)

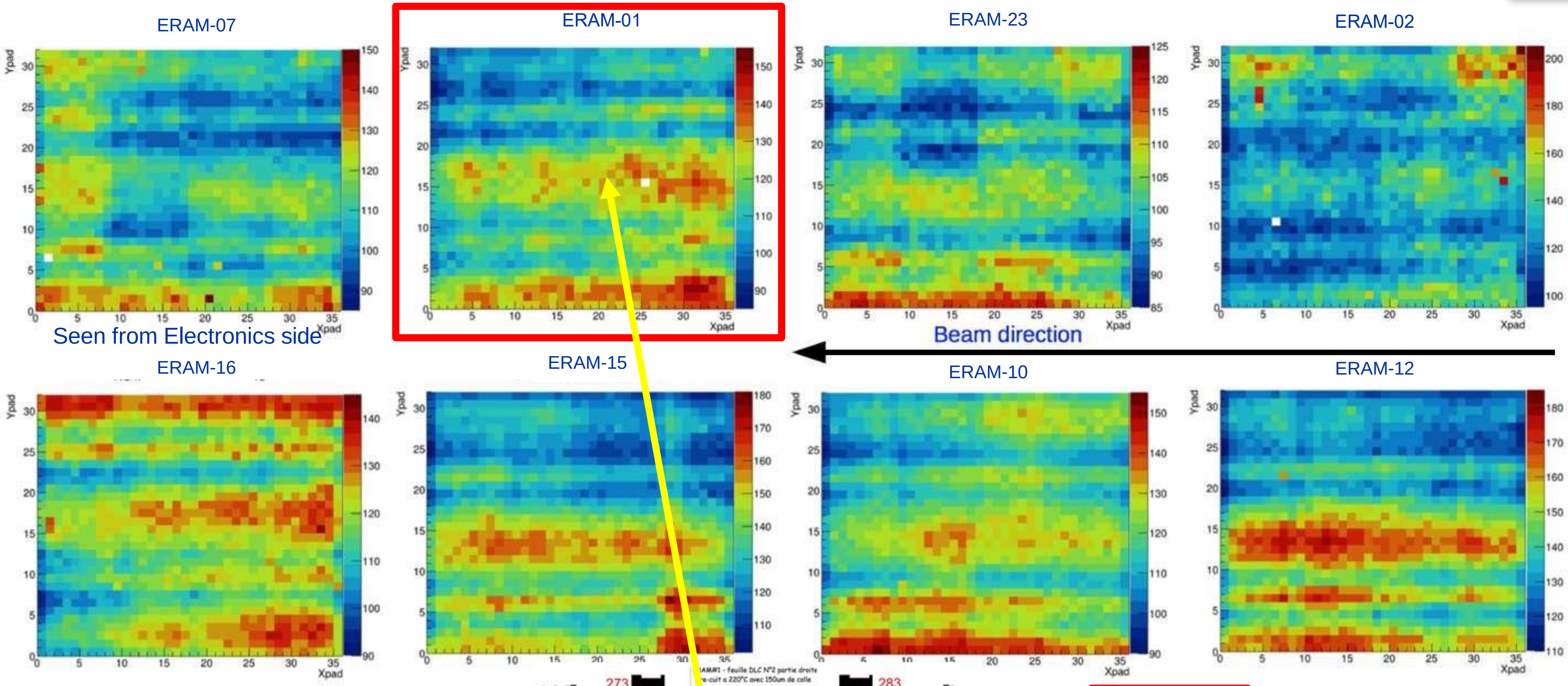

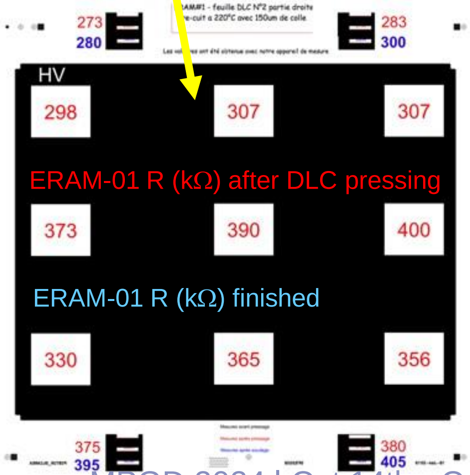

RC is derived from the fit of the pad signal waveforms datas (leading and neighbours) with the complete modelization of the detector response

ERAM	RC_{mean} (ns/mm²)	$Gain_{mean}$	
01	116.9	1944	
02	128.6	1736	
03	116.4	1987	
07	111.8	1898	
10	120.9	1697	
12	145.4	1635	
15	135.1	1629	
16	120.4	1705	
18	68.98	1277	~1/2 RC as expected
23	101.6	1393	
29	102	1318	~ RC as expected
30	114.3	1161	

RC is quite well correlated to the measured DLC resistivity

Spare

Just in Case

bottom layer.

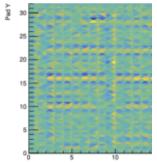

Figure 31: A map of gain non-uniformit
shift of the mean amplitude reconstruct
pad under study with respect to the me

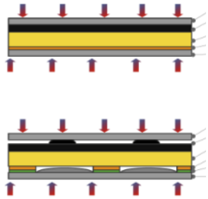

Figure 32: Schematic view of the DLC
resulting in the non-uniformities obser
The arrows represent the mechanical
when the soldermask is removed and re

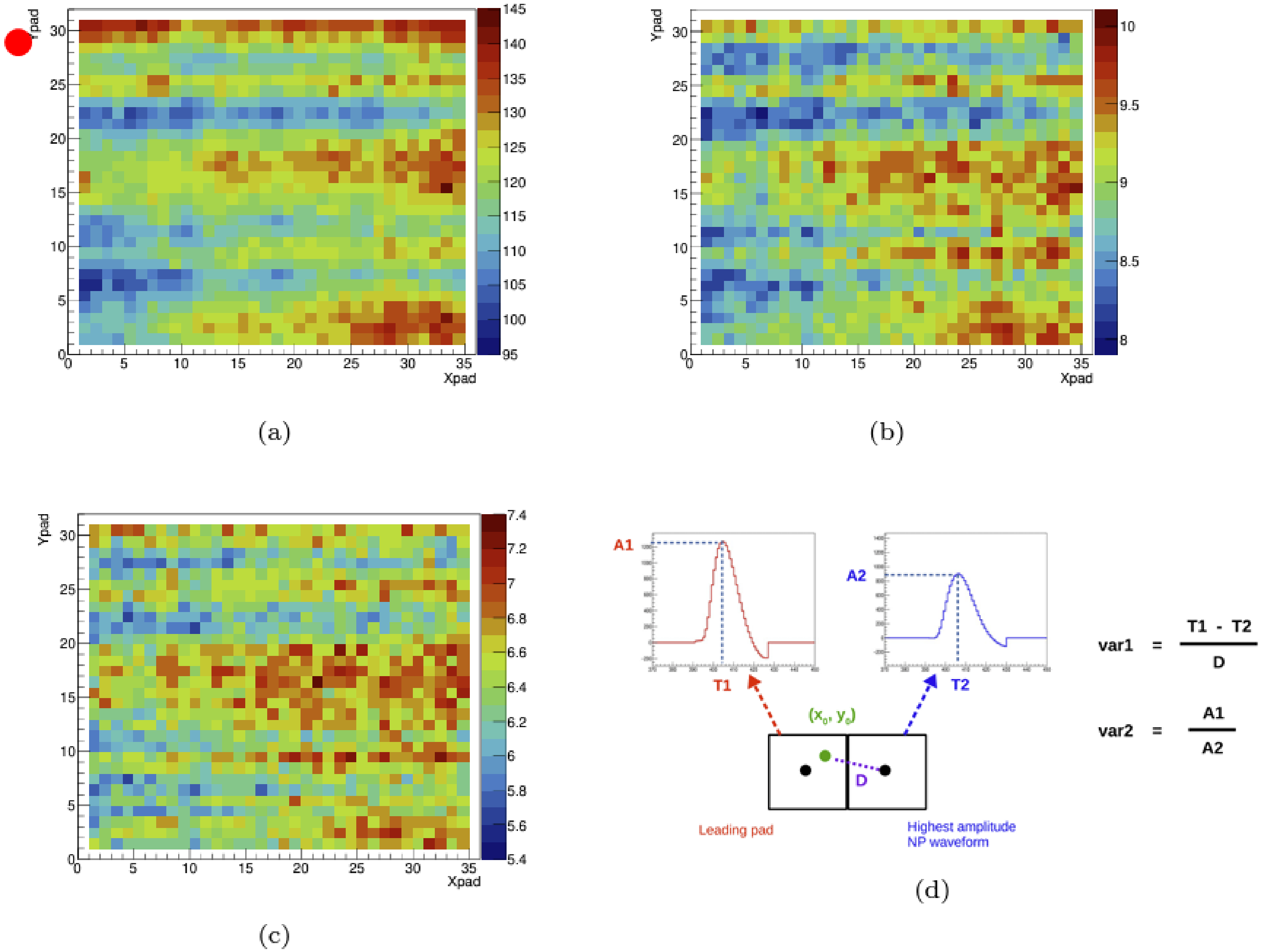

Figure 23: Comparing the features of an *RC* map (a) with the maps of two different basic-level variables (b) and (c) for ERAM-16. Variables var1 and var2 described in plot (d) are used to construct the maps (b) and (c) respectively.

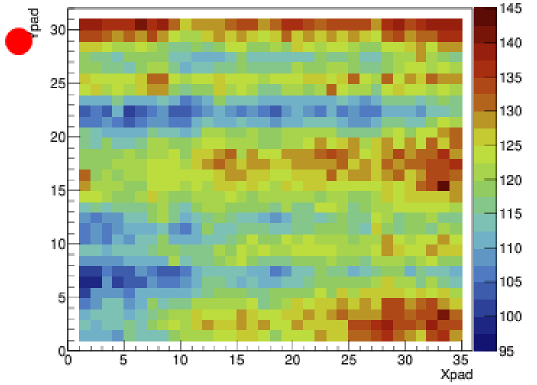

(a)

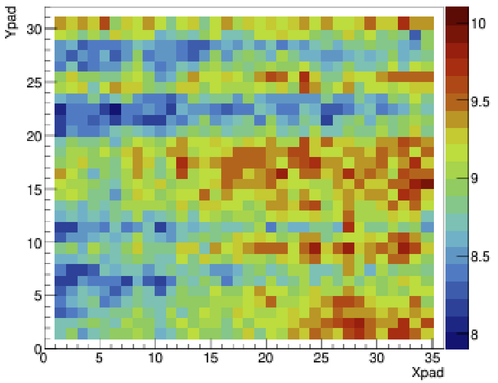

(b)

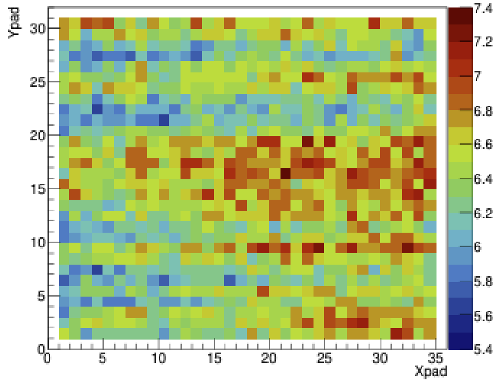

(c)

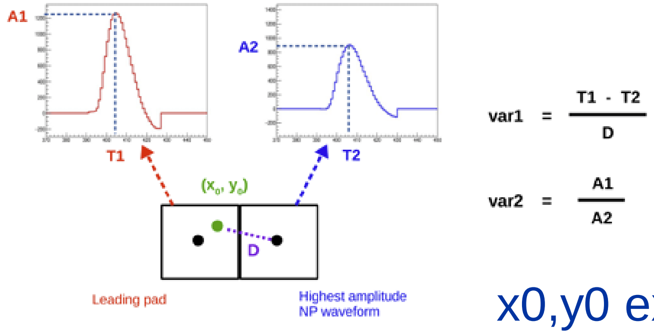

(d)

x0,y0 extracted by baricentrum
Fit independent

Figure 23: Comparing the features of an *RC* map (a) with the maps of two different basic-level variables (b) and (c) for ERAM-16. Variables var1 and var2 described in plot (d) are used to construct the maps (b) and (c) respectively.

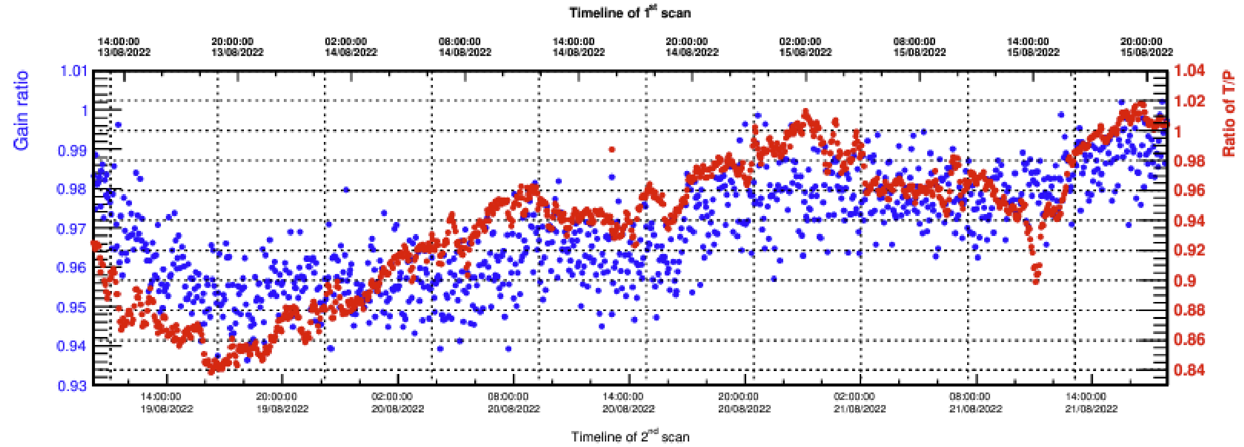

Figure 35: Effect of T/P on gain of an ERAM. The top and bottom x-axes represent the timelines of the two full detector scans.

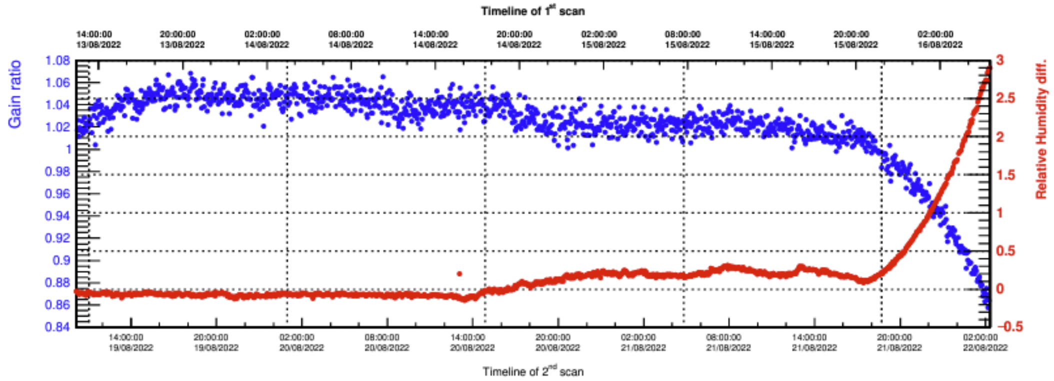

Figure 36: Effect of relative humidity on gain of an ERAM. The top and bottom x-axes represent the timelines of the two full detector scans.

Table 7. Typical Electrical Properties of Kapton® Type HN and HPP-ST Films

Property Film Gauge	Typical Value		Test Condition	Test Method
Dielectric Strength	**V/µm (kV/mm)**	**(V/mil)**		
25 µm (1 mil)	303	(7700)	60 Hz	
50 µm (2 mil)	240	(6100)	1/4 in electrodes	ASTM D-149
75 µm (3 mil)	201	(5,100)	500 V/sec rise	
125 µm (5 mil)	154	(3900)		
Dielectric Constant				
25 µm (1 mil)	3.4			
50 µm (2 mil)	3.4		1 kHz	ASTM D-150
75 µm (3 mil)	3.5			
125 µm (5 mil)	3.5			
Dissipation Factor				
25 µm (1 mil)	0.0018			
50 µm (2 mil)	0.0020		1 kHz	ASTM D-150
75 µm (3 mil)	0.0020			
125 µm (5 mil)	0.0026			
Volume Resistivity	Ω•cm			
25 µm (1 mil)	1.5×10^{17}			
50 µm (2 mil)	1.5×10^{17}			ASTM D-257
75 µm (3 mil)	1.4×10^{17}			
125 µm (5 mil)	1.0×10^{17}			

Although a-C:H and ta-C belong to the same material family, they are not produced by the same coating process.
a-C:H is achieved by PECVD (Plasma Enhanced Chemical Vapor deposition) in a gaseous environment.
Whereas ta-C is produced by PVD-arc (Physical Vapor deposition arc) from a solid carbon target.
PVD-arc technology enables the production of a ta-C coating with a higher percentage of sp^3 hybridization without hydrogen and providing a higher hardness.

- **Thermal annealing of ta-C is well known**
  - a-C:H as well. But,
  - *"Thermal annealing of a-C:H also reduces the stress, as in ta-C. However, as the bonding in a-C:H is less stable during annealing, annealing is less useful in this case."*
- Mechanism described
  - Thermal annealing converts a small fraction of sp^3 (2%) to sp^2
    - Distance between atoms is different between sp^2 and sp^3
    - New sp^2 structure has aligned electron orbitals
  - The conversion causes **exponential decrease** in resistivity
  - Compressive stress relieved by new sp^2 structure with electron orbitals aligned

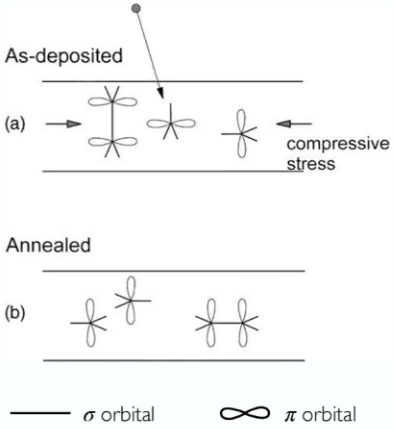

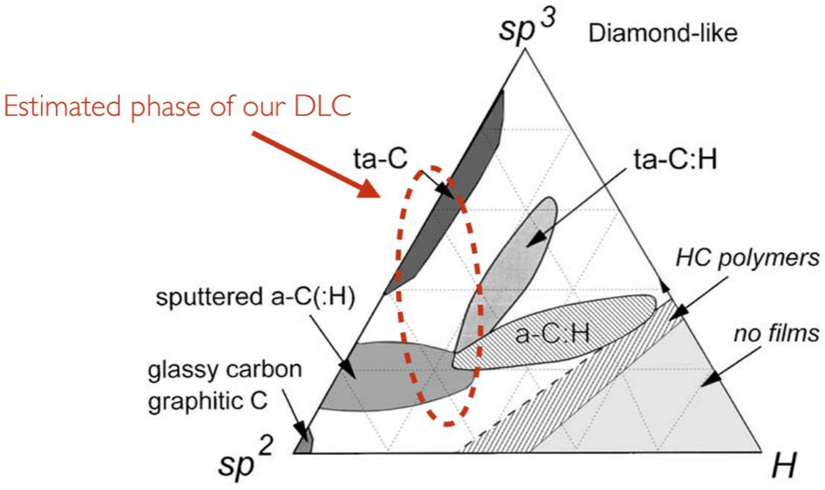

Kensuke Yamamoto[A]

S. Ban[A], W. Li[A], A. Ochi[B], W. Ootani[A], A. Oya[A], H. Suzuki[B], M. Takahashi[B]
([A]The University of Tokyo, [B]Kobe University)

DOCA
(Distance Of Closest Approach)

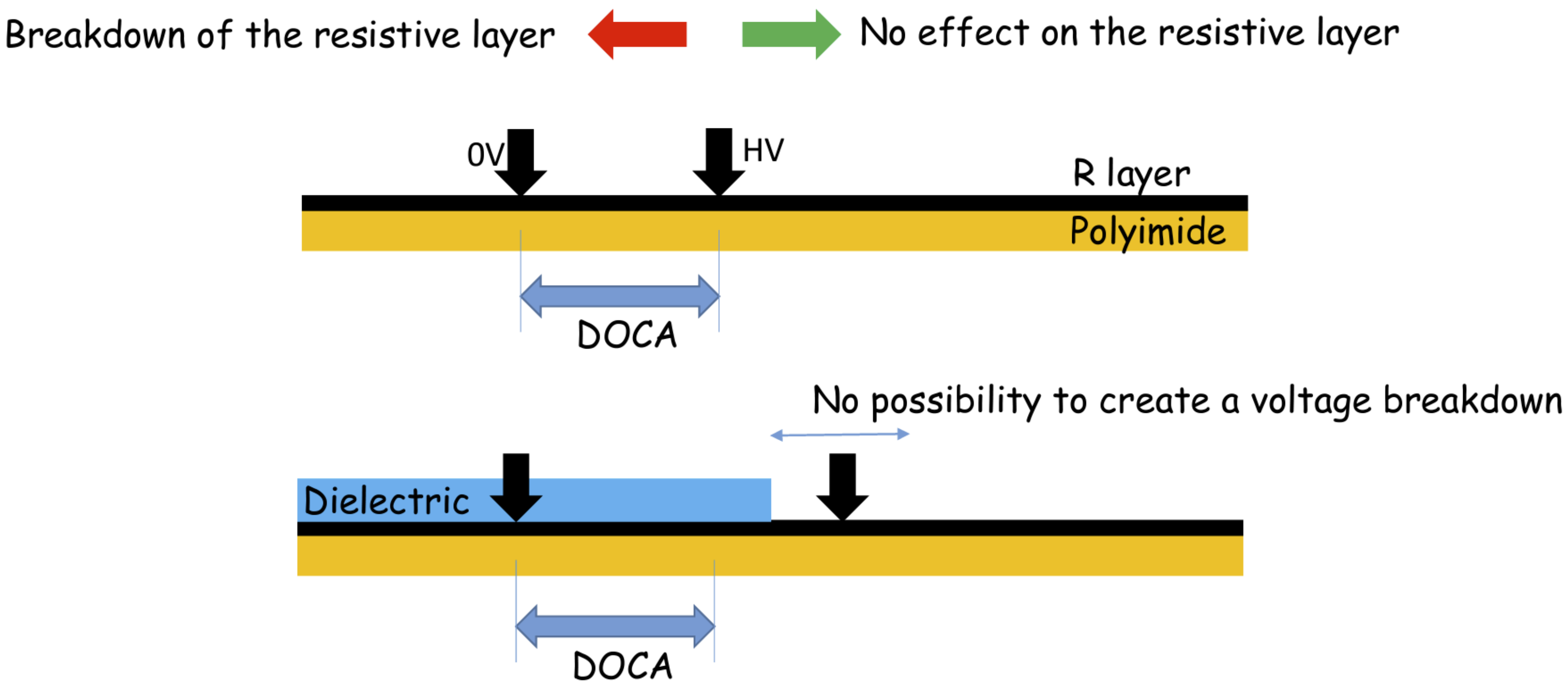

A breakdown of the resistive layer means creating a low Ohmic channel in the layer

T2K+SK joint analysis

- T2K has good sensitivity to δ_{CP} but mild sensitivity to mass ordering
- SK has good constraint on mass ordering but not on δ_{CP}
- Adding SK atmospheric sample allows to break the degeneracies between the CP violation parameter δ_{CP} and the mass ordering → boost sensitivity to CP

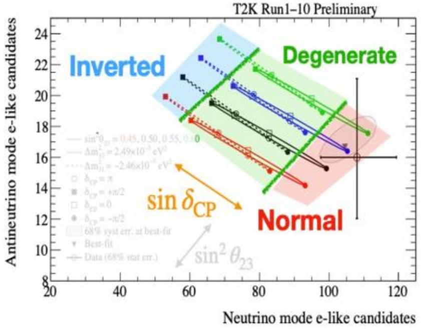

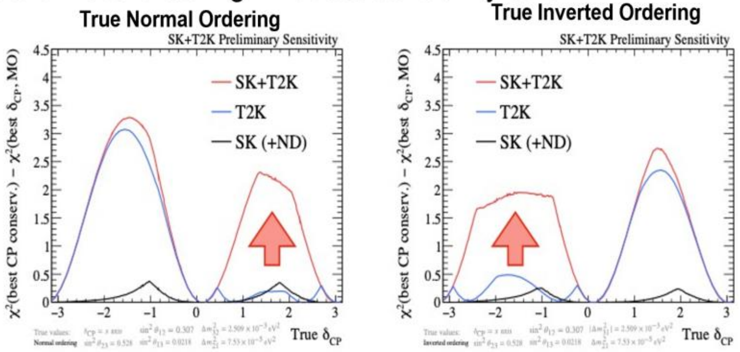

Both experiments individually prefer normal ordering and δCP~-π/2, T2K prefers upper octant, SK prefer lower octant

We performed Bayesian and Frequentist analyses → frequentist analyses shown today

The CP-conserving value of the Jarlskog invariant is excluded with a significance between 1.9 and 2 σ

Mass ordering and θ_{23} octant

- Slight preference for normal ordering and upper octant but none of them is significant
  - Bayes factor NO/IO = 3.3
  - Bayes factor (θ_{23}>0.5)/(θ_{23}<0.5) = 2.6

	$\sin^2\theta_{23} < 0.5$	$\sin^2\theta_{23} > 0.5$	Sum
NH ($\Delta m^2_{32} > 0$)	0.23	0.54	0.77
IH ($\Delta m^2_{32} < 0$)	0.05	0.18	0.23
Sum	0.28	0.72	1.00

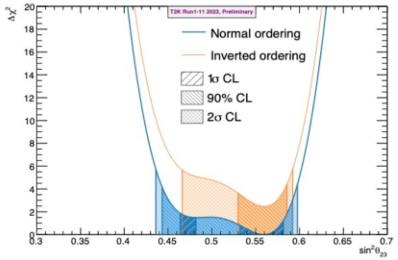

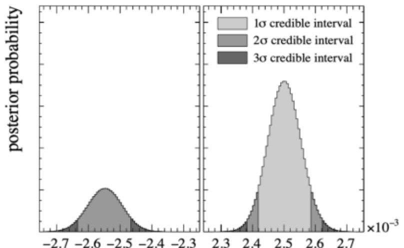

NOvA-T2K joint fit: takeaways

Advancing the precision frontier on $|\Delta m^2_{32}|$
<2% measurement!

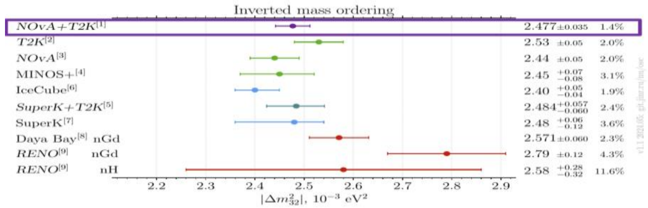

Mild preference for Inverted Ordering but influenced by θ_{13} constraint

NOvA+T2K only	NOvA+T2K + 1D θ_{13}	NOvA+T2K + 2D (θ_{13}, Δm^2_{32})
IO (71%)	IO (57%)	NO (59%)

- NOvA & T2K's **first joint results**:
  - Yield **strong constraint on Δm^2_{32}**
  - Weakly prefer IO or NO depending on which reactor constraint is applied
  - **Strongly favor CP violation in Inverted Ordering**
- Collaborations in active discussion about **joint fit next steps**

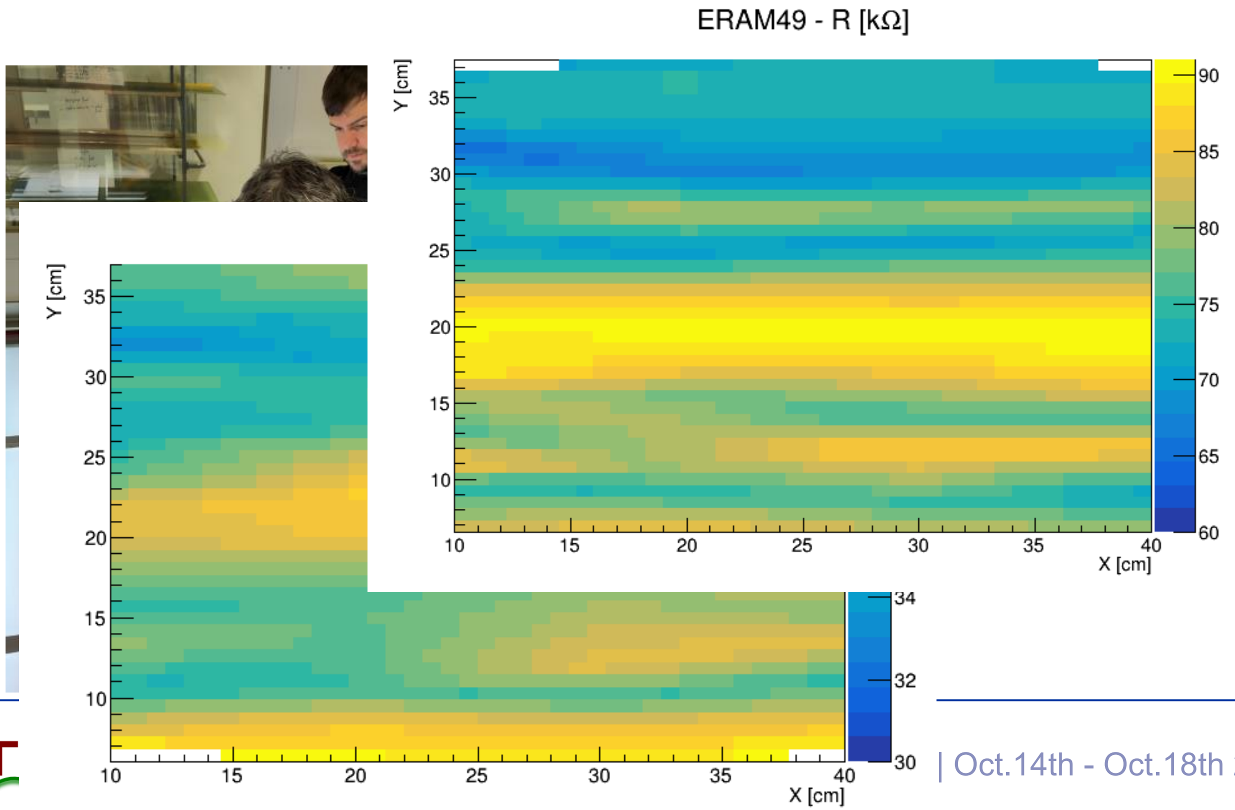

R inhomogeneities in the sputtering are clearly visible in the direction perpendicular to the drum rotation axis.

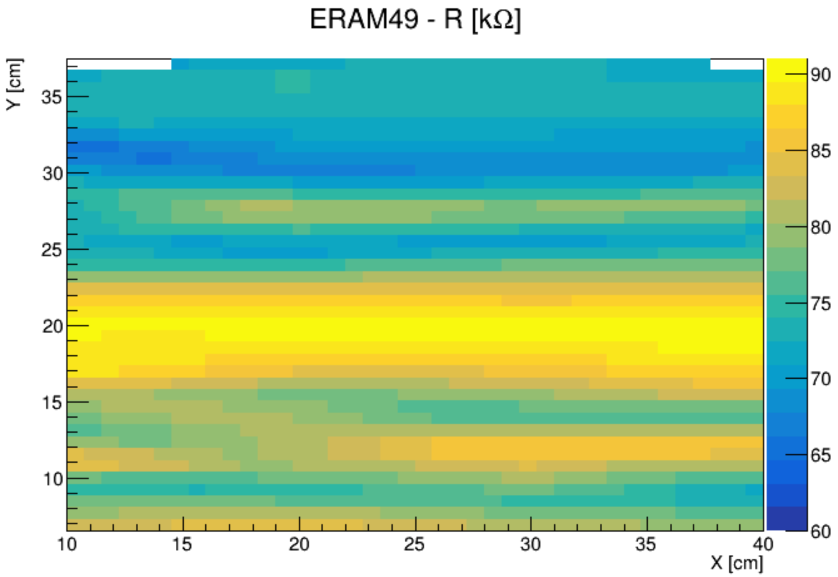

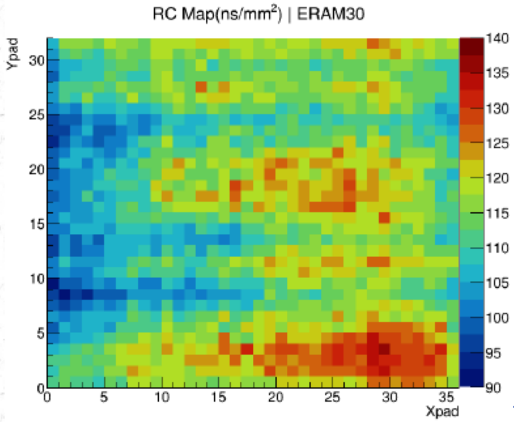

And t
the re
meas
very
const
thickr
insula

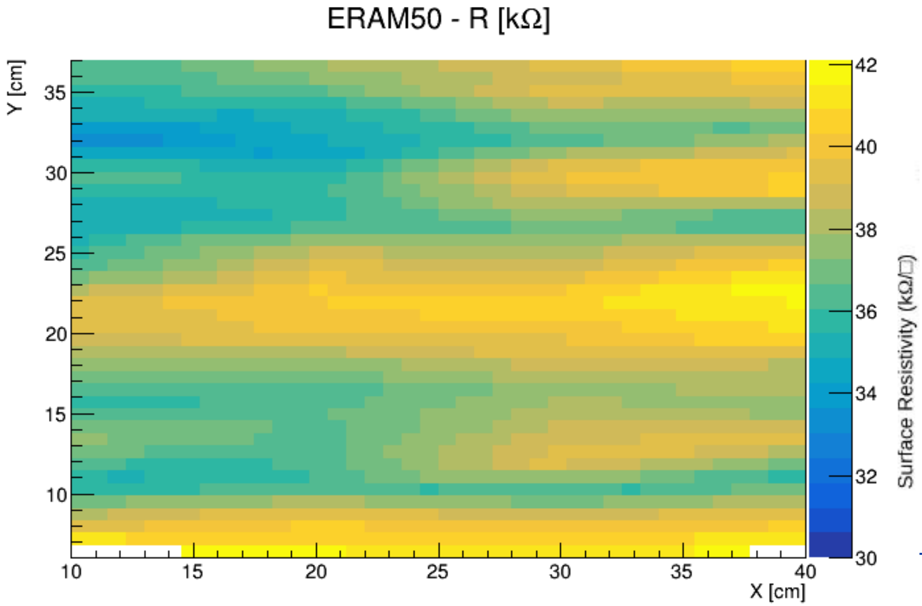

R inhomogeneities in the sputtering are clearly visible in the direction perpendicular to the drum rotation axis.

The ND280 experiment: High Angle TPC highlights

- Field Cage (FC)
  - Assembly and layout
  - Production
  - Characterization and Quality Assessment
    - Mechanical
    - Electrical

An outsider: Field Cage 0 ?
Electrical Issues, what we understood…
and learnt

Insulation issue in full scale FC0 prototype

Innermost layers stack (first full-scale FC prototype)

Material	Thickness
Cu Strips on Kapton foil (electrodes)	Cu 17μm / Kapton 50μm / Cu 17μm
"Coverlay" (strip insulation / protection)	Glue 20μm / Kapton 25μm
Aramid Fiber Fabric (Twaron™)	2mm

Current drawn by voltage divider starting in large excess wrt nominal at power on and slowly decreasing to lower value but still in excess

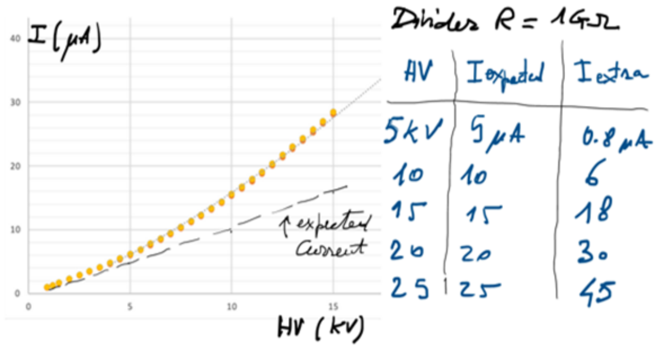

I_{extra} increasing non linearly with voltage

Current drawn by voltage divider starting in large excess wrt nominal at power on and slowly decreasing to lower value but still in excess

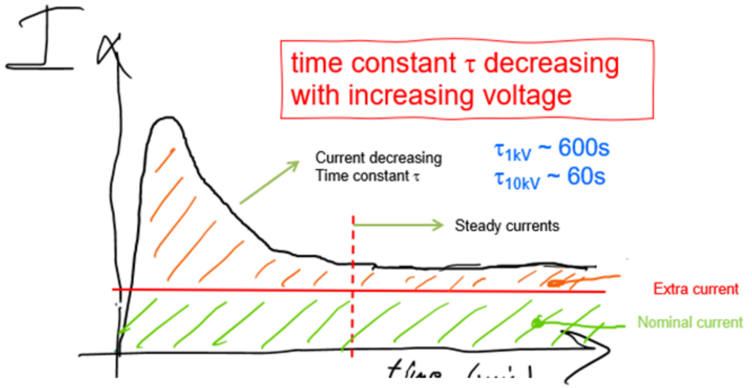

Observed extra-currents in excess w. r. t. expected from voltage divider

Insulation issue in full scale FC0 prototype

Innermost layers stack (first full-scale FC prototype)

Material	Thickness
Cu Strips on Kapton foil (electrodes)	Cu 17µm / Kapton 50µm / Cu 17µm
“Coverlay” (strip insulation / protection)	Glue 20µm / Kapton 25µm
Aramid Fiber Fabric (Twaron™)	2mm

Strip-Strip Potential difference of the strips @ 5kV

Voltage difference between Field strips (every 5 strips)
ie V_1-V_2, V_5-V_6, V_{10}-V_{11}, … V_1 = anode, V_{196} = cathode

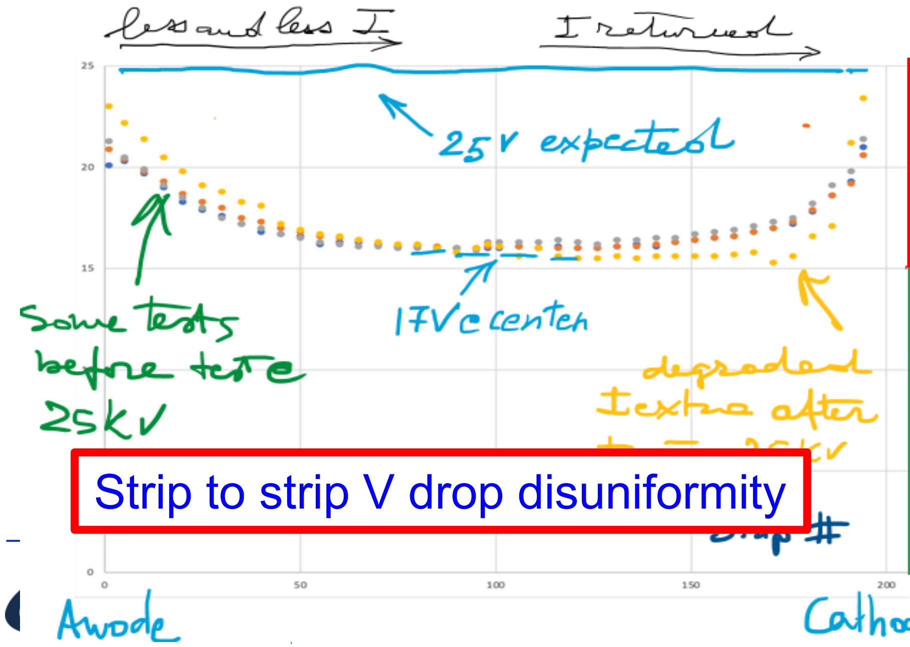

Strip to strip V drop disuniformity

Behaviour explained by either
1) Voltage divider resistors values not uniform along the divider or ~~(ruled out)~~
2) current diverted from voltage divider (drawn from strips) more and more along the 1st half of the cage going from anode to cathode returned to the divider (pulled by the strips) in the 2nd half

Measurement of Surface resistance of strip foil (resistors removed)

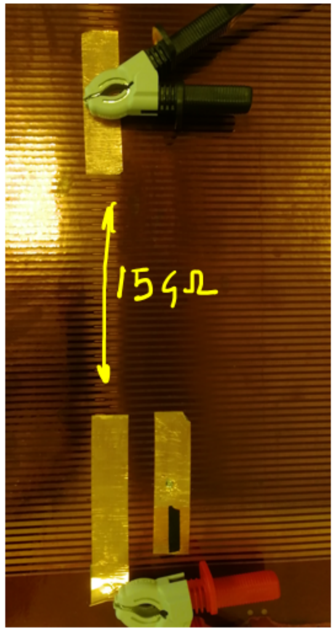

Resistance between single strips is very high O(TΩ)
…but when joining some tens of strips to form a single large electrode then finite resistances are measured

Example: measured R ~15 GΩ @ 1kV between two electrodes formed by 20Field+20Mirror strips each
(surface of single electrode is huge ~ 0.5m²)
! No voltage divider there, ie all strips disconnected

Resistance is
- Independent of the distance between electrodes
- Linearly dependent of the number of the strips

→ not a surface resistance !

Measured R is rising with time (slow) up to saturation
- when repeating measurement, go faster to saturation
- when inverting polarity of electrodes, slow again

→ looks like due to dielectric polarization / relaxation
→ or capacitor charging trough high resistance

Find similar value of Resistance for same dimension electrodes formed in the Field Cage and on a strips foil when aluminum foil is placed underneath the foil → next

Buried resistive layer: a possible explanation

All observed features could be explained by the combination of two factors:

1) Presence of a resistive layer buried underneath the Kapton coverlay layer protecting the mirror Mirror strip
2) Low resistivity of the coverlay Kapton layer

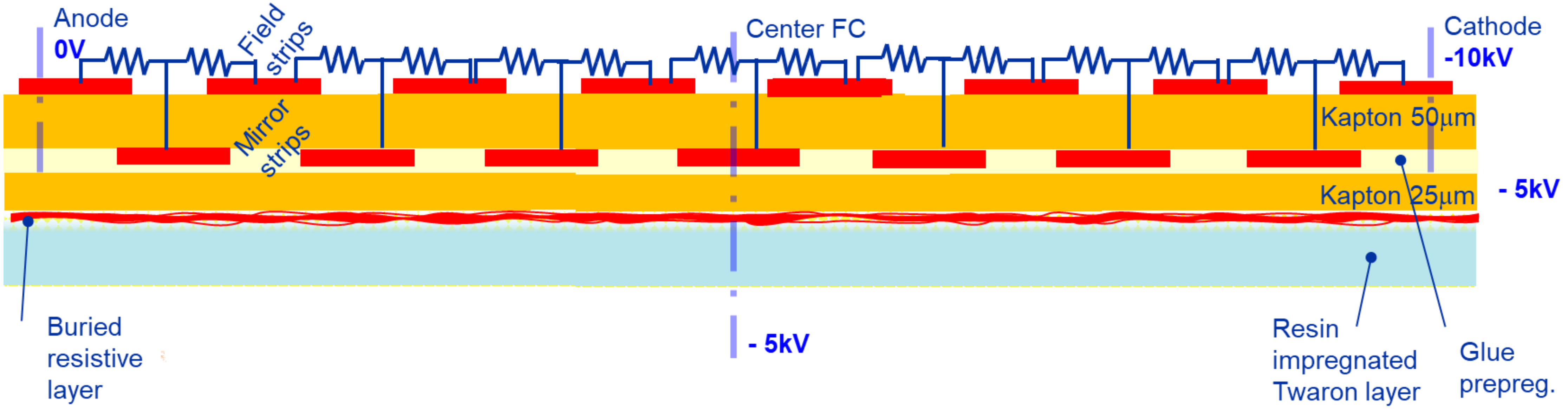

Buried resistive layer: phenomenology

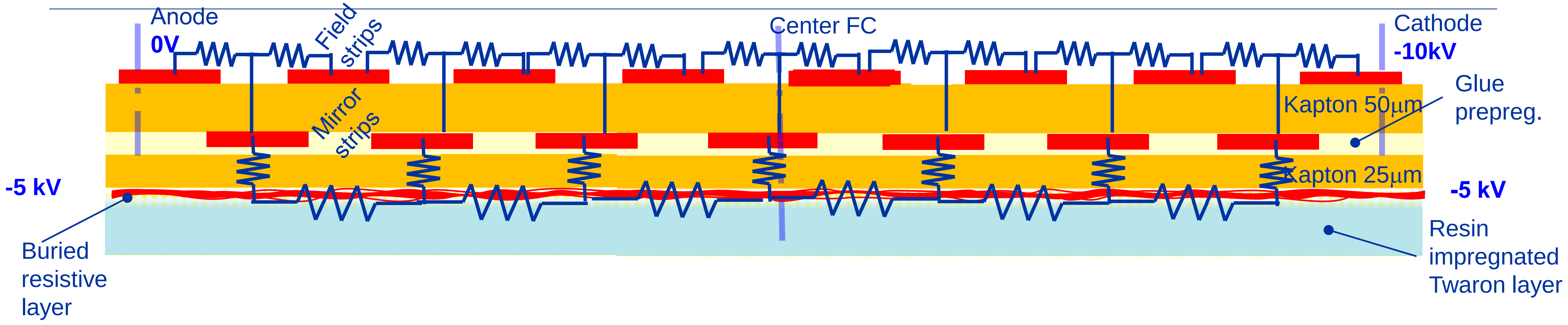

After applying HV after applying HV (eg -10kV) to the cathode, two phases:

1) **Transient state**: in time scale depending on the contaminated layers resistivity (in our case very short O(10s) time scale) the buried resistive layer become ~ equipotential (setting at intermediate potential -5kV) by drawing charge from the strips

2) **Steady state**: Mirror strips on the Anode, first half convey current to the buried layer, while mirror strips on the Cathode side draw currents from the buried layer

Buried resistive layer: phenomenology

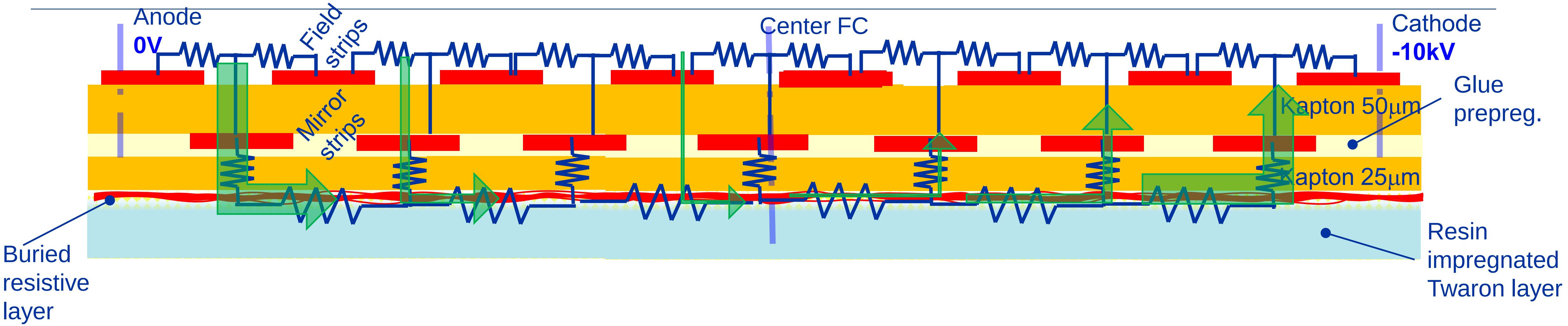

After applying HV after applying HV (eg -10kV) to the cathode, two phases:

1) **Transient state**: in time scale depending on the contaminated layers resistivity (in our case very short O(10s) time scale) the buried resistive layer become ~ equipotential (setting at intermediate potential -5kV) by drawing charge from the strips

2) Steady state: Mirror strips on the Anode, first half convey current to the buried layer, while mirror strips on the Cathode side draw currents from the buried layer

Buried resistive layer: verification

In fact we **verified** the following

1) Coverlay Kapton volume resistivity ~ 1GΩcm much lower than datasheet)
2) Twaron layer facing the coverlay featured surface resistivity ~ 1G/□

Both features could on turn be explained by the **accidental use of antistatic spray (resistive)** on the back of the strip foil (ie on the coverlay) after the strip foil was fixed on the Mould, in order to keep the huge foil surface ($5m^2$) clean from dust and other possible contaminants. The spray contaminated both the Kapton coverlay (being very easily adsorbed) and the innermost layer of the Twaron (being mixed with the resin which impregnates the fiber fabric, during the Twaron lamination phase)

We could not exclude alternative sources of contamination affecting the resin and making it resistive (eg presence of water if epoxy not treated in vacuum after mixing)

Buried resistive layer: electrical model

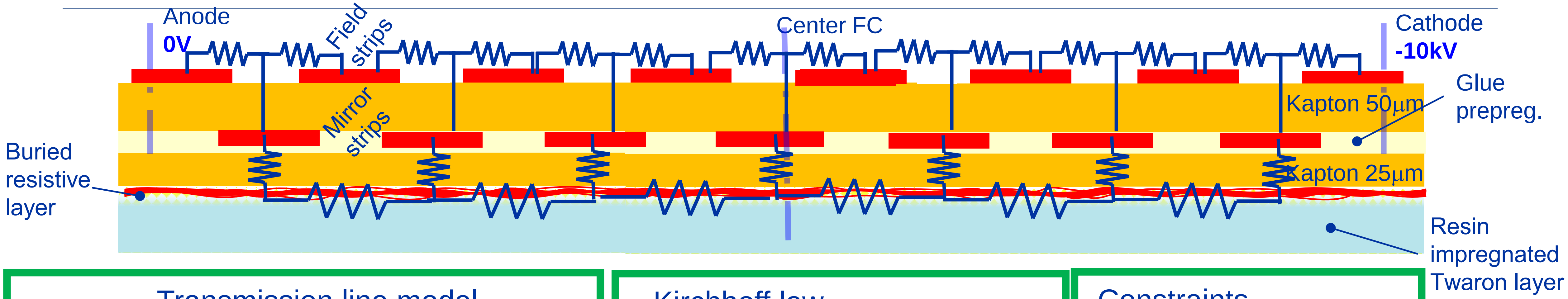

Transmission line model

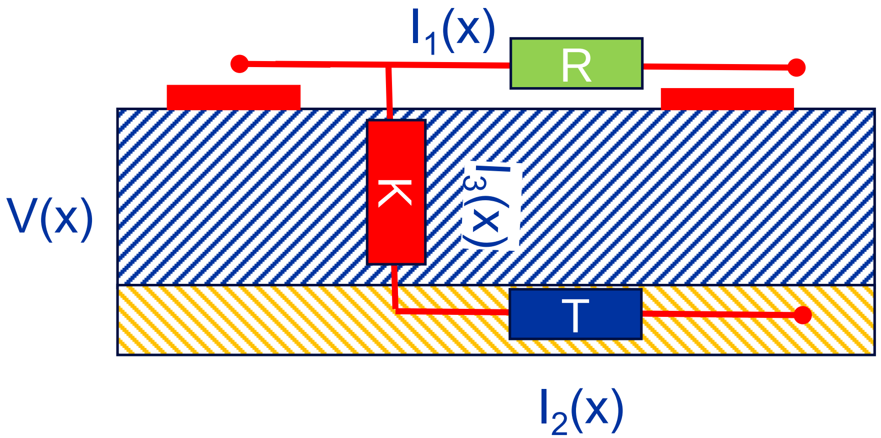

Kirchhoff law

[K]=Ωm, [T]=Ω/□,[R]= Ω

$$T\frac{dI3(x)}{dx} + RI1(x) - KI2(x) = 0$$

$$\frac{dI_1(x)}{dx} + I_3(x) = 0$$

$$\frac{dI_2(x)}{dx} - I3(x) = 0$$

Constraints

$I_1(0)+I_3(0)=I_1(L) - I_3(L)$

$I_2(0)=I_3(0)$ $I_2(L)=-I_3(L)$

Symmetry $\frac{dI_3(x=L/2)}{dx}=0$ (middle of the cage)

Buried resistive layer: electrical model results

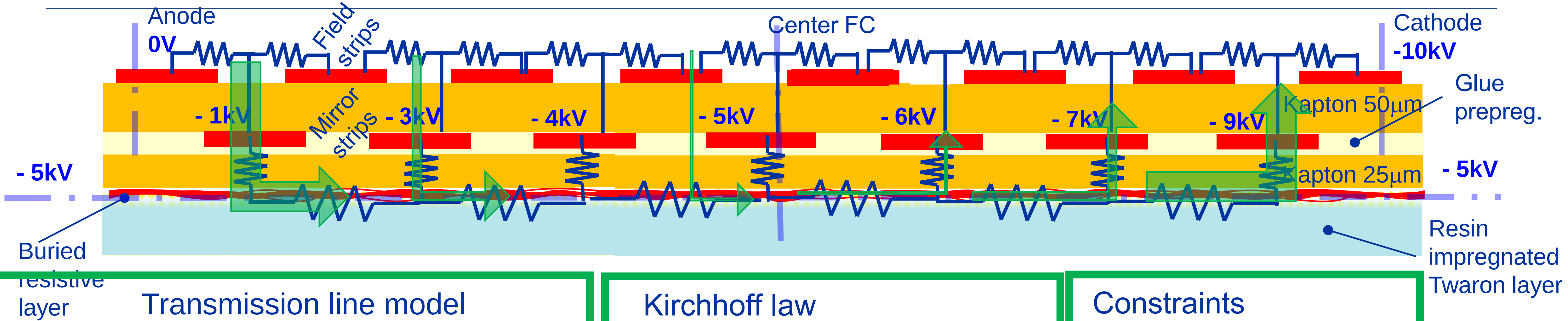

Transmission line model

Kirchhoff law

Constraints

The electric field in the active volume is non uniform

Due to the spurious voltage divider formed in parallel to the regular one

V(x)

Buried resistive layer: electrical model results

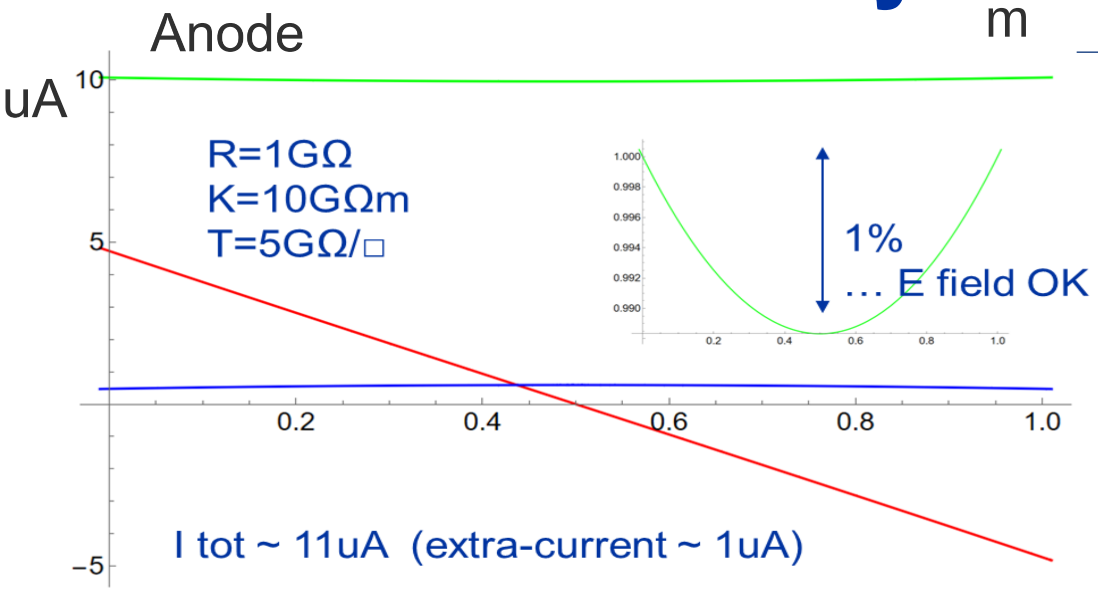

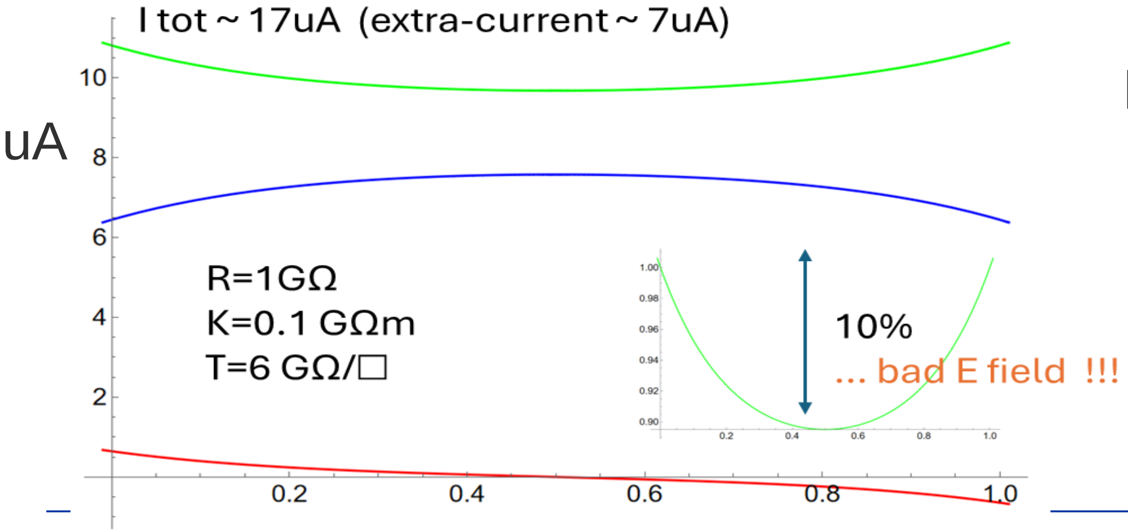

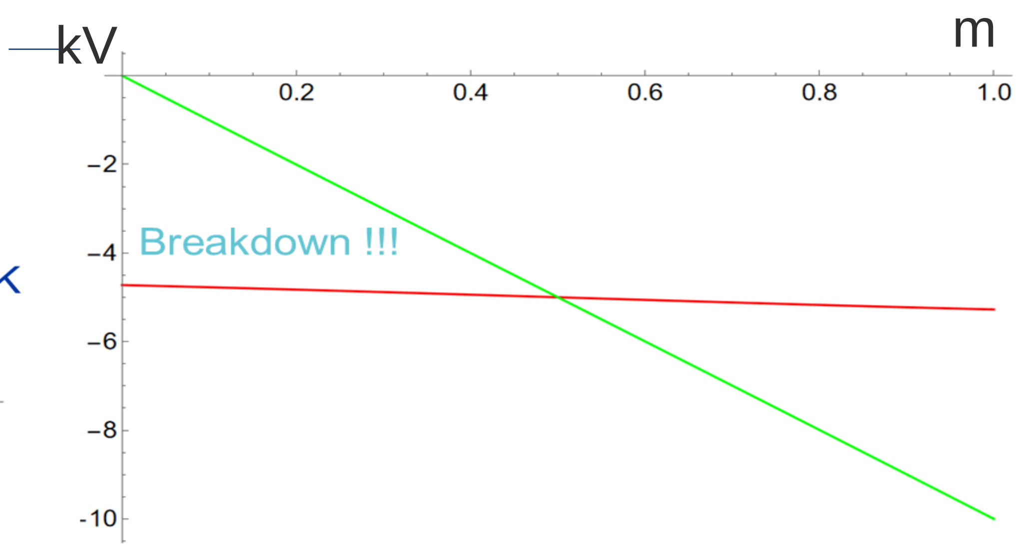

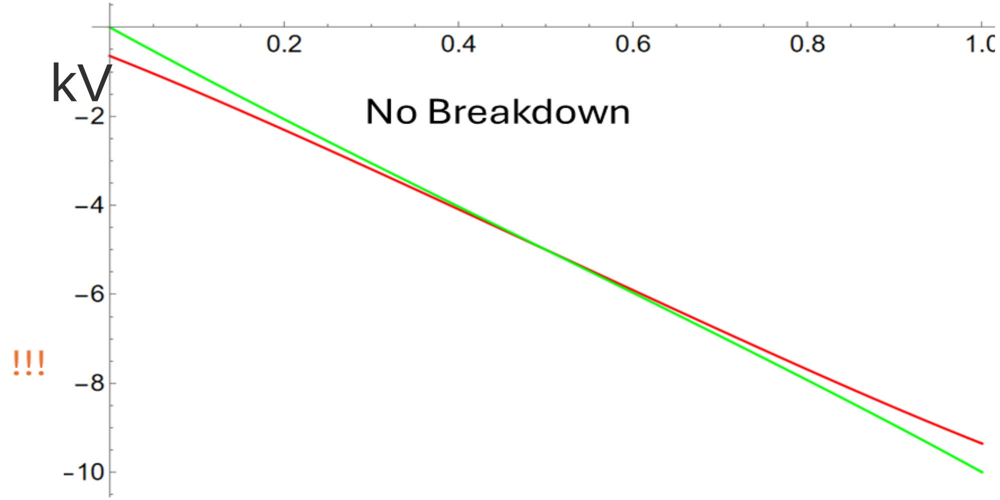

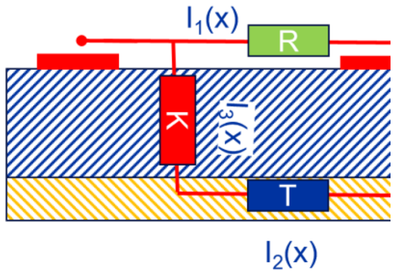

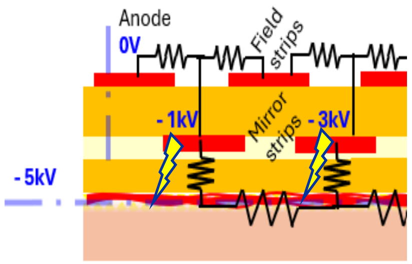

Buried resistive layer: fit to the data

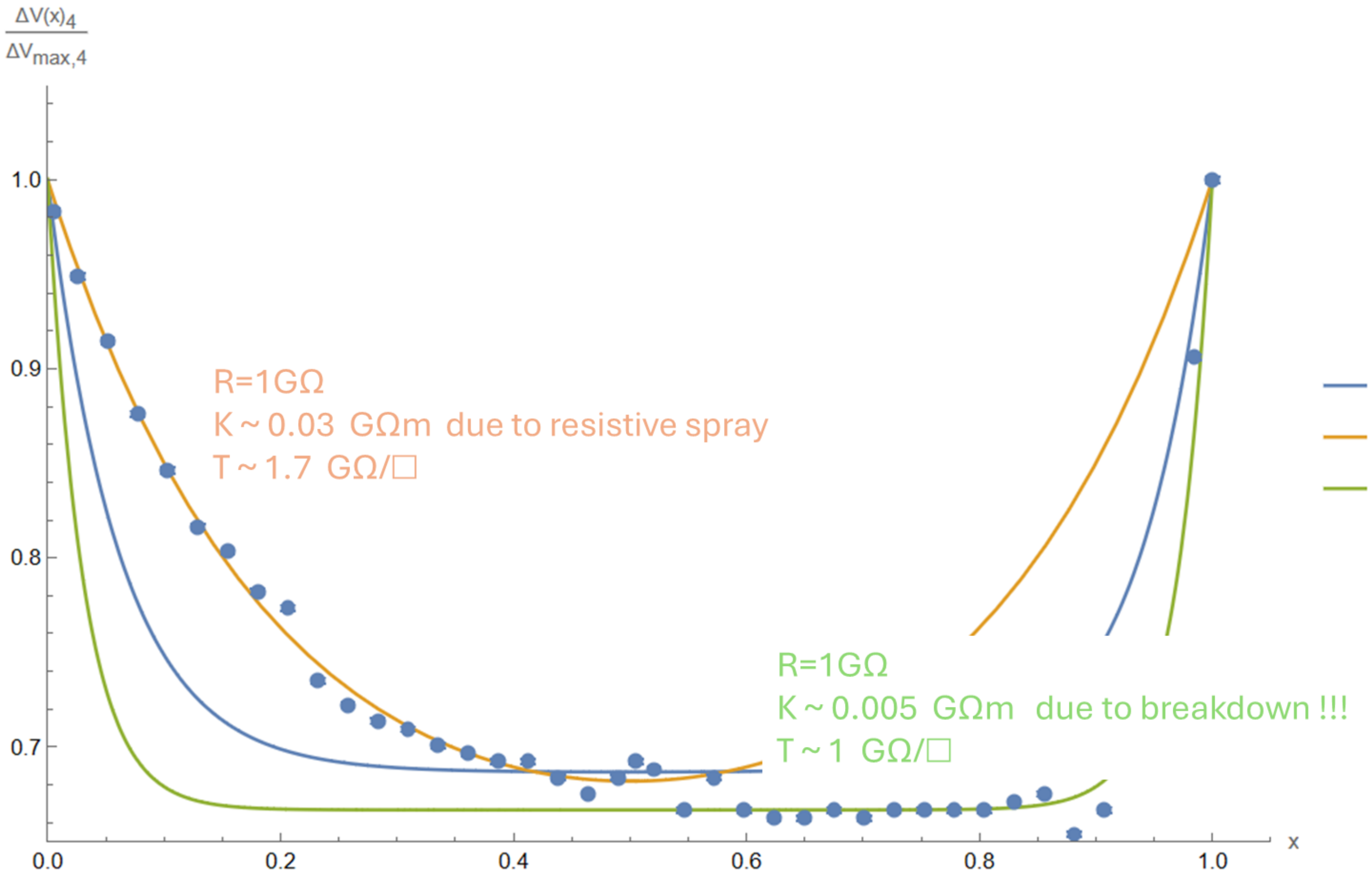

25μm Kapton
Breakdown observed at values much lower than datasheet

Buried resistive layer: electrical model results

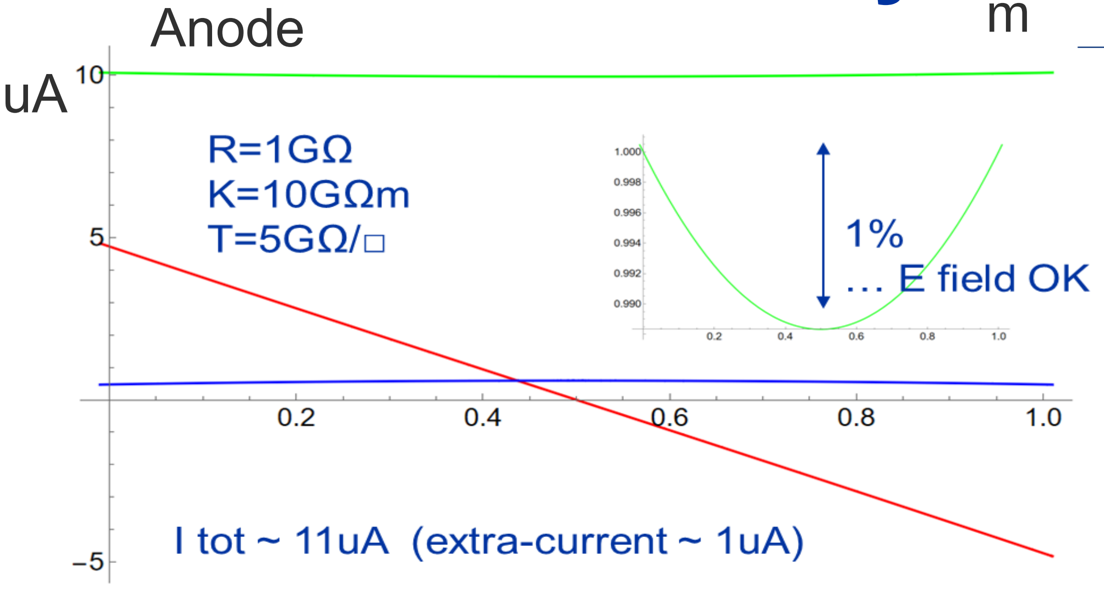

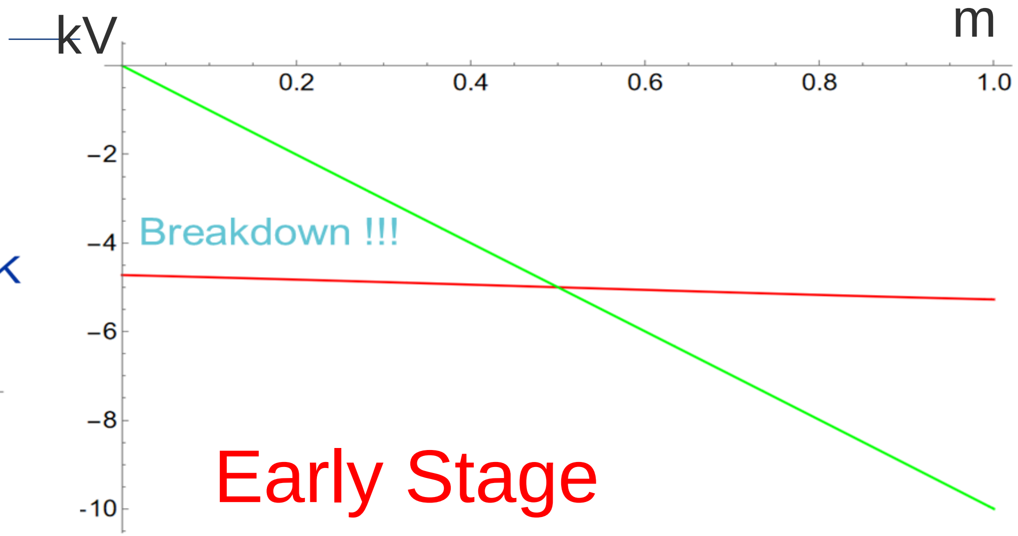

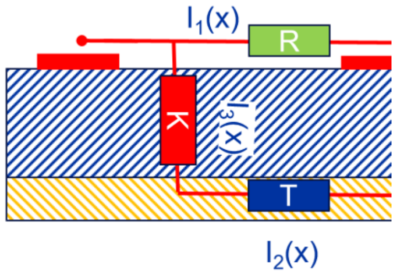

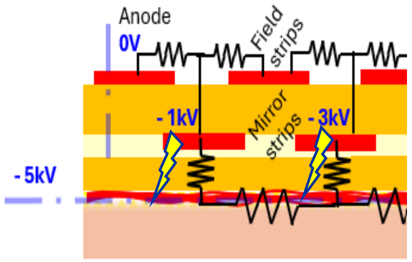

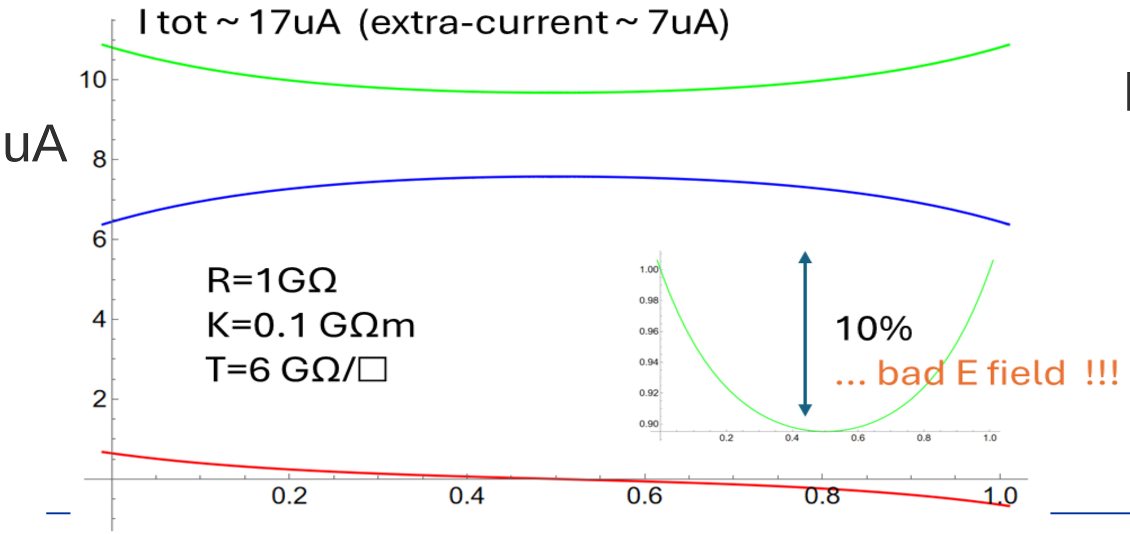

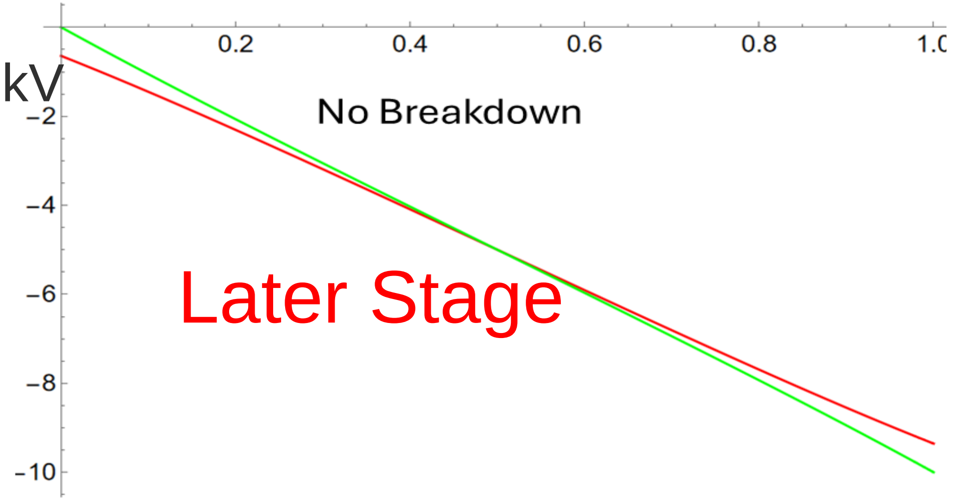

Final layout, materials and procedures fixed for the series production

Key points to avoid failures

- no resin contamination !!! Note: usually glues and resins are the weakest points

- Interpose between strips and Twaron layers a “thick” layer of insulator featuring

  - High resistivity $\rho_v > 10^{15}$ Ωcm
  - Dielectric strength > 150kV/mm

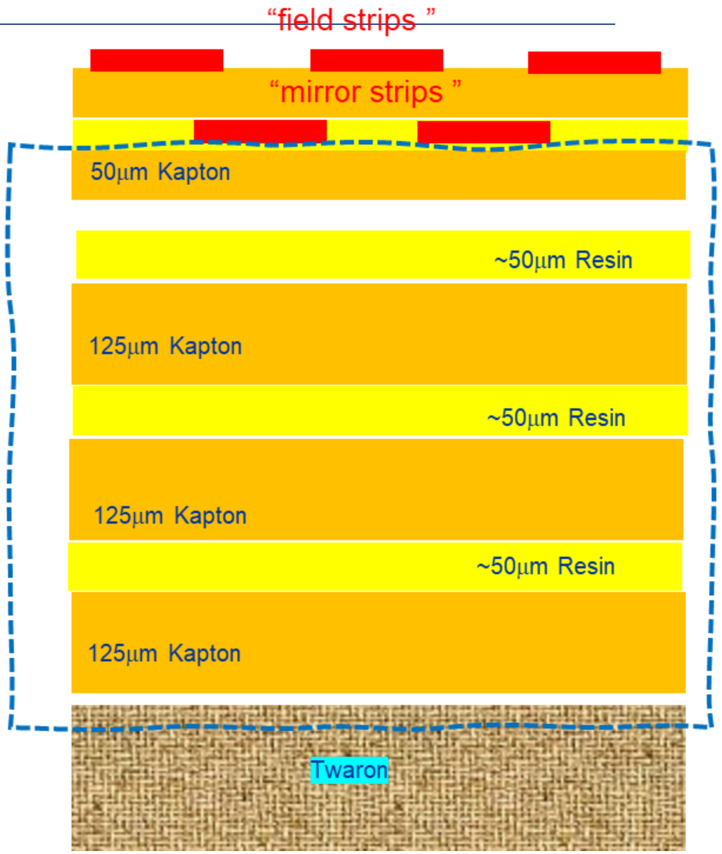

Final layout of the stack: minimal changes to design

- new strip foil w/ thicker Kapton coverlay 50µm + 25µm glue (produced at CERN, gluing in vacuum with press)
- 3 layers of Kapton: 125µm + 50µm resin each (to be laminated on the back of strip foil on the mold)

thickness Kapton+Resin ~0.5mm → “vertical R” below 1 strip O(10TΩ) @ 10kV

Materials: Same insulating materials (Kapton + Aramid) and same resin (Resoltech)

Production procedure and enhanced countermeasures and QC

- Minimize moisture trapped in wall layers: drying in oven Kapton & Twaron just before use
- QC epoxy contamination -> proper control of mixing and de-gassing process (new mixing / degassing tools and QC) and **… avoid antistatic spray…**
- QC electrical resistivity measurements after each early step in the production

ND280: installations at J-PARC

TOF installation (July 2023)

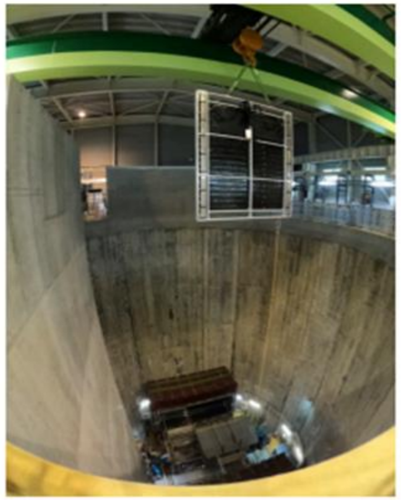

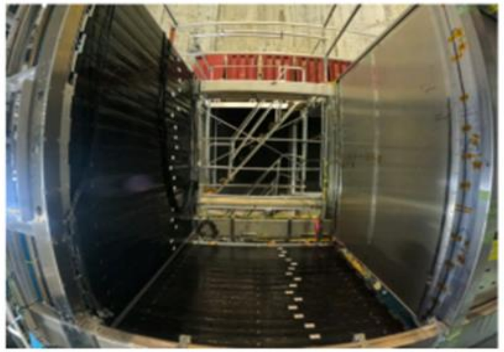

Bottom TPC
installation (September 2023)

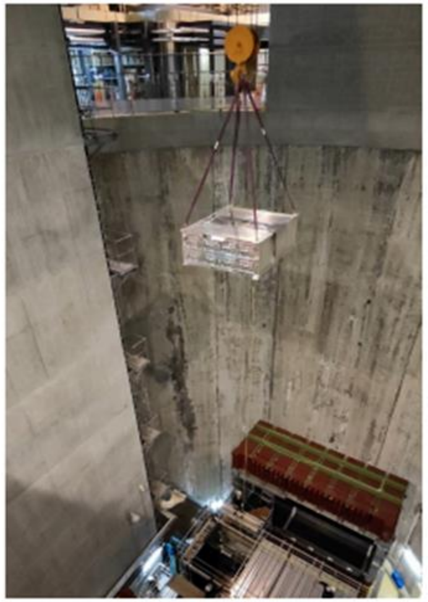

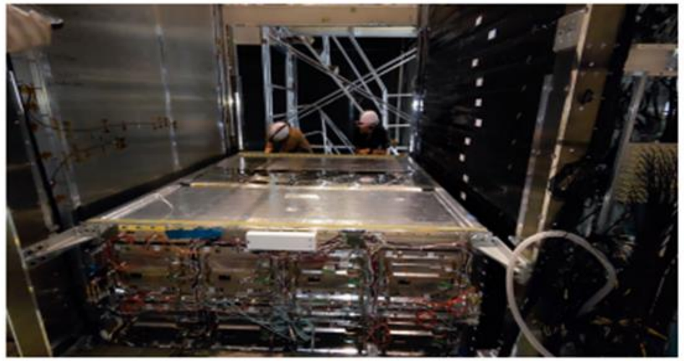

Super-FGD
installation (October 2023)

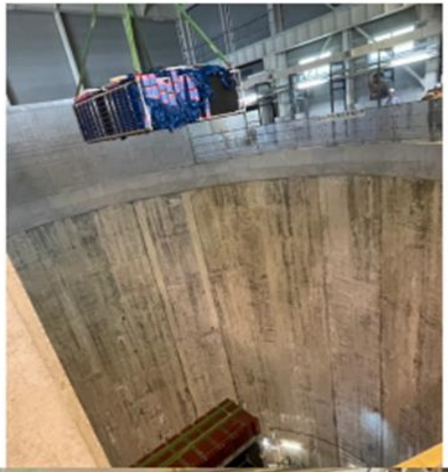

N280: commissioning at JPARC with cosmics

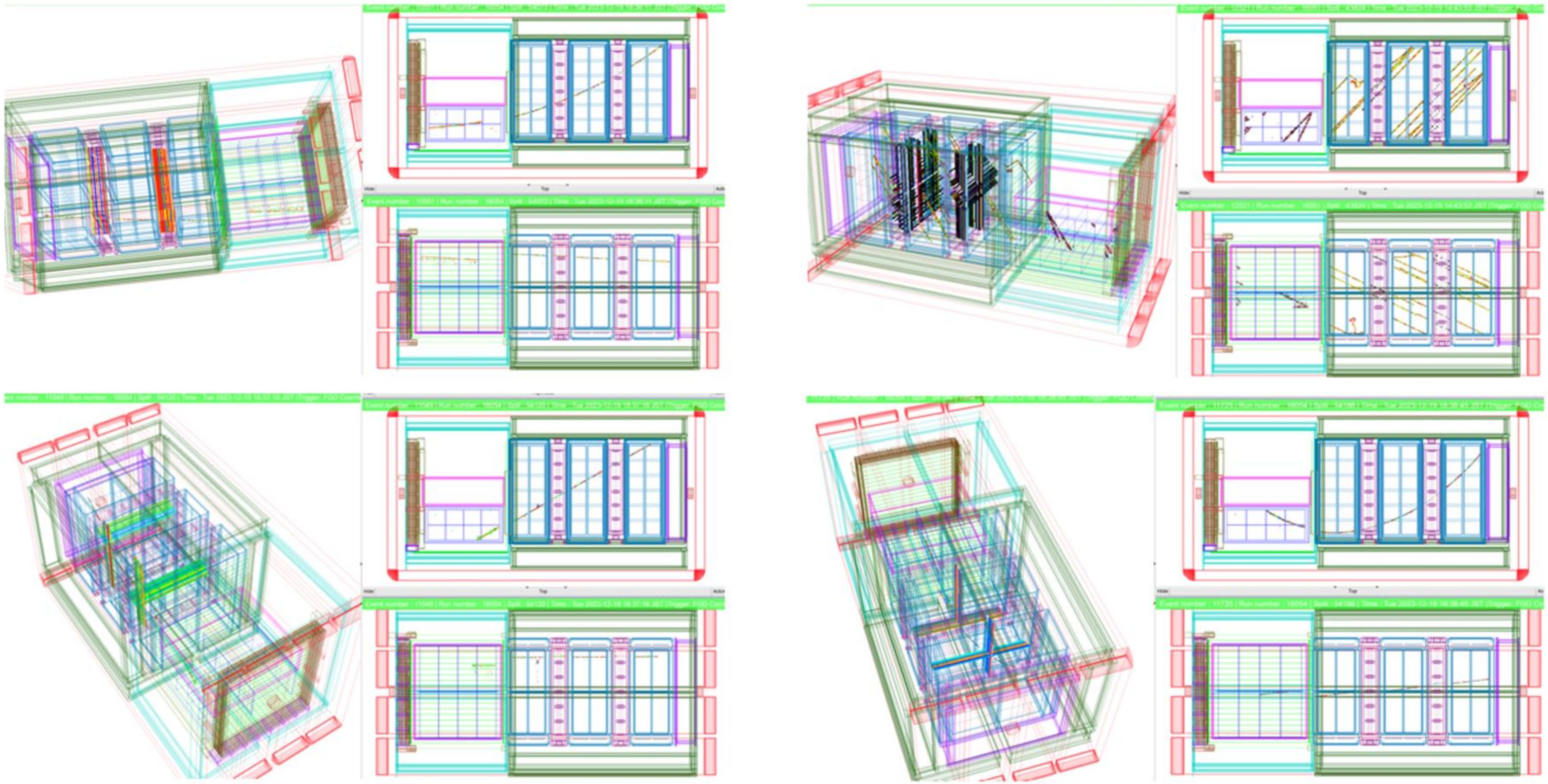

- Detector commissioning with and without magnetic field
- Alignment runs
- New software deployment
- New T2K gas system commissioning for both vertical and horizontal TPCs

N280: ν technical runs in December 2023 and February 2024 physics run

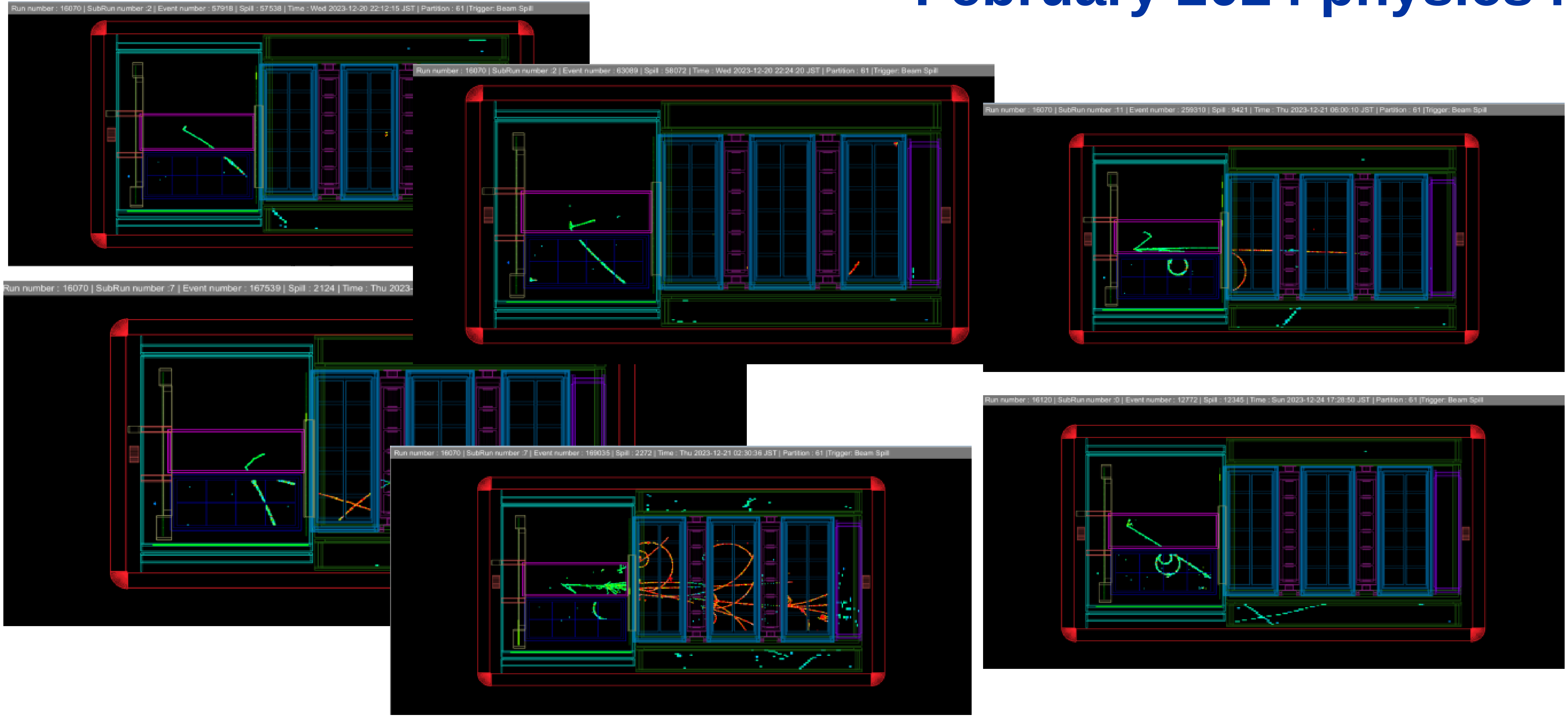

The T2K run schedule: beam upgrade

ν beam @ J-PARC: dedicated upgrade of the MR facility to reach the 1.3 MW beam power

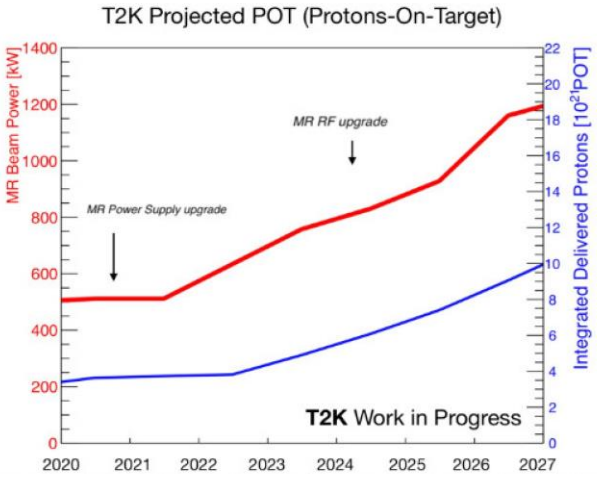

Beam and Window Parameters

		750 kW	1.3MW
		Design	T2KII path
Beam Energy	[Gev]	30	30
Protons per spill	[-]	3.30E+14	3.20E+14
Energy deposited per kg per proton	[J/kg/proton]	2.52E-10	2.52E-10
Energy deposited per kg per pulse	[J/kg/pulse]	83300	80640
Cycle time	[s]	2.1	1.16
Spill length	[s]	4.13E-06	4.11E-06
Number of bunches	[-]	8	8
Bunch length	[ns]	58	40
Gap length	[ns]	523	541
Peak Heat Generation	[J/m^3/s]	8.15E+14	1.14E+15
Beam sigma	[mm]	4.24	4.24
Heat load per spill	[J/cc/pulse]	378.18	366.11
Heat load per sec	[W/cc]	180.09	315.61
Peak Temp per bunch	[C]	19.78	19.15
Thermal stress per bunch	[MPa]	61.27	59.32
Peak Temp per pulse	[C]	158.27	153.22

3

Science & Technology Facilities Council
Rutherford Appleton Laboratory

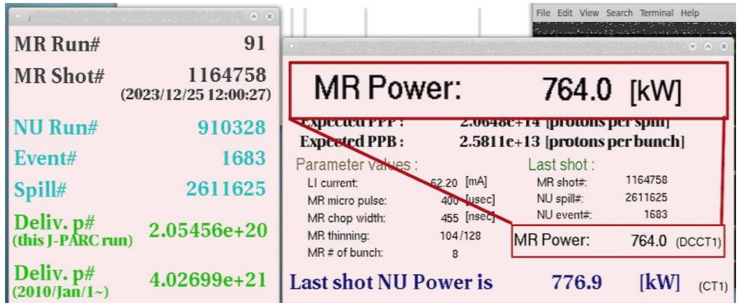

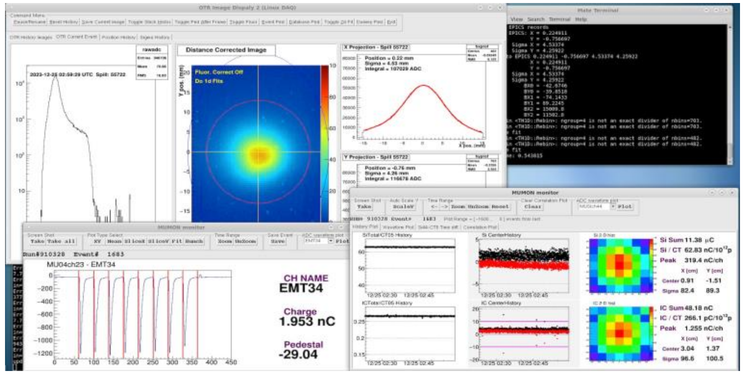

Expect to select 20k ν_μ CC0pi interactions in the super-FGD for 0.2e21 POT (1 month)

December 2023 → Beam power increased from 500 to 760 kW stable mode
800 kW reached in 2024 for the first run with the fully upgraded ND280

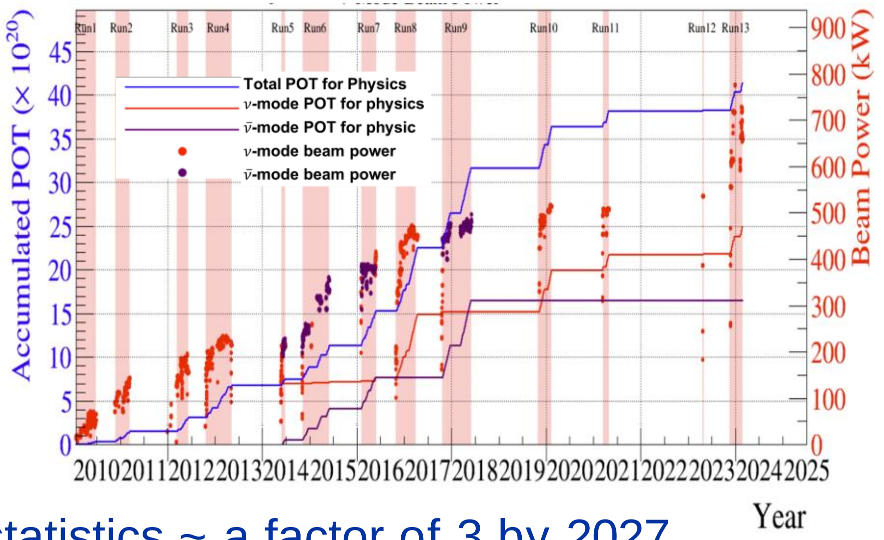

Steady improvements to reach 1.3 MW by 2027 with an increase T2K statistics ~ a factor of 3 by 2027